

**DEVELOPMENT OF AN UNCONDITIONALLY STABLE  
FINITE-DIFFERENCE TIME-DOMAIN METHOD FOR  
ELECTROMAGNETIC MODELING AND APPLICATIONS**

by

**CHENGHAO YUAN**

Submitted

in partial fulfillment of the requirements

for the degree of

**DOCTOR OF PHILOSOPHY**

Major Subject: Electrical and Computer Engineering

at

**DALHOUSIE UNIVERSITY**

Halifax, Nova Scotia, Canada

August, 2003

©Copyright by Chenghao Yuan, 2003



National Library  
of Canada

Bibliothèque nationale  
du Canada

Acquisitions and  
Bibliographic Services

Acquisitions et  
services bibliographiques

395 Wellington Street  
Ottawa ON K1A 0N4  
Canada

395, rue Wellington  
Ottawa ON K1A 0N4  
Canada

*Your file    Votre référence*

*ISBN: 0-612-89101-1*

*Our file    Notre référence*

*ISBN: 0-612-89101-1*

The author has granted a non-exclusive licence allowing the National Library of Canada to reproduce, loan, distribute or sell copies of this thesis in microform, paper or electronic formats.

L'auteur a accordé une licence non exclusive permettant à la Bibliothèque nationale du Canada de reproduire, prêter, distribuer ou vendre des copies de cette thèse sous la forme de microfiche/film, de reproduction sur papier ou sur format électronique.

The author retains ownership of the copyright in this thesis. Neither the thesis nor substantial extracts from it may be printed or otherwise reproduced without the author's permission.

L'auteur conserve la propriété du droit d'auteur qui protège cette thèse. Ni la thèse ni des extraits substantiels de celle-ci ne doivent être imprimés ou autrement reproduits sans son autorisation.

---

In compliance with the Canadian Privacy Act some supporting forms may have been removed from this dissertation.

Conformément à la loi canadienne sur la protection de la vie privée, quelques formulaires secondaires ont été enlevés de ce manuscrit.

While these forms may be included in the document page count, their removal does not represent any loss of content from the dissertation.

Bien que ces formulaires aient inclus dans la pagination, il n'y aura aucun contenu manquant.

**Canada**

**Dalhousie University**  
**Faculty of Engineering**


The undersigned hereby certify that they have examined, and recommend to the Faculty of Graduate Studies for acceptance, the thesis (*or project*) entitled "Development of an unconditionally stable finite-difference time-domain method for electromagnetic modeling and applications" by Chenghao Yuan in partial fulfillment of the requirements for the degree of Doctor of Philosophy.

Dated: August 29<sup>th</sup>, 2003


Supervisor:

  
**Dr. Zhizhang Chen**

External Examiner (Ph. D. only)

  
**Royal Military College of Canada**  
**Dr. Yahia M. Antar**

Examiners:

  
**Dr. Sherwin Nugent**

  
**Dr. Matiur Rahman**

**Dalhousie University**  
**Faculty of Engineering**

DATE: August 29<sup>th</sup>, 2003

**AUTHOR:** Chenghao Yuan


**TITLE:** DEVELOPMENT OF AN UNCONDITIONALLY STABLE  
FINITE-DIFFERENCE TIME-DOMAIN METHOD FOR  
ELECTROMAGNETIC MODELING AND APPLICATIONS

**MAJOR SUBJECT:** Electrical & Computer Engineering

**DEGREE:** Doctor of Philosophy

**CONVOCA TION:** October, 2003

Permission is herewith granted to Dalhousie University to circulate and to have copied for non- commercial purposes, at its discretion, the above thesis upon the request of individuals or institutions.

 Signature of Author

The author reserves other publication rights, and neither the thesis nor extensive extracts from it may be printed or otherwise reproduced without the author's written permission.

The author attests that permission has been obtained for the use of any copyrighted material appearing in this thesis (*or project*) (other than brief excerpts requiring only proper acknowledgement in scholarly writing), and that all such use is clearly acknowledged.

## **Dedication**

To my parents, Yuan Rongji, Shen Guangzi,  
my sister Yuan Yanhua, my niece Li Zhenggen  
and my dearest Fangyi Liu who has been always supporting me

## TABLE OF CONTENTS

<b>LIST OF TABLES.....</b>	<b>VIII</b>
<b>LIST OF FIGURES.....</b>	<b>IX</b>
<b>LIST OF SYMBLES AND ABBREVIATIONS.....</b>	<b>XI</b>
<b>ACKNOWLEDGEMENTS.....</b>	<b>XII</b>
<b>ABSTRACT.....</b>	<b>XIII</b>
 <b>CHAPTER 1 INTRODUCTION</b>	
1.1 Maxwell's Equations and Their Solutions.....	1
1.2 Brief Review of the State-of-the-art.....	2
1.3 Inducement of the Thesis.....	20
1.4 Purviews and Organization of the Thesis.....	21
 <b>CHAPTER 2 DEVELOPMENT OF THE FINITE- DIFFERENCE TIME-DOMAIN METHOD</b>	
2.1 Introduction.....	23
2.2 Yee's Grid and FDTD Algorithm in the Rectangular Coordinates.....	24
2.3 FDTD Algorithm in the Cylindrical Coordinate Systems.....	29
2.4 FDTD Algorithm in the Spherical Coordinate System.....	33
2.5 Properties of the FDTD Algorithm.....	36
2.5.1 Nonuniform Mesh.....	36
2.5.2 Two Inherent Constraints of the FDTD Algorithm.....	38
2.5.2.1 Numerical Stability.....	39
2.5.2.2 Numerical Dispersion.....	39
2.6 Absorbing Boundary Conditions.....	40
2.6.1 Mur First-order Boundary Conditions.....	41
2.6.2 Perfectly Matched Layers Boundary Conditions.....	42
2.6.3 Stretched Coordinates PML Boundary Conditions.....	46
2.7 Conclusions.....	52

## **CHAPTER 3 THE UNCONDITIONAL STABLE ADI-FDTD METHOD FOR ELETROMAGNETIC MODELING**

3.1 Introduction.....	53
3.2 ADI Fundamentals.....	53
3.3 Development of the Cylindrical ADI-FDTD Algorithm.....	55
3.3.1 Formulation of the Cylindrical ADI-FDTD Scheme .....	55
3.3.2 Advantages of the ADI Technique.....	57
3.3.3 Efficient Computations of the ADI-FDTD Method.....	58
3.4 Numerical Verification of the ADI-FDTD Algorithm.....	61
3.5 Conclusions.....	63

## **CHAPTER 4 A NOVEL METHOD FOR THE ANALYSIS OF NUMERICAL STABILITY**

4.1 Introduction.....	65
4.2 SCHUR-COHN-FUJIWA Criterion.....	65
4.3 Analytical Proof of Unconditional Stability of the Cylindrical ADI-FDTD Method.....	67
4.4 Numerical Experiments on Unconditional Stability.....	74
4.4.1 Numerical Verification of the Unconditional Stability.....	74
4.4.2 Numerical Accuracy with Different Time Steps.....	75
4.5 Conclusions.....	76

## **CHAPTER 5 ADI-FDTD MODELING OF CLOSED STRUCTURES**

5.1 Introduction.....	78
5.2 Approximation of Medium Parameters in ADI-FDTD Algorithm.....	78
5.3 Modified ADI-FDTD Algorithm for Solving Highly Conductive Materials.....	80
5.4 Padé Approximation.....	83
5.5 Experiments on Circular Resonators.....	86
5.6 Experiments on the Resonators with Lossy Materials.....	90

5.7 Conclusions.....	95
----------------------	----

## **CHAPTER 6 ADI-FDTD MODELING OF OPEN STRUCTURES**

6.1 Introduction.....	96
6.2 The Cylindrical ADI-FDTD Method with the Mur Boundary Condition.....	96
6.3 The Cylindrical ADI-FDTD Method with Uniaxial PML Boundary Condition...	97
6.4 Performance of the Absorbing Boundary Conditions.....	101
6.5 Numerical Simulations for Analyzing General Conductive Materials.....	106
6.5.1 Experiments on the Waveguide with Highly Conductive Materials.....	106
6.5.2 Experiments on the Waveguide with Copper Wall.....	111
6.6 Conclusions.....	118

## **CHAPTER 7 SUMMARY AND FUTURE DIRECTIONS**

7.1 Summary.....	119
7.2 Future Directions.....	120

<b>References.....</b>	<b>123</b>
------------------------	------------

<b>Appendix A Equations of the Cylindrical ADI-FDTD Algorithm.....</b>	<b>137</b>
--	------------

<b>Appendix B Rearranged Equations of ADI-FDTD Equations for Computer Programming.....</b>	<b>141</b>
--	------------

<b>Appendix C Maple Outputs of the Expressions of the Coefficients of the Characteristic Equation.....</b>	<b>146</b>
--	------------

<b>Appendix D Modified ADI-FDTD Algorithm for Solving Conductive Materials.....</b>	<b>150</b>
---	------------



## List of Tables

### Chapter 3

Table 1	Resonant frequencies computed with the conventional FDTD and the ADI-FDTD .....	62
---------	---	----

### Chapter 4

Table 1	Simulation results with different time steps.....	76
---------	---	----

### Chapter 5

Table 1	Resonant frequencies of the dielectric rod resonator compared with different methods .....	87
Table 2	Resonant frequencies of the dielectric resonator computed with different methods .....	89
Table 3	Resonant frequencies of with the presented method .....,.....	94
Table 4	Q-factors of each mode with the presented method .....	94
Table 5	Q-factor of $TM_{010}$ mode with the presented method .....	95

### Chapter 6

Table 1	Computed attenuation constants with different conductivities .....	108
Table 2	Computed phase shift constants with different conductivities .....	109
Table 3	Computed time by FDTD and ADI-FDTD .....	110
Table 4	Memory usage by FDTD and ADI-FDTD methods .....	110

## List of Figures

### Chapter 1

Figure 1.1 A typical mesh for a two-dimensional finite difference method.....	3
Figure 1.2 One half of the cross section of a microstrip line for the <i>MoL</i> procedure.....	8
Figure 1.3 A hybrid TLM cell.....	13

### Chapter 2

Figure 2.1 Position of electric and magnetic field components in Yee's grid.....	26
Figure 2.2 Field Placement in cylindrical Yee's grid.....	30
Figure 2.3 (a) A portion of the lattice at $r=0$ (b) the integral path to obtain $E_z$ at $r=0$ .....	32

### Chapter 3

Figure 3.1 The geometry of the resonator cavity (dimensions in centimeter).....	62
---	----

### Chapter 4

Figure 4.1 Electric field $E_z$ recorded in time domain with the time steps larger than the CFL limit.....	75
Figure 4.2 Relative error of the proposed scheme with various time steps.....	76

### Chapter 5

Figure 5.1 Interfaces of an inhomogeneous medium.....	79
Figure 5.2 The geometry of a dielectric rod resonator.....	86
Figure 5.3 The geometry of the dielectric disk resonator (side view).....	87
Figure 5.4 Discretization of the computation area.....	88
Figure 5.5 Computation errors of the cylindrical ADI-FDTD with the uniform and nonuniform grid.....	89
Figure 5.6 The geometry of the selected cylindrical cavity: (a) Side view (b) Bottom view.....	91
Figure 5.7 (a) Nonuniform mesh in the air-filled area (b) Uniform fine mesh inside the conducting walls.....	91
Figure 5.8 The comparison between DFT and DFT/Padé method for a certain mode with the cylindrical ADI-FDTD method.....	93

### Chapter 6

Figure 6.1	A circular waveguide with ABCs.....	101
Figure 6.2	The perfect cylindrical waveguide terminated with UPML at both ends.....	102
Figure 6.3	The $E_r$ of 2000 iterations.....	104
Figure 6.4	Numerical reflections from the UPML layers.....	105
Figure 6.5	Reflection Error of Mur Boundary Condition.....	106
Figure 6.6	The non-perfect waveguide under study.....	107
Figure 6.7	The z-directed wave impedance in the air-filled area with different conductivities .....	111
Figure 6.8	A Field attenuation along propagation direction .....	112
Figure 6.9	Wave impedance in the air-filled area .....	113
Figure 6.10	Wave impedance in the air-filled area .....	113
Figure 6.11	(a) Field distribution in the conductive region in the radial direction at 40GHz.....	114
	(b) Field distribution in the conductive region in the azimuthal direction at 40GHz.....	115
	(c) Field distribution in the conductive region in the propagation direction.....	115
Figure 6.12	(a) Wave impedance in the radial direction in the conductive area.....	117
	(b) Wave impedance in the azimuthal direction in the conductive area .....	117
	(c) Wave impedance in the propagation direction in the conductive area .....	118

## List of Symbols and Abbreviations

$\omega$	Angular frequency
$\alpha$	Attenuation constant
$\beta$	Phase constant
$\gamma$	Propagation constant
$\delta$	Skin depth
$\epsilon$	Permittivity
$\epsilon_r$	Relative permittivity
$\mu$	Permeability
$\kappa$	Complex frequency shift
$\lambda$	Wave length
$\sigma$	Conductivity
$c$	Velocity of light
$k$	Wave number
$u$	Velocity of wave
ABCs	Absorbing Boundary Conditions
ADI	Alternating Direction Implicit
BOR	Body of Rotation
CFL	Courant-Friedrich-Levy
CFS	Complex Frequency Shift
EM	Electromagnetic
EMP	Electromagnetic Pulse
DFT	Discrete Fourier Transform
FD	Frequency Domain
FDM	Finite Difference Method
FDTD	Finite-difference Time-domain
FEM	Finite Element Method
FFT	Fast Fourier Transform
MoL	Method of Line
MoM	Method of Moments
MRTD	Multiresolution Time-domain
PEC	Perfect Electric Conductor
PML	Perfectly Matched Layers
PSTD	Pseudospectral Time-domain
RF	Radio Frequency
SDM	Spectral Domain Method
TD	Time Domain
TDFEM	Time Domain Finite Element Method
TODE	Time-domain Difference Equation
TE	Transverse Electric
TM	Transverse Magnetic
TLM	Transmission Line Method
UPML	Uniaxial Perfectly Matched Layers

## **Acknowledgements**

The author would like to thank Dr. Zhizhang Chen for his support and guidance throughout this thesis work. His advice and opinions were highly valued at all stages of the research project. The author also wishes to thank the other members of the Guiding Committee, for their advice and evaluating this work.

My appreciations also go to the Natural Science and Engineering Research Council of Canada for its financial support. All of the members at the Microwave and Wireless Research Laboratory of Dalhousie University are also greatly appreciated for their assistance.

Thanks to Dr. S. Nugent for his advice on the theory of electromagnetism and the guidance for my comprehensive exams. Thanks to Dr. M. Rahman for his helpful advice and suggestions, especially on solving higher order complex matrix.

Special thanks to Ms. S. Pace and Ms. N. Smith for their kind assistance during the period of my study.

## ABSTRACT

Maxwell's equations, which represent a fundamental relationship between electric and magnetic fields, have been studied for decades. Although the analytical solutions have been given for analyzing many microwave structures, it is difficult to obtain them for predicting field behaviors in complex structures with composite materials. Consequently, numerical techniques have been studied, applied and proven to be effective in both time domain and frequency domain. With the particular desire of obtaining the full wave analysis for the microwave devices in an efficient manner, researchers have been driven into finding novel time domain techniques. The Finite-difference Time-domain (FDTD) method was then developed and has been extensively investigated and employed in solving electromagnetic problems due to its simplicity, effectiveness and flexibility. It has become one of the most popular time-domain methods so far. For the electrically large structures and highly conductive materials, however, the FDTD algorithm requires large computation resources and prohibitively long simulation time owing to its two inherent limits: dispersion errors and Courant-Friedrich-Levy (CFL) stability condition. Several FDTD-based algorithms, aiming at removing or alleviating the two constraints, have been recently developed. They include multiresolution time-domain (MRTD) method and pseudospectral time-domain (PSTD) method for reduction of numerical dispersion, and alternating direction implicit FDTD (ADI-FDTD) method for complete removal of CFL condition.

So far, the ADI-FDTD method has been applied only to the Cartesian coordinates system. As well, its exclusive advantages have not been fully explored in solving practical electromagnetic problems. In this thesis, the newly developed three-dimensional ADI-FDTD method in the cylindrical coordinates system is presented for effectively analyzing cylindrical microwave devices, especially body of rotational (BOR) structures. Unlike the conventional ADI algorithm, however, the alternation is performed in a term-wise manner rather than in the coordinates at each time step. As a result, for the three-dimensional case, only two alternations are required to obtain the unconditionally stable scheme. The CFL stability condition that exists in the conventional FDTD method is completely removed. The time step of the ADI-FDTD method is no longer determined by the CFL stability condition but by the modeling accuracy.

Theoretical proof of the unconditional stability of the ADI-FDTD method in cylindrical coordinates system is given with the help of SCHUR-COHN-FUJIWA Criterion. The numerical verification of the unconditional stability as well as the effectiveness and efficiency of the proposed method are also demonstrated in experiments. It is found that the required iteration number can be at least three times less than that of the conventional FDTD method that can result in great saving in CPU time.

To further demonstrate the exclusive advantages of the ADI-FDTD method in solving practical electromagnetic problems, two resonant structures with conductive materials have been computed with the proposed method. A modified ADI-FDTD method in cylindrical coordinates system is specifically derived for solving highly conductive materials. The detailed field behavior in the conductive materials is then computed, which can not be easily done with the conventional FDTD method. It is shown that the ADI-FDTD method is remarkably effective and efficient for solving the structures with conductive materials, especially the highly conductive materials.

Finally, the ADI-FDTD algorithm is successfully combined with the popular absorbing boundary conditions (ABCs) for simulating open structures. The detailed implementation of the uniaxial perfectly matched layers (UPML) boundary conditions in stretched coordinates is presented for modeling general open media. With the comparison between the Mur ABC and the UPML ABC, it is shown that the UPML ABC has smaller reflection errors and is more capable of absorbing evanescent waves. It is also shown that the ADI-FDTD method combined with the UPML absorbing boundary conditions is more effective and accurate in modeling the structures with arbitrary conductivities than the Surface Impedance Boundary Condition (SIBC) method.

In conclusion, the ADI-FDTD method is an effective and efficient tool in simulating the field behaviors in RF/Microwave circuits and devices, especially where the fine mesh is indispensable. The exclusive feature of the unconditional stability allows it to be particularly useful in Monolithic Microwave Integrated Circuit (MMIC) and nanotechnology designs in the future.

# **Chapter 1    Introduction**

## **1.1    Maxwell's Equations and Their Solutions**

Maxwell's partial differential equations represent the spectral-temporal relationship of electric and magnetic fields. Based on these equations together with certain principles and theorems, such as duality, reciprocity, uniqueness, image theory, induction theorem and Green's functions, a variety of the electromagnetic phenomena can be interpreted and described. More specifically, since they were firstly introduced in 1870, their applications can be found in various areas, such as fundamental physics, remote sensing, satellite communication, optical fiber communication, electromagnetic compatibility, military electronic warfare, and wireless communications. As a result, seeking the solutions to Maxwell's equations in different environmental settings has been one of the most interesting topics in electromagnetism.

The primary ways to find electromagnetic solutions can be categorized into experimental, analytical and numerical approaches. Experimental approach obtains the electrical parameters by measuring the subjects under study with electronic testing equipment. Analytical approach solves the Maxwell's equations directly, most likely in geometries of regular shapes. Numerical approach employs the numerical methods to solve Maxwell's equations. Each approach has its advantages and disadvantages. The practical experiment can provide electronically measured references for the parameters of interest such as field strength, waveform, field attenuation etc. However, it is subject to the environmental interference, the accuracy of apparatus as well as potential high cost of setting up testing facilities. Therefore it is not feasible and practical sometimes for the accurate scientific research or theoretical study. Analytical approach is the most accurate way for analyzing the field behavior. But it is difficult or impossible to perform for complex structures or composite materials. Numerical techniques are currently the burgeoning approach that is applied for solving arbitrary complex circuit structures. Their flexibility, effectiveness and ability make them useful tools in electromagnetics. Thanks to the rapidly increased



computing power, it can now be used to cope with heavy computation loads associated with simulating complex structures [1-87].

On the other hand, for modern electronic system design, proper electromagnetic modeling and accurate computation play an increasingly indispensable role before the system is fabricated due to the demands for performance at high frequency band. Novel MIC/MMIC techniques allow hundreds or even thousands of electronic components to be integrated into a single package or circuit board. Such a high-density integration introduces non-negligible various electromagnetic interactions and interference such as cross-talk among different circuit parts or different layers of the circuit board. In addition, thin film techniques and nanotechnology enable the circuits of much smaller size than before. With such a small or even tiny size, electromagnetic effects that were ignored in the conventional design needs to be taken into account. Consequently, low-cost and reliable numerical analysis has become an essential procedure for the design of today's electronic systems.

The normal procedure of an electromagnetic computation technique includes developing a proper mathematical model, running numerical simulation to validate it, and modifying the model based on the simulation results. Many numerical models have been developed in the past twenty years. In the following section, several widely used numerical methods will be briefly discussed for a better understanding of the state-of-the-art in computational electromagnetics.

## **1.2 Brief Review of the State-of-the-art**

### A. Finite Difference Method (FDM)

Finite difference method [1] is a simple method for solving partial differential equations. This method can be applied to a wide range of EM problems even with irregular boundary shapes and different boundary conditions [1] [2]. The least analytical property with minimal mathematical preprocessing made it be a prevailing method during 1950~1970 [3] [4]. However, the simplicity of the method is at the cost of numerical inefficiency. For structures with good many grid points, it needs more storage memory

and faster computer processor to accomplish computation. Certain precautions have to be considered when it is applied to an open problem in which an infinite solution region is truncated to a finite size.

The basic idea of FDM method can be summarized as:

- 1) Discretize the whole solution domain into a grid structure with the mesh points lying on the boundary.
- 2) Replace the derivatives of the partial differential governing equations with the difference quotients related to adjacent points.
- 3) Form a system of linear equations with unknowns being the field variable for each point.
- 4) Solve the linear equations with known boundary conditions and obtain field value at each point.

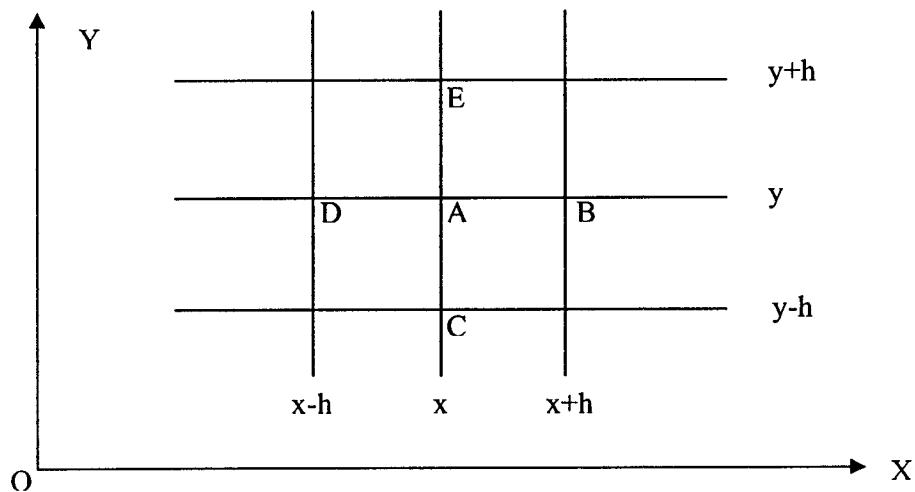


Figure 1.1 A typical mesh for a two-dimensional finite difference method

Figure 1.1 shows a typical 2-D computation area. Suppose that the governing function is:

$$\frac{\partial^2 \phi}{\partial x^2} + \frac{\partial^2 \phi}{\partial y^2} = 0 \quad (1.1)$$

Replacement of the derivatives with their corresponding finite-difference quotients leads to:

$$\frac{\partial^2 \phi_A}{\partial x^2} + \frac{\partial^2 \phi_A}{\partial y^2} \approx \frac{\phi_B + \phi_D - 2\phi_A}{h^2} + \frac{\phi_E + \phi_C - 2\phi_A}{h^2} = 0 \quad (1.2)$$

or, the field value at point A can be expressed as:

$$\phi_A = \frac{\phi_B + \phi_C + \phi_D + \phi_E}{4} \quad (1.3)$$

After forming the equation for each grid point, the field value at each point can be obtained by solving the system of linear equations with the help of known boundary conditions.

For complicated structures or the structures with complex shapes or different materials, the programming of the FDM method may become complicated. The computation accuracy may also decrease when the fields change rapidly. Nevertheless, with the development of high-speed computers with large storage capability, the easy application of the finite differential method has made it popular in solving EM problems [5] [6].

#### B. Finite Element Method (FEM)

Finite element method [7] is one of the widely used numerical methods for solving electromagnetic problems [8] [9]. Instead of dealing with partial differential equations with certain boundary conditions, it solves energy functional that represents the total energy in a particular system. By discretizing the whole solution area into small element areas or cells, functionals are set up and variational expressions are established in terms of the small element areas. These small areas or cells, unlike those in *FDM* method, are usually polygons such as triangles and rectangles for two-dimensional problems and tetrahedral for three-dimensional problems. Such choices of the elements render FEM the flexibility in matching its cells with irregular boundary shapes. The field quantities with each element are expanded in terms of basis functions, usually linear basis functions. By minimizing the functional over the whole domain that consists of elements, a system of linear equations is obtained for the expansion coefficients. Solving the set of linear

equations for the coefficients, the *FEM* solutions are obtained. For example, the solution to the two dimensional Laplace equation is equivalent to minimizing the functional:

$$I(\phi) = \langle \phi, \nabla^2 \phi \rangle = \iint_S \phi \left( \frac{\partial^2 \phi}{\partial x^2} + \frac{\partial^2 \phi}{\partial y^2} \right) dx dy = - \iint_S \left[ \left( \frac{\partial \phi}{\partial x} \right)^2 + \left( \frac{\partial \phi}{\partial y} \right)^2 \right] dx dy \quad (1.4)$$

$S$  in the above equation is then discretized as the sum of small element areas. The functional becomes a collection of the contributions from all of the small elements. By expanding  $\phi$  in each small element in terms of known basis functions with unknown coefficients and minimizing the functional by setting its first derivatives with respect to all coefficients to be zero, a matrix equation is then generated. By solving the set of equations for the coefficients, the solutions are obtained.

One of the problems of *FEM* methods is the numerical spurious solutions which correspond to nonphysical field structures [10]. Several schemes are available to reduce or eliminate these spurious solutions, such as edge-based *FEM* method [11] [12] [13] [14]. In addition, the complex data processing and tremendous number of elements are two scabrous topics for practical applications.

### C. Method of Moments (MoM)

Method of Moments [15] is a popular means for discretizing a continuous operator equation such as an integral equation. By employing weighted residuals techniques, the method has been widely used in computational electromagnetics since Harrington first introduced it into electromagnetic field theory [15]. It has been shown that the method is extremely suitable for solving antenna radiation and scattering problems [16-20].

The normal procedure of the method can be described as follows. Assume that the equation to be solved is:

$$Lu = f \quad (1.5)$$

where  $L$  is an operator-differential or integral,  $f$  is known force function and  $u$  is the solution to be determined. The first step in the moment method is to expand the unknown function  $u$  in terms of the approximate solution  $\bar{u}$  that is a linear combination of known basis functions  $\phi_n$  with  $n=1,2,\dots,N$ :

$$\bar{u} = \sum_{n=1}^N \alpha_n \phi_n \quad (1.6)$$

where the  $\alpha_n$ 's are the unknown expansion coefficients of the approximate solution and the  $\phi_n$ 's are the basis functions. The second step is to select a set of linear independent test functions  $w_n$  ( $n=1,2,\dots,N$ ), and then set to zero of the inner product of each test function and the residual:

$$R = \bar{u} - f = \sum \alpha_n \phi_n - f$$

$$\langle R, w_n \rangle = 0$$

or

$$\sum_{n=1}^N \alpha_n \langle L\phi_n, w_m \rangle = \langle f, w_m \rangle \quad m = 1, 2, \dots, N \quad (1.7)$$

In a matrix form:

$$A[\alpha] = B \quad (1.8)$$

where  $\alpha$  is a column vector which is composed of the unknown expansion coefficients, and:

$$A = \begin{bmatrix} \langle L\phi_1, w_1 \rangle & \langle L\phi_2, w_1 \rangle & \cdots & \langle L\phi_n, w_1 \rangle \\ \langle L\phi_1, w_2 \rangle & \langle L\phi_2, w_2 \rangle & \cdots & \langle L\phi_n, w_2 \rangle \\ \vdots & \vdots & \vdots & \vdots \\ \langle L\phi_1, w_n \rangle & \langle L\phi_2, w_n \rangle & \cdots & \langle L\phi_n, w_n \rangle \end{bmatrix} \quad (1.9)$$

$$B = \begin{bmatrix} \langle f, w_1 \rangle \\ \langle f, w_2 \rangle \\ \vdots \\ \langle f, w_n \rangle \end{bmatrix} \quad (1.10)$$

By solving equation (1.8), the approximate solution to coefficient  $\alpha$ 's are obtained and therefore is found. There are several choices available for the basis functions and test functions, such as unit pulse function and delta function etc. When the test functions are identical with the basis functions, the method is called Galerkin's method. Due to the flexible choice of the basis functions as well as the test functions, the method of moments can be used to solve static, quasi-static and dynamic problems expressed by differential or integral equations. Some commercial EM simulators such as HP-ADS Momentum are based on this technique.

#### D. Method of Lines (MoL)

Method of lines [21] was developed for solving partial difference equations. The method was firstly applied to the calculation of planar microwave circuits by Schulz and Pregla [22]. The primary concept of the method is that all but one of the independent variables of partial differential equations are discretized for numerical processing while the analytical expressions are sought for the remaining one variable, which actually results in a dimension-reduced system.

For example, the cross section a microstrip line is shown in Fig. 1.2. The governing equation to be solved is the homogeneous Helmholtz equation:

$$\frac{\partial^2 \phi}{\partial x^2} + \frac{\partial^2 \phi}{\partial y^2} + (k^2 - \beta^2) \phi = 0 \quad (1.11)$$

where  $\phi$  is the electric or magnetic field,  $k$  is the wave number and  $\beta$  is the propagation constant.

The  $x$  direction is discretized by a family of  $N$  straight lines parallel to the  $y$  axis separated by  $h$ .

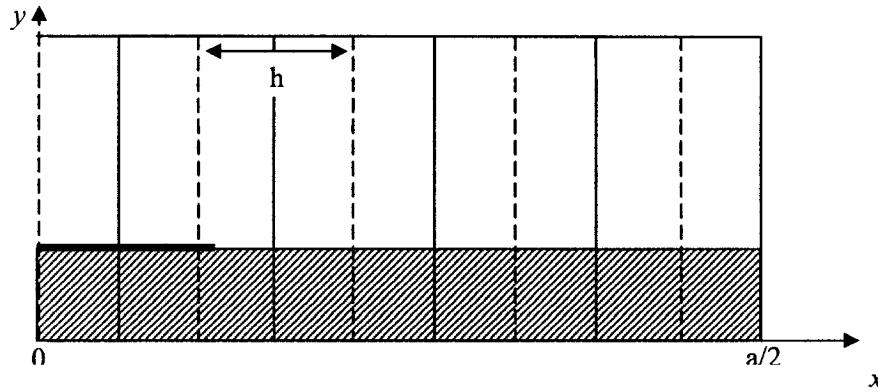


Figure 1.2 One half of the cross section of a microstrip line for the *MoL* procedure

By replacing the partial derivative with respect to the  $x$  coordinate with difference expression, the two scalar functions for  $E$  or  $H$  that satisfy the Helmholtz equation become:

$$\frac{\partial^2 \varphi}{\partial^2 y} + \frac{1}{h^2} [\varphi_{i-1}(y) - 2\varphi_i(y) + \varphi_{i+1}(y)] + (k^2 - \beta^2) \varphi_i(y) = 0 \quad (1.12)$$

$i = 1, 2, \dots, N$

or in matrix form,

$$h^2 \frac{d\Phi}{dy^2} - [P - h^2(k^2 - \beta^2)I] \Phi = 0 \quad (1.13)$$

where  $I$  is the identity matrix and  $P$  is a tridiagonal matrix determined by the lateral boundary conditions at  $x=0$  and  $x=a/2$ . The discretization lines for  $E$  and  $H$  are shifted by half the discretization distance,  $h/2$ , so that the boundary conditions can be easily implemented.

Because  $P$  is a real symmetric matrix, there is an orthogonal matrix  $T$  such that:

$$T' P T = \text{diag}(\lambda) \quad (1.14)$$

where  $T'$  denotes the transpose of  $T$  and the elements of the diagonal matrix  $diag(\lambda)$  are eigenvalues of  $P$ . By introducing

$$T'\Phi = U \quad (1.15)$$

the system of  $N$  coupled ordinary equations (1.12) can be decoupled as:

$$h^2 \frac{\partial^2 U}{\partial y^2} + [\lambda_i - h^2 (k^2 - \beta^2)] U_i = 0 \quad i = 1, 2, \dots, N \quad (1.16)$$

The equations of this form can then be analytically solved for each homogeneous region.

The method of lines has been extensively used in a number of practical but analytically complex structures such as microstrip resonator, stripline coupler, and via hole in multilayer packaging [23] [24] [25]. However, in most cases MoL is restricted to the analysis of planar and quasiplanar waveguide structures.

#### E. Spectral Domain Method (SDM)

Unlike the above methods that are conducted in temporal and spatial domain, SDM [26] is a Fourier-transformed version of integral equation method applied to planar structures. The purpose of Fourier transform is to convert a multidimensional problem into an ordinary one-dimensional problem. It was originally proposed by Itoh and Mittra on the dispersion analysis of microstrip lines. This method has been widely used in analyzing planar structures including microstrip line, finline, slotline and coplanar waveguide [27-30].

Basically SDM can be summarized in three formulation steps:

1. Associate two scalar potentials  $\phi$  and  $\psi$  with electric and magnetic fields of one dimension in all the regions. The field components are then Fourier transformed in other dimensions. The governing equations are reduced to one-dimensional ordinary differential equations for the untransformed dimension.



2. Determine an appropriate Green's function for  $\phi$  and  $\psi$  by means of immittance approach.
3. Solve the equations for the Fourier transformed unknown current distribution for a strip by means of Galerkin's method. The unknown currents are solved and expressed in terms of known basis functions.

The primary advantage of the SDM is the numerical efficiency due to the decreased dimensions. However, the significant amount of analytical preprocessing restricts its applicability to a limited number of cases. The method is generally used in well-shaped structures with infinitely thin conductors, having perfect conduction.

The numerical computation methods described so far are generally used for solving the EM problems in frequency domain, and therefore are called frequency domain numerical methods. Naturally, frequency domain methods are computationally efficient since only a narrow range of frequency is under study. During the period of the pre-computer era when large scale computation was impossible, these methods had been the primary tools for analyzing EM problems.

With the arrival of cheap powerful digital computers in recent years, large scale computation becomes possible. There have been growing interests in the direct time domain (TD) methods to calculate the electromagnetic scattering and interaction phenomena. This may be due to the surge in the activities in such areas as:

- 1) Electromagnetic pulse (EMP) application and short pulse radar that involve strong transient effects.
- 2) High speed digital circuit packaging and interconnects which include the propagation, crosstalk and radiation of electronic digital pulses.
- 3) Broad band signal transmission, where signals are mostly interpreted in time domain.

Direct transient analysis is preferred in these applications. Therefore, the time domain methods are the natural choice because they have several advantages over conventional frequency domain methods:

- 1) They can provide wideband analysis with recorded time domain signature.
- 2) The field behavior can be visually studied in time domain.
- 3) The simulation needs to be run only once to obtain the information over a wide range of frequencies, and the frequency domain information can be extracted from the time domain data by Fourier transform.
- 4) They can handle very short pulse excitations such as electromagnetic pulse and lighting which are not very suitable for frequency domain methods.

Typical examples of the growing variety of TD research include the original time-domain differential equation (TDDE) approach by Yee [31], which is the basis of the widely used finite difference time domain (FDTD) model [32]. An alternative implementation of TDDE models was shortly thereafter developed as the transmission line method (TLM) by John and Beurle [33]. Some of the frequency domain methods were also studied and transformed to their time domain counterpart, such as TDFEM [34] and TDMoL [35]. In the following section, several popularly used time domain methods are reviewed and discussed.

#### A. Finite-Difference Time Domain Method (FDTD)

Finite-difference time-domain is one of the most popular numerical methods that is widely used and of important research interest at present due to its simplicity for numerical implementation and relatively less requirements of computation resources [36]. By directly differencing Maxwell's time-dependent curl equations or their equivalent integral equations, FDTD can predict the field behaviors in a certain structure in time domain as well as in frequency domain by Fourier transforming time domain responses. Its simplicity and flexibility enable its applications to various types of electromagnetic problems, such as anisotropic and nonlinear problems. With the development of other related numerical techniques, such as Perfectly Matched Layers Absorbing Boundary Condition (PML-ABC) [37], and Efficient Techniques of Frequency Response Extraction [38] etc., FDTD has been extended to a variety of research areas, such as bio-electromagnetics [39].

Like other numerical techniques, FDTD method has its own disadvantages which are mainly originated from its two inherent modeling constraints [36] [40]. Theoretical studies show that FDTD is not computationally efficient when it is applied to electrically small and electrically large structures. The main reasons are due to the following limits:

1. In the spatial domain, the maximum spatial increment must be small enough in comparison with the wavelength (usually 8-10 steps per smallest wavelength) in order to obtain accurate field components values.
2. In the temporal domain, the time marching step must be small enough to meet the Courant-Friedrich-Levy (CFL) stability condition.

The above two limits makes FDTD too difficult to be applied to the problems where fine grid mesh or long simulation time is inevitable. Since this thesis work is based on the FDTD, more detailed discussions of FDTD will be given in Chapter 2.

#### B. Transmission Line Method (TLM)

TLM is another popular time domain method developed by Johns and Beurle [41] in 1971. It is a conceptually different approach from that of the straightforward differencing method of the Maxwell equations [42] [43] [44]. It employs the analogy between voltage and current propagation on a transmission line network and plane wave propagation in space. Consequently, field space is discretized into 2D or 3D grid of transmission lines interconnected at nodes. By analyzing the incident voltage wave and reflected voltage wave propagating along the transmission lines in the structure, the field behavior in the structure can be obtained.

In the generic form of the three dimensional TLM method, the space is discretized into a three dimensional lattice with a period of  $\Delta l$ . Six field components are represented by a hybrid TLM cell as shown in Figure 3. Boundaries corresponding to the electric wall and the magnetic wall are represented by short-circuiting shunt nodes and open-circuiting shunt nodes on the boundary. Magnetic and dielectric materials can be introduced by adding short-circuited series stubs of length  $\Delta l / 2$  at the series nodes (magnetic field components) and open-circuited  $\Delta l$  stubs at the shunt nodes (electric field components).

The losses can be represented by resistively loading the shunt nodes. The three dimensional nodes in TLM lattice are currently expressed with three dimensional condensed nodes.

In general TLM can be viewed as a transmission-line discrete-model of Maxwell's equations. The method can also be interpreted as an implementation of Huygen's principle, in which fields spreading in space can develop and form as a series of secondary sources. Since both TLM and FDTD methods are modeling of the Maxwell's equations in a march-on-time fashion, they can be made equivalent. The equivalence of the TLM and a modified FDTD method was shown by Chen et al. [45].

Similar to FDTD, TLM models involve space and time discretization. Therefore they are also subject to problems of mesh dispersion and anisotropy [46] [47] [48]. In addition, due to the introduction of periodic lattice structure, a typical passband-stopband phenomenon appears in the frequency data. Thus the frequency range must be lower than the upper bound of the lowest passband and is determined by the mesh size. An extensively study on TLM can be found in [49].

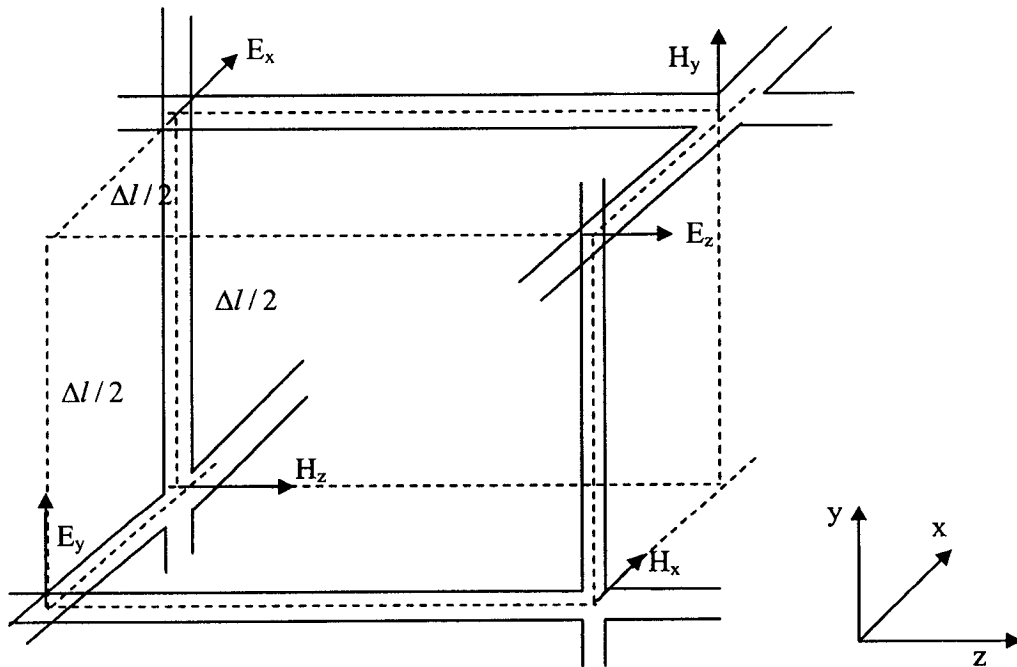


Figure 1.3 A hybrid TLM cell

### C. Time Domain Finite Element Method (TDFEM)

Due to the advantage of unstructured grid that is generally used in FEM, FEM is capable of modeling the structures with arbitrary geometries. The FEM introduced before was originally applied for solving boundary value problems. It was a natural step to develop the method for solving initial value time domain problems, which resulted in the TDFEM that were presented in [34] [50-52]. TDFEM is based on solving the wave equations for electric or magnetic field. For example, the wave equation can be expressed as:

$$\nabla^2 u - \varepsilon\mu \frac{\partial^2 u}{\partial t^2} = 0 \quad (1.17)$$

The corresponding functional equation is:

$$F(u) = \int_v \left( 0.5 |\nabla u|^2 + u \varepsilon \mu \frac{\partial u}{\partial t} \right) dv \quad (1.18)$$

where  $u$  is electric or magnetic field,  $\varepsilon$  is the medium permittivity and  $\mu$  is the medium permeability.

By following the general FEM procedure for space discretization and field expansion, and minimizing the functional, a system of ordinary differential equations can be obtained:

$$\varepsilon\mu A \frac{\partial^2 u}{\partial t^2} + Bu = C \quad (1.19)$$

where  $A$  and  $B$  are known matrices related to discretization steps and geometry,  $C$  consists of known elements related to excitation functions and boundary conditions. By discretizing the partial differential in time domain, the above equation can be solved by updating the electromagnetic field distribution in a leapfrog fashion.

Unlike the FDTD method, TDFEM techniques have the remarkable stability and the flexibility of modeling complex structures with curved and irregular boundaries. A lot of

research [53-56] has been conducted on the improvement of TDFEM. Nevertheless TDFEM techniques have not been widely used in solving EM problems. The reasons are:

1. The unstructured 3-D mesh generation takes a significant effort to develop, especially when the structure necessitate considerable mesh cells to simulate the field behavior.
2. It needs large pre and post-data processing, which adds more computation loads.
3. It is more time consuming than FDTD method on every time step marching.

Due to the above disadvantages, some research [57-61] has been focused on hybrid methods that take advantage of both finite-difference and finite element time domain techniques.

#### D. Time Domain Method of Lines (TDMoL)

With the fast development of planar microwave circuit, accurate full wave analysis of planar transmission line and its discontinuities became one of the important research topics in 1980s. By analyzing modal field distributions and input pulse behavior for a shielded microstrip line, Itoh *et al.* first formulated the time domain solution to MoL [62] [63]. The general procedure of TDMoL can be described as:

1. Discretize the computation area with field lines, which properly satisfy the boundary conditions
2. Express the field distribution as an expanded modal field distribution.
3. Find the coefficients of the expansion.

After the above operations, the field values at each grid point at any time step can be obtained so that the full wave analysis can be conducted for a certain structure. However, TDMoL techniques have not been widely used for analyzing planar type structures. The reasons are that:

- a. Modal field distributions are not always known, especially for complex structures;
- b. There is additional complexity when solving non time harmonic problems;
- c. It is not computationally easy to find the coefficient of the expansion;

- d. Large pre- and post-data processing.

#### E. Multi-resolution Time Domain Method (MRTD)

FDTD method requires large memory and CPU time consumption due to small spatial discretization and CFL constraint. To relax or even remove the above constraints, various time domain techniques have been developed [64-84] for improved computation efficiency. In 1996, a multi-resolution time-domain method [64] was proposed based on Battle-Lemarie wavelets, which shows an excellent capability to approximate the exact solution with negligible error at the Nyquist sampling rates in space. At the same time, Daubechies-wavelet-based technique [65], and a multigrid technique using Haar wavelets [66] [67] were reported. These MRTD have been employed to analyze cavity resonators [64] [66] [68], microstrip lines [69] [70], patch antennas [71], and nonlinear problems [72].

The general idea of MRTD method is to expand the field components with scaling functions. Basically, by applying method of moments to Maxwell's equations in its temporal form, the MRTD can be derived with the use of scaling and wavelet functions as a set of basis functions, such as:

$$E = \sum_{k,l,m,n=-\infty}^{+\infty} E_{l+\frac{1}{2},m,n}^{\phi} h(t) \phi_{l+\frac{1}{2}}(x) \phi_m(y) \phi_n(z) \quad (1.20)$$

where the indices  $k,l,m,n$  are the discrete time and space indices related to the time and space coordinates via  $t=k\Delta t$ ,  $x=l\Delta x$ ,  $y=m\Delta y$ ,  $z=n\Delta z$ . The  $\Delta t$ ,  $\Delta x$ ,  $\Delta y$ ,  $\Delta z$  represent the time and space discretization steps. The function  $h_m(x)$  is defined as:

$$h_m(x) = h\left(\frac{x}{\Delta x} - m\right) \quad (1.21)$$

with

$$h(x) = \begin{cases} 1 & \text{for } |x| < \frac{1}{2} \\ \frac{1}{2} & \text{for } |x| = \frac{1}{2} \\ 0 & \text{for } |x| > \frac{1}{2} \end{cases} \quad (1.22)$$

The function  $\phi_m(x)$  is defined as:

$$\phi_m(x) = \phi\left(\frac{x}{\Delta x} - m\right) \quad (1.23)$$

where  $\phi(x)$  is the scaling function. By inserting the above field expansions into Maxwell's equations and sampling the equations with pulse function as test functions in time and scaling functions as test functions in space, MRTD formulas can be obtained.

The MRTD algorithm is much more complicated than that of FDTD due to the field expansion. The field at one grid point is related to the field at its several neighboring points. With more smooth function such as cubic spline Battle-Lemarie scaling function, the number of the relevant points can be limited. [64].

Although MRTD can greatly reduce the dispersion of FDTD and therefore reduce the memory requirement for space gridding, the stability condition for MRTD still remains and actually becomes more stringent [73] [74]. The scheme itself has less physical meaning than FDTD by calculating the coefficients instead of real field values. In addition, it is essentially a high-order technique, which does not seem more advantageous over the high-order conventional FDTD [75].

#### F. Pseudo-Spectral Time-Domain (PSTD)

Pseudo-spectral Time-domain method was firstly introduced by Q. H. Liu [76] [77] in 1997. It used the Fast Fourier Transform (FFT) instead of finite difference to compute spatial derivatives in the spatial spectral domain. The main advantage of the method is its spatial grid upper bound can reach two grids per wavelength, which is the Nyquist



Sampling limit. Compared to at least 8~10 grids per wavelength needed by FDTD method, PSTD method has much less computation memory requirement.

To be more explicit, the following paragraphs explain the main difference between the PSTD and the FDTD in the representation of spatial derivatives. In the Yee's FDTD algorithm, central difference approximation for space derivatives is used:

$$\frac{\partial f(n\Delta x, m\Delta y, l\Delta z, k\Delta t)}{\partial x} = \frac{f(n\Delta x + \frac{\Delta x}{2}, m\Delta y, l\Delta z, k\Delta t) - f(n\Delta x - \frac{\Delta x}{2}, m\Delta y, l\Delta z, k\Delta t)}{\Delta x} \quad (1.24)$$

In the PSTD method, the space derivative is computed through the Fourier transform:

$$\frac{\partial f(n\Delta x, m\Delta y, l\Delta z, k\Delta t)}{\partial x} = -F^{-1}[ik_x F\{f(n\Delta x, m\Delta y, l\Delta z, k\Delta t)\}] \quad (1.25)$$

where  $F$  and  $F^{-1}$  denote the forward and inverse Fourier transform, and  $k_x$  is Fourier transform variable, or spatial frequency along the  $x$  direction.

Compared to FDTD, PSTD method use only  $(1/8)^D - (1/4)^D$  [77] ( $D$  is the dimensionality) memory that required by FDTD, and it is simple to implement because the nodes are condensed. In addition, the dispersion error of the PSTD method is smaller than that of FDTD method.

However, because spatial Fourier transform requires the fields to be continuous within the whole spatial domain, problems arise when the fields are discontinuous, for example, at the boundary of perfect conductor where the magnetic field components are not continuous [76]. In such a case, the PSTD method is not effective. Furthermore, PSTD is not suitable for highly inhomogeneous media. A hybrid method combining the FDTD and the PSTD method [78] was developed recently to retain the merits of each individual method.

It should be noted that as an explicit approach, the PSTD is still constrained by the CFL stability condition. Furthermore, the complex computations inherited from FFT doubles the computer memory requirement and results in less saving in computation time than expected. In addition, it is still a high-order technique, which has a dispersion property not much better than that of the high-order FDTD method.

#### *F Alternating-Direction Implicit FDTD (ADI-FDTD)*

ADI-FDTD method was first applied to Yee's grid by R. Holland in 1984 [79]. Instead of directly calculating field values, the finite-difference operator for 3-D solution to Maxwell's equations was factored into three operators. Each operator is performed in respect to the three coordinate directions. However, the scheme required three implicit sub-step computations for each FDTD recursive cycle and it was never found to be completely stable without adding significant dielectric loss.

In 1990, a specially designed two dimensional FDTD algorithm, which employed time step larger than that allowed by explicit FDTD method, was presented in [80]. Nevertheless, it was based on a new staggered grid different from Yee's and the grid points and field components were twice of the Yee's on a body surface. Consequently, the method consumes more computer memory and computation resources. Very recently, a new two dimensional FDTD algorithm free of the Courant stability conditions was proposed for a 2D-TE wave [81]. The resulting FDTD formulation was found to be unconditionally stable. Consequently, the second constraint of the FDTD modeling is completely removed. F. Zheng et al. successfully developed ADI-FDTD method for general three dimensional problems [82] [83]. The applications of ADI-FDTD method in solving EM problems have subsequently been reported, such as [84], especially for problems that the conventional FDTD method is incapable of solving due to CFL condition.

Since this thesis work is based on ADI-FDTD method, the detailed description to ADI-FDTD method will be introduced in Chapter 3.

In the above sections, several numerical methods for solving electromagnetic problems have been introduced and discussed. Each method has its own distinct advantages and

disadvantages in respect to different types of electromagnetic problems. For a specific problem, an appropriate method needs to be selected in order to effectively and efficiently obtain the desired computation results. Memory requirement, total computation time, modeling accuracy and data processing of pre- (post-) computation are the important factors to be under consideration.

### **1.3 Inducement of the Thesis**

F. Zheng, Z. Chen and J. Zhang have reported the unconditional stability of ADI-FDTD scheme in the three dimensional Cartesian coordinates system with emphasis on the theoretical validations, such as mathematical proof of unconditional stability and dispersion analysis. The attractive features of unconditional stability of ADI-FDTD and its relatively shorter simulation time have made it a promising numerical method.

However, all of the previous work so far has been confined to the Cartesian coordinates system with very limited applications. If the ADI-FDTD method is applied to curvilinear boundaries and other extended applications, studies must be required with the changed environmental settings. Therefore it is desired to:

1. extend ADI-FDTD algorithm to other coordinate system, such as cylindrical coordinate system, to broaden the applications of ADI-FDTD method.
2. enhance the scheme's capability by implementing certain absorbing boundary conditions (ABC), such as PML boundary conditions, for solving open boundary structures and scattering EM problems.
3. study the effectiveness and efficiency of ADI-FDTD method when it is applied to the structures with arbitrary media parameters, including highly conductive media that is insolvable with the conventional FDTD method, and
4. draw up criteria on what problems can be more effectively and efficiently solved with ADI-FDTD method than with other numerical methods

This thesis work is undertaken along these lines to give a more detailed insight in the ADI-FDTD method that is particularly associated with solving practical EM problems,

and in commonly used RF and microwave devices, such as resonators, waveguides, microstrip lines etc.

## **1.4 Purviews and Organization of the Thesis**

The thesis includes three primary parts:

1. Theoretical development of the cylindrical ADI-FDTD method, including formulation of the cylindrical ADI-FDTD method, mathematical proof of the unconditional stability of the algorithm and numerical validation of the algorithm
2. The applications of the method to close structures, including experiments on various resonator type structures with general media parameters
3. The applications of the method to open structures, including incorporation of the absorbing boundary media into the ADI-FDTD method and numerical analysis of circular waveguide structures and cylindrical microstrip lines.

The thesis is organized in the following manner:

Chapter 2 introduces the Yee's grid and conventional FDTD method, which are the basis of the ADI-FDTD method. As an indispensable part for solving open structures and scattering problems, several popularly used absorbing boundary schemes are also discussed.

Chapter 3 is the primary theoretical part of the thesis, in which the formulation of the cylindrical ADI-FDTD method is presented for the first time. The numerical validation of the algorithm is then given in comparison with conventional FDTD method.

Chapter 4 introduces a novel theoretical approach for determining the numerical stability. Extensive numerical experiments are conducted to verify the theoretical results.

Chapter 5 focuses on solving close structures, such as circular resonators, circular resonators with rods, circular disk resonator. The nonuniform gridding method is

developed for efficient computation. The influence of the nonuniform mesh on numerical results is also presented.

Chapter 6 gives applications to open structures. In it, the Uniaxial Perfectly Matched Layers (UPML) is incorporated with the cylindrical ADI-FDTD that allows modeling of open conducting structures. Numerical validations were performed with waveguide structures. Walls of arbitrary conductivities are computed for the first time. The results are compared to those with the Surface Impedance Boundary Conditions (SIBC) method.

Chapter 7 concludes the thesis by reviewing the theoretical and experimental results of cylindrical ADI-FDTD method, and indicating the possible directions of the future research work in this field.

## **Chapter 2    The Finite-Difference Time-Domain (FDTD) Method**

### **2.1        Introduction**

In this chapter, the FDTD method is introduced and described. It provides the basis for the ADI-FDTD method to be developed in the later chapters.

The FDTD method has become one of the most popular numerical methods in computational electromagnetics for many years. Theoretically it is capable of predicting the field behavior regardless shape and material parameters of a subject under study. It can incorporate materials of any conductivity of a real metal or of zero conductivity dielectric. It can model various types of materials such as magnetic materials, anisotropic plasma and magnetic ferrites. As a result, FDTD is suitable for a wide range of applications, including microwave circuit analysis [85-92], photonic device analysis [93-95], packaging and interconnection modeling [96-99], antenna design and analysis [100-102], and bioelectromagnetic applications [103-105].

However, it suffers from great difficulty when simulating electrically small and electrically large objects. Such difficulty is mainly derived from its two inherent constraints:

1. relatively fine mesh, compared to either smallest wavelength or minimum structure dimension, must be taken to make the numerical errors negligible.
2. simulation time step must be smaller than or equal to Courant-Friedrich-Levy stability condition.

In the following sections, the fundamental knowledge and the primary points of FDTD method will be discussed.

This chapter is organized in the following manner: Firstly the fundamentals of FDTD technique are reviewed; secondly the FDTD algorithms in cylindrical and spherical coordinates system are discussed; then the two restrictions as well as the resultant numerical stability conditions of FDTD method are presented; finally the commonly used absorbing boundary conditions are described. Other relevant knowledge, such as nonuniform gridding method as well as numerical dispersion will also be given.

## 2.2 Yee's Grid and FDTD Algorithm in the Rectangular Coordinates

As having been discussed in Chapter 1, many numerical methods for solving Maxwell's equations have been developed in order to predict the field behavior in both time and frequency domains. In 1966, K. Yee originated the FDTD scheme which solves the time dependent Maxwell's curl equation for the lossless materials in a straightforward manner [31]. In this numerical scheme, the continuous electromagnetic fields in a finite volume of space are sampled at certain points discretely in space and time. The electromagnetic wave propagation is modeled by finite-differencing of Maxwell's equation at each spatial lattice point at corresponding time step and advancing in time step. The field solution at the current time step is deduced from the field values at the previous time steps, which leads to a recursive leap-frog algorithm. This approach basically results in a simulation of actual coupled full wave solutions by the numerically sampled data that propagates in a data space (the simulation region) stored in a computer. Space and time sampling increments are selected to avoid aliasing of the continuous field distribution and to guarantee stability of the time marching algorithm. Time marching is completed when the desired late time or steady-state field behavior is observed.

The time dependent Maxwell's curl equations in a linear, lossless and isotropic medium may be written as:

$$\frac{\partial \mathbf{H}}{\partial t} = -\frac{1}{\mu} \nabla \times \mathbf{E}, \quad (2.1a)$$

$$\frac{\partial \mathbf{E}}{\partial t} = \frac{1}{\varepsilon} \nabla \times \mathbf{H}. \quad (2.1b)$$

where  $\varepsilon$  and  $\mu$  are electrical permittivity and magnetic permeability respectively.

The vector curl equations (2.1) can be rewritten as scalar equations in a certain coordinate system. In cartesian coordinates, for example, the six scalar equations are:

$$\frac{\partial H_x}{\partial t} = \frac{1}{\mu} \left( \frac{\partial E_y}{\partial z} - \frac{\partial E_z}{\partial y} \right), \quad (2.2a)$$

$$\frac{\partial H_y}{\partial t} = \frac{1}{\mu} \left( \frac{\partial E_z}{\partial x} - \frac{\partial E_x}{\partial z} \right), \quad (2.2b)$$

$$\frac{\partial H_z}{\partial t} = \frac{1}{\mu} \left( \frac{\partial E_x}{\partial y} - \frac{\partial E_y}{\partial x} \right), \quad (2.2c)$$

$$\frac{\partial E_x}{\partial t} = \frac{1}{\varepsilon} \left( \frac{\partial H_z}{\partial y} - \frac{\partial H_y}{\partial z} \right), \quad (2.2d)$$

$$\frac{\partial E_y}{\partial t} = \frac{1}{\varepsilon} \left( \frac{\partial H_x}{\partial z} - \frac{\partial H_z}{\partial x} \right), \quad (2.2e)$$

$$\frac{\partial E_z}{\partial t} = \frac{1}{\varepsilon} \left( \frac{\partial H_y}{\partial x} - \frac{\partial H_x}{\partial y} \right). \quad (2.2f)$$

A continuous solution domain is then discretized based on the proposal by Yee as illustrated in Fig. 2.1. For convenience, a space point can be denoted as:

$$(i, j, k) = (x = i\Delta x, y = j\Delta y, z = k\Delta z) \quad (2.3)$$

and any function of time and space as:

$$u^n(i, j, k) = u(x = i\Delta x, y = j\Delta y, z = k\Delta z, t = n\Delta t) \quad (2.4)$$

in which  $\Delta x$ ,  $\Delta y$ ,  $\Delta z$  and  $\Delta t$  are the spatial and temporal increment steps respectively. By using the second order central difference approximation as indicated in (2.5) for space and time derivatives,



$$\frac{\partial(u^n(i, j, k))}{\partial x} = \frac{u^n(i + \frac{1}{2}, j, k) - u^n(i - \frac{1}{2}, j, k)}{\Delta x} + O(\Delta x^2), \quad (2.5a)$$

$$\frac{\partial(u^n(i, j, k))}{\partial t} = \frac{u^{n+\frac{1}{2}}(i, j, k) - u^{n-\frac{1}{2}}(i, j, k)}{\Delta t} + O(\Delta t^2) \quad (2.5b)$$

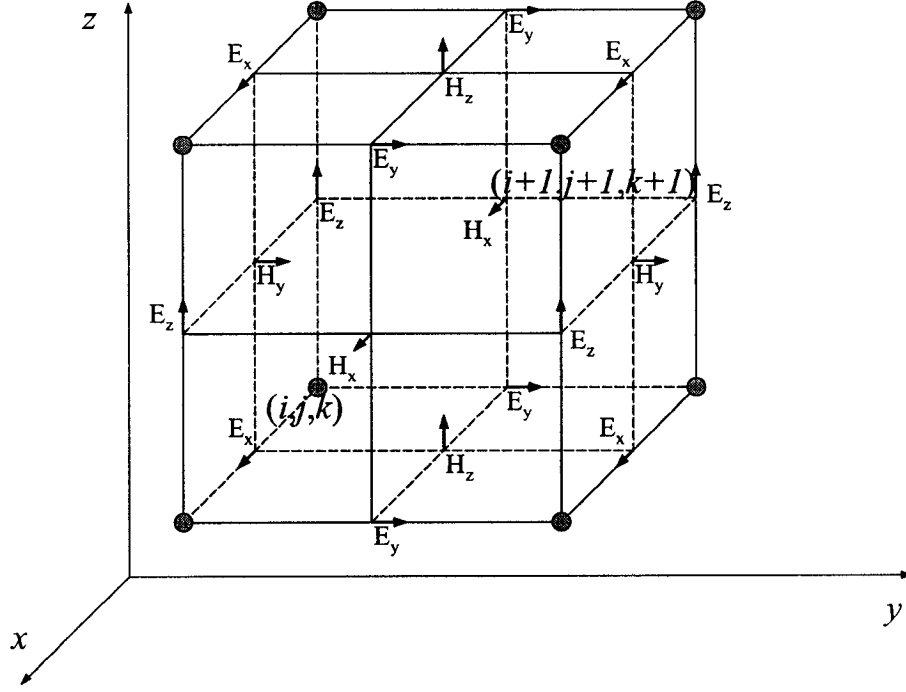


Figure 2.1 Position of electric and magnetic field components in Yee's grid

the explicit finite difference approximation of six Maxwell's scalar equations in (2.2) can be obtained as:

$$H_x^{n+\frac{1}{2}}(i, j + \frac{1}{2}, k + \frac{1}{2}) = H_x^{n-\frac{1}{2}}(i, j + \frac{1}{2}, k + \frac{1}{2}) + \frac{\Delta t}{\mu} \left[ \frac{E_y^n(i, j + \frac{1}{2}, k + 1) - E_y^n(i, j + \frac{1}{2}, k)}{\Delta z} \right] - \frac{\Delta t}{\mu} \left[ \frac{E_z^n(i + \frac{1}{2}, j + \frac{1}{2}, k) - E_z^n(i + \frac{1}{2}, j - \frac{1}{2}, k)}{\Delta y} \right] \quad (2.6a)$$

$$H_y^{n+\frac{1}{2}}(i+\frac{1}{2}, j, k+\frac{1}{2}) = H_y^{n-\frac{1}{2}}(i+\frac{1}{2}, j, k+\frac{1}{2}) + \frac{\Delta t}{\mu} \left[ \frac{E_z^n(i+1, j, k+\frac{1}{2}) - E_z^n(i, j, k+\frac{1}{2})}{\Delta x} \right] - \frac{\Delta t}{\mu} \left[ \frac{E_x^n(i+\frac{1}{2}, j, k+1) - E_x^n(i+\frac{1}{2}, j, k)}{\Delta z} \right] \quad (2.6b)$$

$$H_z^{n+\frac{1}{2}}(i+\frac{1}{2}, j+\frac{1}{2}, k) = H_z^{n-\frac{1}{2}}(i+\frac{1}{2}, j+\frac{1}{2}, k) + \frac{\Delta t}{\mu} \left[ \frac{E_x^n(i+\frac{1}{2}, j+1, k) - E_x^n(i+\frac{1}{2}, j, k)}{\Delta y} \right] - \frac{\Delta t}{\mu} \left[ \frac{E_y^n(i+1, j+\frac{1}{2}, k) - E_y^n(i, j+\frac{1}{2}, k)}{\Delta x} \right] \quad (2.6c)$$

$$E_x^{n+1}(i+\frac{1}{2}, j, k) = E_x^n(i+\frac{1}{2}, j, k) + \frac{\Delta t}{\varepsilon} \left[ \frac{H_z^{n+\frac{1}{2}}(i+\frac{1}{2}, j+\frac{1}{2}, k) - H_z^{n+\frac{1}{2}}(i+\frac{1}{2}, j-\frac{1}{2}, k)}{\Delta y} \right] - \frac{\Delta t}{\varepsilon} \left[ \frac{H_y^{n+\frac{1}{2}}(i+\frac{1}{2}, j, k+\frac{1}{2}) - H_y^{n+\frac{1}{2}}(i+\frac{1}{2}, j, k-\frac{1}{2})}{\Delta z} \right] \quad (2.6d)$$

$$E_y^{n+1}(i, j+\frac{1}{2}, k) = E_y^n(i, j+\frac{1}{2}, k) + \frac{\Delta t}{\varepsilon} \left[ \frac{H_x^{n+\frac{1}{2}}(i, j+\frac{1}{2}, k+\frac{1}{2}) - H_x^{n+\frac{1}{2}}(i, j+\frac{1}{2}, k-\frac{1}{2})}{\Delta z} \right] - \frac{\Delta t}{\varepsilon} \left[ \frac{H_z^{n+\frac{1}{2}}(i+\frac{1}{2}, j+\frac{1}{2}, k) - H_z^{n+\frac{1}{2}}(i-\frac{1}{2}, j+\frac{1}{2}, k)}{\Delta x} \right] \quad (2.6e)$$

$$E_z^{n+1}(i, j, k+\frac{1}{2}) = E_z^n(i, j, k+\frac{1}{2}) + \frac{\Delta t}{\varepsilon} \left[ \frac{H_y^{n+\frac{1}{2}}(i+\frac{1}{2}, j, k+\frac{1}{2}) - H_y^{n+\frac{1}{2}}(i-\frac{1}{2}, j, k+\frac{1}{2})}{\Delta x} \right] - \frac{\Delta t}{\varepsilon} \left[ \frac{H_x^{n+\frac{1}{2}}(i, j+\frac{1}{2}, k+\frac{1}{2}) - H_x^{n+\frac{1}{2}}(i, j-\frac{1}{2}, k+\frac{1}{2})}{\Delta y} \right] \quad (2.6f)$$

As can be seen from (2.6) each field component at a certain time step is evaluated with the field components at the previous time step, which leads to a leapfrog time recursive scheme. In space, each field component at a certain grid point is described by the four surrounding counterpart field points, which forms an interlaced E-H pattern in spatial domain. Once a certain grid point is illuminated by a wave source, such as the simple

point source, the accordingly generated waves will be propagating in the Yee's grid at a certain wave speed. As a result, the field behavior at a certain point as well as in the whole structure can be obtained by observing the time domain signature of a certain grid point and the field distribution within the structure. By applying Fourier transform, the wave properties in frequency domain can also be obtained for further investigation of the field solutions.

It should be pointed out that the equations in (2.6) are only the basic representation of FDTD algorithm without considering medium anisotropy, nonuniform cell sizes, nonuniform medium distribution, and boundary problems. They can be modified and extended to different EM problems by either changing some terms in the basic equations or introducing other auxiliary field components. In essence, Yee's FDTD scheme provides a simple structure of three-dimensional space being filled by an interlinked array of Faraday's Law and Ampere's Law contours [36]. It is very simple in concept and implementation by directly representing Maxwell's equations in a discrete form.

In the actual circuit design and EM problem analysis, there exist a variety of structures and devices with curvilinear contour or other nonrectangular boundaries, such as Body of Rotation (BOR) structures, Spherical Structures etc. For these kinds of structures, it is often awkward using cartesian coordinate system to discretize the computation domain due to the irregularities involved. For example, for a ceramic resonator filter of cylindrical shape, if the rectangular coordinate system is used, staircase boundaries may result, which may then compromise the modeling accuracy. It may lead to a long computation time and huge memory consumption.

To circumvent the difficulty, much research work has been done in recent years on non-rectangular coordinates, nonuniform orthogonal grids [106], locally conformal grids and globally orthogonal [107], global curvilinear coordinates [108], irregular nonorthogonal structured grids [109], and irregular nonorthogonal structured grids [110]. Among those, gridding the structures in other orthogonal coordinate systems is a simple but effective way to obtain satisfactory numerical results with minor change to the Cartesian FDTD algorithm. In the following subsections, FDTD algorithms in the cylindrical and spherical coordinate systems are presented and discussed.

## 2.3 FDTD Algorithm in the Cylindrical Coordinates

The basic theory of FDTD algorithm in cylindrical coordinate system is the same as that in Cartesian coordinate system. In an isotropic lossless region with permittivity  $\epsilon$  and permeability  $\mu$ , the six scalar equations that relate the components of electric field  $E$  and magnetic field  $H$  in the cylindrical coordinate can be expressed as:

$$\epsilon \frac{\partial E_r}{\partial t} = \frac{\partial H_z}{r \partial \phi} - \frac{\partial H_\phi}{\partial z} \quad (2.7a)$$

$$\epsilon \frac{\partial E_\phi}{\partial t} = \frac{\partial H_r}{\partial z} - \frac{\partial H_z}{\partial r} \quad (2.7b)$$

$$\epsilon \frac{\partial E_z}{\partial t} = \frac{\partial(rH_\phi)}{r \partial r} - \frac{\partial H_r}{r \partial \phi} \quad (2.7c)$$

$$-\mu \frac{\partial H_r}{\partial t} = \frac{\partial E_z}{r \partial \phi} - \frac{\partial E_\phi}{\partial z} \quad (2.7d)$$

$$-\mu \frac{\partial H_\phi}{\partial t} = \frac{\partial E_r}{\partial z} - \frac{\partial E_z}{\partial r} \quad (2.7e)$$

$$-\mu \frac{\partial H_z}{\partial t} = \frac{\partial(rE_\phi)}{r \partial r} - \frac{\partial E_r}{r \partial \phi} \quad (2.7f)$$

As can be seen, the electric field is decomposed into three orthogonal field components, which are  $E_r$ ,  $E_\phi$  and  $E_z$  respectively; similarly the magnetic field is decomposed into  $H_r$ ,  $H_\phi$  and  $H_z$  respectively.

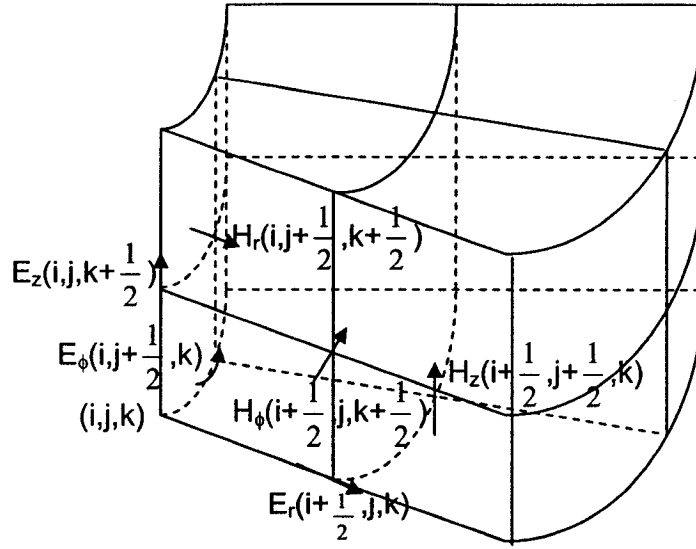


Figure 2.2 Field Placement in cylindrical Yee's grid

The space is then discretized with a cell shown in Figure 2.2. Denote  $(i, j, k) = (r = i\Delta r, \phi = j\Delta\phi, z = k\Delta z)$  as well as a function  $u|_{i,j,k}^n = u(r = i\Delta r, \phi = j\Delta\phi, z = k\Delta z, t = n\Delta t)$  like in (2.5), the finite-differenced form of (2.2) can be obtained as:

$$\frac{H_r^{n+\frac{1}{2}}(i, j + \frac{1}{2}, k + \frac{1}{2}) - H_r^{n-\frac{1}{2}}(i, j + \frac{1}{2}, k + \frac{1}{2})}{\Delta t} = \frac{1}{\mu} \left[ \frac{E_\phi^n(i, j + \frac{1}{2}, k + 1) - E_\phi^n(i, j + \frac{1}{2}, k)}{\Delta z} - \frac{E_z^n(i, j + 1, k + \frac{1}{2}) - E_z^n(i, j, k + \frac{1}{2})}{\Delta\phi \cdot i \cdot \Delta r} \right] \quad (2.8a)$$

$$\frac{H_\phi^{n+\frac{1}{2}}(i + \frac{1}{2}, j, k + \frac{1}{2}) - H_\phi^{n-\frac{1}{2}}(i + \frac{1}{2}, j, k + \frac{1}{2})}{\Delta t} = \frac{1}{\mu} \left[ \frac{E_z^n(i + 1, j, k + \frac{1}{2}) - E_z^n(i, j, k + \frac{1}{2})}{\Delta r} - \frac{E_r^n(i + \frac{1}{2}, j, k + 1) - E_r^n(i + \frac{1}{2}, j, k)}{\Delta z} \right] \quad (2.8b)$$

$$\frac{H_z^{n+1}(i+\frac{1}{2}, j+\frac{1}{2}, k) - H_z^n(i+\frac{1}{2}, j+\frac{1}{2}, k)}{\Delta t} = \frac{1}{\mu \cdot (i+\frac{1}{2}) \cdot \Delta r} \left[ \frac{E_r^n(i+\frac{1}{2}, j+1, k) - E_r^n(i+\frac{1}{2}, j, k)}{\Delta \phi} - \frac{(i+1) \cdot \Delta r \cdot E_\phi^n(i+1, j+\frac{1}{2}, k) - i \cdot \Delta r \cdot E_\phi^n(i, j+\frac{1}{2}, k)}{\Delta r} \right] \quad (2.8c)$$

$$\frac{E_r^{n+1}(i+\frac{1}{2}, j, k) - E_r^n(i+\frac{1}{2}, j, k)}{\Delta t} = \frac{1}{\varepsilon} \left[ \frac{H_z^{n+1}(i+\frac{1}{2}, j+\frac{1}{2}, k) - H_z^{n+1}(i+\frac{1}{2}, j-\frac{1}{2}, k)}{\Delta \phi \cdot (i+\frac{1}{2}) \cdot \Delta r} - \frac{H_\phi^{n+1}(i+\frac{1}{2}, j, k+\frac{1}{2}) - H_\phi^{n+1}(i+\frac{1}{2}, j, k-\frac{1}{2})}{\Delta z} \right] \quad (2.8d)$$

$$\frac{E_\phi^{n+1}(i, j+\frac{1}{2}, k) - E_\phi^n(i, j+\frac{1}{2}, k)}{\Delta t} = \frac{1}{\varepsilon} \left[ \frac{H_r^{n+1}(i, j+\frac{1}{2}, k+\frac{1}{2}) - H_r^{n+1}(i, j+\frac{1}{2}, k-\frac{1}{2})}{\Delta z} - \frac{H_z^{n+1}(i+\frac{1}{2}, j+\frac{1}{2}, k) - H_z^{n+1}(i-\frac{1}{2}, j+\frac{1}{2}, k)}{\Delta r} \right] \quad (2.8e)$$

$$\frac{E_z^{n+1}(i, j, k+\frac{1}{2}) - E_z^n(i, j, k+\frac{1}{2})}{\Delta t} = \frac{1}{\varepsilon \cdot i \cdot \Delta r} \left[ \frac{(i+\frac{1}{2}) \cdot \Delta r \cdot H_\phi^{n+1}(i+\frac{1}{2}, j, k+\frac{1}{2}) - (i-\frac{1}{2}) \cdot \Delta r \cdot H_\phi^{n+1}(i-\frac{1}{2}, j, k+\frac{1}{2})}{\Delta r} - \frac{H_r^{n+1}(i, j+\frac{1}{2}, k+\frac{1}{2}) - H_r^{n+1}(i, j-\frac{1}{2}, k+\frac{1}{2})}{\Delta \phi} \right] \quad (2.8f)$$

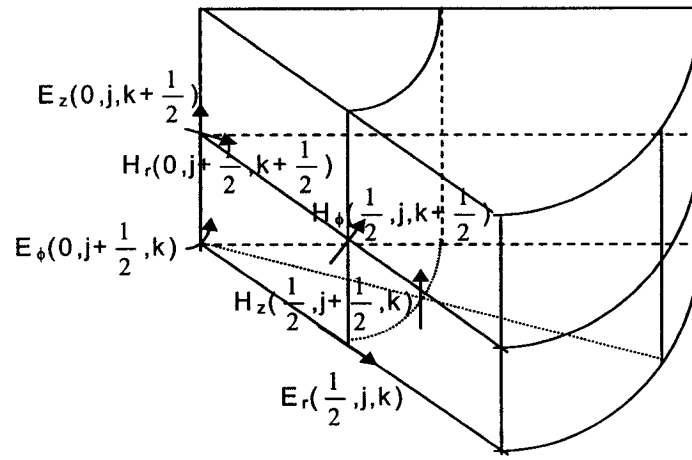
Note in the above equation, there is a singularity at  $r=0$  as  $i=0$ . The reason is that in the original discretized Maxwell's equation (2.8),  $1/r$  term exists which leads to infinity at  $r=0$ . Therefore a special treatment is required at the axial points to remove such a singularity. Figure 2.3(a) shows a grid cell at  $r=0$ .

As can be seen from Figure 2.3(a), there are totally three field components that are defined at the axis  $r=0$  (or simply the  $z$ -axis),  $E_z$ ,  $E_\phi$  and  $H_r$ . Because of the symmetry,  $E_\phi=0$  and  $H_r=0$ . As a result, only  $E_z$  at  $r=0$  is left to be computed specially.

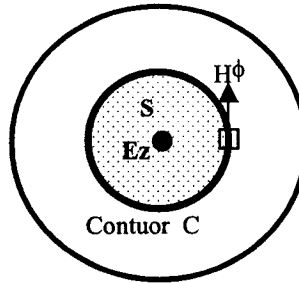
To compute or update  $E_z$ , the following integral form of Maxwell's equation in the time domain is used and applied:

$$\oint_C \vec{H} \cdot d\vec{l} = \varepsilon \cdot \int_S \frac{\partial \vec{E}}{\partial t} \cdot d\vec{s} \quad (2.9)$$

where  $C$  is a closed contour surrounding the  $z$ -axis, and  $S$  is the surface bounded by the contour  $C$ .



(a)



(b)

Figure 2.3 (a) A portion of the lattice at  $r=0$  (b) the integral path to obtain  $E_z$  at  $r=0$

By using the closed circular path of radius  $\Delta r/2$  around the  $z$ -axis as shown in Figure 2.3(b), the following finite-difference equation for  $E_z$  at  $r=0$  can be obtained:

$$E_z^{n+1}(0, j, k) = E_z^n(0, j, k) + \frac{4\Delta t}{\epsilon \cdot \Delta r} H_\phi^{n+\frac{1}{2}}(0, j, k) \quad (2.10)$$

The above equation is explicit for computing  $E_z$  at  $r=0$  with the use of the central finite difference.

In [36], a 2.5-dimension method is proposed for computing the field component on the axis which eliminates azimuthal ( $\phi$ ) dependence of the field by expanding it as a Fourier series. The algorithm is able to compute all the Fourier modes providing it converges for each mode. This method is essentially applicable only for BOR structures since the assumption of the Fourier expansion is not valid when the field distribution in azimuthal direction can not be expanded in sinusoidal forms. However, (2.8) and (2.10) are general formulations without assumptions and will be employed in this thesis.

## 2.4 FDTD Algorithm in Spherical Coordinates

In the spherical coordinate system, the electric field and the magnetic field are decomposed in three orthogonal directions, which are  $R$ ,  $\theta$  and  $\phi$  respectively. The Maxwell's equations can thus be expressed as:

$$\epsilon \frac{\partial E_R}{\partial t} = \frac{\partial(\sin \theta H_\phi)}{R \sin \theta \partial \theta} - \frac{\partial H_\theta}{\partial \phi} \quad (2.11a)$$

$$\epsilon \frac{\partial E_\theta}{\partial t} = -\frac{\partial H_R}{R \sin \theta \partial \phi} - \frac{\partial(R H_\phi)}{R \partial R} \quad (2.11b)$$

$$\epsilon \frac{\partial E_\phi}{\partial t} = \frac{\partial(R H_\theta)}{R \partial R} - \frac{\partial H_R}{R \partial \theta} \quad (2.11c)$$

$$-\mu \frac{\partial H_R}{\partial t} = \frac{\partial(\sin \theta E_\phi)}{R \sin \theta \partial \theta} - \frac{\partial E_\theta}{R \sin \theta \partial \phi} \quad (2.11d)$$

$$-\mu \frac{\partial H_\theta}{\partial t} = \frac{\partial E_R}{R \sin \theta \partial \phi} - \frac{\partial(R E_\phi)}{R \partial R} \quad (2.11e)$$

$$-\mu \frac{\partial H_\phi}{\partial t} = \frac{\partial(R E_\theta)}{R \partial r} - \frac{\partial E_R}{R \partial \theta} \quad (2.11f)$$



Similar with the process described before for the Cartesian and cylindrical coordinates, the discretized form of (2.11) can be similarly obtained by direct finite-differencing method, which is:

$$\frac{H_R^{n+\frac{1}{2}}(i, j + \frac{1}{2}, k + \frac{1}{2}) - H_R^{n-\frac{1}{2}}(i, j + \frac{1}{2}, k + \frac{1}{2})}{\Delta t} = \frac{1}{\mu \cdot i \cdot \Delta R \cdot \sin\left[\left(j + \frac{1}{2}\right)\Delta\theta\right]} \left[ \frac{E_\theta^n(i, j + \frac{1}{2}, k + 1) - E_\theta^n(i, j + \frac{1}{2}, k)}{\Delta\phi} - \frac{\sin[(j+1)\Delta\theta]E_\phi^n(i, j + 1, k + \frac{1}{2}) - \sin[j\Delta\theta]E_\phi^n(i, j, k + \frac{1}{2})}{\Delta\theta} \right] \quad (2.12a)$$

$$\frac{H_\theta^{n+\frac{1}{2}}(i + \frac{1}{2}, j, k + \frac{1}{2}) - H_\theta^{n-\frac{1}{2}}(i + \frac{1}{2}, j, k + \frac{1}{2})}{\Delta t} = \frac{1}{\mu} \left[ \frac{(i+1)\Delta R \cdot E_\phi^n(i+1, j, k + \frac{1}{2}) - i\Delta R \cdot E_\phi^n(i, j, k + \frac{1}{2})}{(i + \frac{1}{2}) \cdot \Delta R^2} - \frac{E_R^n(i + \frac{1}{2}, j, k + 1) - E_R^n(i + \frac{1}{2}, j, k)}{(i + \frac{1}{2})\Delta R \cdot \sin(j \cdot \Delta\theta)\Delta\phi} \right] \quad (2.12b)$$

$$\frac{H_\phi^{n+\frac{1}{2}}(i + \frac{1}{2}, j + \frac{1}{2}, k) - H_\phi^{n-\frac{1}{2}}(i + \frac{1}{2}, j + \frac{1}{2}, k)}{\Delta t} = \frac{1}{\mu} \left[ \frac{E_R^n(i + \frac{1}{2}, j + 1, k) - E_R^n(i + \frac{1}{2}, j, k)}{(i + \frac{1}{2})\Delta R \cdot \Delta\theta} - \frac{(i+1)\Delta R \cdot E_\theta^n(i+1, j + \frac{1}{2}, k) - i\Delta R \cdot E_\theta^n(i, j + \frac{1}{2}, k)}{(i + \frac{1}{2})\Delta R^2} \right] \quad (2.12c)$$

$$\begin{aligned}
& \frac{E_R^{n+1}(i+\frac{1}{2}, j, k) - E_R^n(i+\frac{1}{2}, j, k)}{\Delta t} = \\
& \frac{1}{\varepsilon} \left[ \frac{\sin\left[\left(j+\frac{1}{2}\right)\Delta\theta\right] H_\phi^{n+\frac{1}{2}}(i+\frac{1}{2}, j+\frac{1}{2}, k) - \sin\left[\left(j-\frac{1}{2}\right)\Delta\theta\right] H_\phi^{n+\frac{1}{2}}(i+\frac{1}{2}, j-\frac{1}{2}, k)}{\Delta\theta \cdot \sin(j\Delta\theta) \cdot (i+\frac{1}{2}) \cdot \Delta R} \right. \\
& \left. \frac{H_\theta^{n+\frac{1}{2}}(i+\frac{1}{2}, j, k+\frac{1}{2}) - H_\theta^{n+\frac{1}{2}}(i+\frac{1}{2}, j, k-\frac{1}{2})}{\sin(j\Delta\theta) \cdot (i+\frac{1}{2}) \cdot \Delta R \cdot \Delta\phi} \right] \quad (2.12d)
\end{aligned}$$

$$\begin{aligned}
& \frac{E_\theta^{n+1}(i, j+\frac{1}{2}, k) - E_\theta^n(i, j+\frac{1}{2}, k)}{\Delta t} = \\
& \frac{1}{\varepsilon} \left[ \frac{H_R^{n+\frac{1}{2}}(i, j+\frac{1}{2}, k+\frac{1}{2}) - H_R^{n+\frac{1}{2}}(i, j+\frac{1}{2}, k-\frac{1}{2})}{i\Delta R \cdot \sin\left[\left(j+\frac{1}{2}\right)\Delta\theta\right] \Delta\phi} - \right. \\
& \left. \frac{\left(i+\frac{1}{2}\right)\Delta R \cdot H_\phi^{n+\frac{1}{2}}(i+\frac{1}{2}, j+\frac{1}{2}, k) - \left(i-\frac{1}{2}\right)\Delta R \cdot H_\phi^{n+\frac{1}{2}}(i-\frac{1}{2}, j+\frac{1}{2}, k)}{i\Delta R^2} \right] \quad (2.12e)
\end{aligned}$$

$$\begin{aligned}
& \frac{E_\phi^{n+1}(i, j, k+\frac{1}{2}) - E_\phi^n(i, j, k+\frac{1}{2})}{\Delta t} = \\
& \frac{1}{\varepsilon \cdot i \cdot \Delta R} \left[ \frac{(i+\frac{1}{2}) \cdot \Delta R \cdot H_\theta^{n+\frac{1}{2}}(i+\frac{1}{2}, j, k+\frac{1}{2}) - (i-\frac{1}{2}) \cdot \Delta R \cdot H_\theta^{n+\frac{1}{2}}(i-\frac{1}{2}, j, k+\frac{1}{2})}{\Delta r} \right. \\
& \left. \frac{H_R^{n+\frac{1}{2}}(i, j+\frac{1}{2}, k+\frac{1}{2}) - H_R^{n+\frac{1}{2}}(i, j-\frac{1}{2}, k+\frac{1}{2})}{\Delta\theta} \right] \quad (2.12f)
\end{aligned}$$

where:

$$(i, j, k) = (r = i\Delta R, \phi = j\Delta\phi, z = k\Delta z),$$

and

$$u^n(i, j, k) = u(r = i\Delta R, \phi = j\Delta\phi, z = k\Delta z, t = n\Delta t)$$

The spherical FDTD algorithm is generally used for solving scattering electromagnetic problems, especially for near field behavior of antenna systems. However, the spherical FDTD is not recommended for solving the problems with dimensions large in terms of the wavelength under consideration. That is due to the increasing sizes in radial direction, which may result in large modeling errors [110]. Other techniques can be employed for efficient computation for these problems, such as nonorthogonal gridding method [110].

## 2.5 Properties of FDTD Algorithm

To effect the efficient computation and reduce the modeling errors, behaviors and properties of the FDTD algorithm need to be investigated. In the following sections, these properties are discussed, including meshing schemes, numerical stability and dispersion.

### 2.5.1 *Nonuniform Mesh*

The discretized Maxwell's equations in (2.6), (2.8) and (2.12) are all written with a uniform Yee's grid, that is, time and space steps are uniformly the same across the whole computation domains. However, the uniform grid is not suitable for modeling the structures with fine geometrical features that can not conform to the edges of the uniform lattice. Further it may result in a global dense mesh when modeling the regions where electromagnetic fields rapidly change, such as near sharp edges or corners, leading to a large computation expenditures. Therefore, a reduction in the actual cell size in certain regions while not necessary in other regions is desired to more accurately model the local fields. In other words, a non-uniform mesh is required.

A non-uniform mesh scheme was introduced by Monk [111] [112]. However, it is cautioned that a non-uniform grid should not change size too rapidly. As a rule of thumb, one should try to maintain  $0.5\Delta x_{\pm 1} \leq \Delta x_i \leq 2\Delta x_{\pm 1}$  to avoid large local numerical errors [36].

The discretized Maxwell's equations of a nonuniform cylindrical mesh can be written as:

$$\frac{H_r^{n+\frac{1}{2}}(i, j + \frac{1}{2}, k + \frac{1}{2}) - H_r^{n-\frac{1}{2}}(i, j + \frac{1}{2}, k + \frac{1}{2})}{\Delta t} = \frac{1}{\mu} \left[ \frac{E_\phi^n(i, j + \frac{1}{2}, k + 1) - E_\phi^n(i, j + \frac{1}{2}, k)}{\Delta z 2(k + 1)} - \frac{E_z^n(i, j + 1, k + \frac{1}{2}) - E_z^n(i, j, k + \frac{1}{2})}{\Delta \phi 2(j + 1) \cdot r(i)} \right] \quad (2.13a)$$

$$\frac{H_\phi^{n+\frac{1}{2}}(i + \frac{1}{2}, j, k + \frac{1}{2}) - H_\phi^{n-\frac{1}{2}}(i + \frac{1}{2}, j, k + \frac{1}{2})}{\Delta t} = \frac{1}{\mu} \left[ \frac{E_z^n(i + 1, j, k + \frac{1}{2}) - E_z^n(i, j, k + \frac{1}{2})}{\Delta r 2(i + 1)} - \frac{E_r^n(i + \frac{1}{2}, j, k + 1) - E_r^n(i + \frac{1}{2}, j, k)}{\Delta z 2(k + 1)} \right] \quad (2.13b)$$

$$\frac{H_z^{n+\frac{1}{2}}(i + \frac{1}{2}, j + \frac{1}{2}, k) - H_z^{n-\frac{1}{2}}(i + \frac{1}{2}, j + \frac{1}{2}, k)}{\Delta t} = \frac{1}{\mu \cdot r(i + \frac{1}{2})} \left[ \frac{E_r^n(i + \frac{1}{2}, j + 1, k) - E_r^n(i + \frac{1}{2}, j, k)}{\Delta \phi 2(j + 1)} - \frac{(i + 1) \cdot \Delta r \cdot E_\phi^n(i + 1, j + \frac{1}{2}, k) - i \cdot \Delta r \cdot E_\phi^n(i, j + \frac{1}{2}, k)}{\Delta r 2(i + 1)} \right] \quad (2.13c)$$

$$\frac{E_r^{n+1}(i + \frac{1}{2}, j, k) - E_r^n(i + \frac{1}{2}, j, k)}{\Delta t} = \frac{1}{\varepsilon} \left[ \frac{H_z^{n+\frac{1}{2}}(i + \frac{1}{2}, j + \frac{1}{2}, k) - H_z^{n-\frac{1}{2}}(i + \frac{1}{2}, j - \frac{1}{2}, k)}{\Delta \phi 1(j) \cdot r(i + \frac{1}{2})} - \frac{H_\phi^{n+\frac{1}{2}}(i + \frac{1}{2}, j, k + \frac{1}{2}) - H_\phi^{n-\frac{1}{2}}(i + \frac{1}{2}, j, k - \frac{1}{2})}{\Delta z 1(k)} \right] \quad (2.13d)$$

$$\frac{E_\phi^{n+1}(i, j + \frac{1}{2}, k) - E_\phi^n(i, j + \frac{1}{2}, k)}{\Delta t} = \frac{1}{\varepsilon} \left[ \frac{H_r^{n+\frac{1}{2}}(i, j + \frac{1}{2}, k + \frac{1}{2}) - H_r^{n-\frac{1}{2}}(i, j + \frac{1}{2}, k - \frac{1}{2})}{\Delta z 1(k)} - \frac{H_z^{n+\frac{1}{2}}(i + \frac{1}{2}, j + \frac{1}{2}, k) - H_z^{n-\frac{1}{2}}(i - \frac{1}{2}, j + \frac{1}{2}, k)}{\Delta r 1(i)} \right] \quad (2.13e)$$

$$\begin{aligned}
& \frac{E_z^{n+1}(i, j, k + \frac{1}{2}) - E_z^n(i, j, k + \frac{1}{2})}{\Delta t} = \\
& \frac{1}{\epsilon \cdot r(i)} \left[ \frac{(i + \frac{1}{2}) \cdot \Delta r \cdot H_\phi^{n+\frac{1}{2}}(i + \frac{1}{2}, j, k + \frac{1}{2}) - (i - \frac{1}{2}) \cdot \Delta r \cdot H_\phi^{n+\frac{1}{2}}(i - \frac{1}{2}, j, k + \frac{1}{2})}{\Delta r l(i)} - \right. \\
& \left. \frac{H_r^{n+\frac{1}{2}}(i, j + \frac{1}{2}, k + \frac{1}{2}) - H_r^{n+\frac{1}{2}}(i, j - \frac{1}{2}, k + \frac{1}{2})}{\Delta \phi l(j)} \right] \quad (2.13f)
\end{aligned}$$

where  $\Delta r l(i), \Delta \phi l(j), \Delta z l(k)$  represent the distance between two local cell center,  $\Delta r 2(i), \Delta \phi 2(j), \Delta z 2(k)$  are the local cell size in three directions respectively, and  $r(i)$  is the distance from the field position to the z-axis.

It is shown in [36] that for complex and highly detailed circuits, the nonuniform grid can easily conform to such geometries without substantially increasing the lattice dimensions and without losing accuracy.

### 2.5.2 Two Inherent Constraints of the FDTD Algorithm

In spite of the fact that the FDTD is popular, it is normally memory and CPU-time intensive. Such intensive memory and CPU time requirements are due to the two physical constraints.

- 1) the spatial increment steps must be small enough in comparison with the wavelength (usually 10-20 steps per wavelength) in order to make the numerical dispersion error negligible. More details will be given in the next subsection.
- 2) the time step must be small enough to ensure that the FDTD computation errors do not grow with the time and therefore the computations remain stable. More specifically, the time step should satisfy the following Courant-Friedrich-Levy (CFL) condition in the cylindrical coordinates: [36]

$$u_{\max} \Delta t \leq \left[ \frac{1}{\Delta r_{\min}^2} + \frac{4}{(\Delta \phi_{\min} \cdot \Delta r_{\min})^2} + \frac{1}{\Delta z_{\min}^2} \right]^{-1/2} \quad (2.14)$$

Here  $u_{\max}$  is the maximum wave phase velocity within the model.

### 2.5.2.1 Numerical Stability

As shown above, the time increment  $\Delta t$  has a specific bound relative to the lattice space increments  $\Delta r, \Delta \phi, \Delta z$ . This bound is necessary to avoid numerical instability. It is an undesirable and unavoidable feature with explicit differential equation solvers that can cause the computed results to spuriously increase without limit as time-marching continues.

In [36], the detailed derivation of the time step bounds was provided in cartesian coordinate system. In the cylindrical coordinates, however, a more complicated derivation is involved due to the presence of the Bessel function and its derivatives [36]. Much research work on the numerical stability of the cylindrical FDTD has been conducted as described in [36] [113] [114]. The popularly accepted stability condition is shown in (2.14).

### 2.5.2.2 Numerical Dispersion

Like any other time-domain numerical schemes, FDTD embodies numerical dispersion of the simulated wave modes in its discrete computational lattice. The dispersion phenomenon can be understood as slow-wave properties of a discrete FDTD grid. It is represented by the variations of the phase velocity of the numerical waves that now change with wavelength, direction of propagation in the grid, and the grid cell size. As a result, numerical dispersion is a factor in FDTD modeling that needs to be accounted for in order to understand FDTD operation and its accuracy limits.

Dispersion errors can be reduced to zero by perturbing the normal unity coefficient in the Yee space derivative analog or by using a higher order accurate central-difference scheme for the space derivatives of the curl operator. Since dispersion analysis is not a

main topic of the thesis, the detailed discussion is not listed here. More information on dispersion analysis can be found in [36].

## 2.6 Absorbing Boundary Conditions

A commonly encountered problem is that many geometries and structures under consideration are defined in “open” regions where the spatial domain of the computed field is unbounded in one or more coordinate directions. However, no computer can store unlimited data. Therefore, the field computation domain must be truncated by a certain absorbing boundary condition (ABC) that simulates the truncated space that extends to infinity.

Since the 1970s, many absorbing techniques have been constructed for solving scattering and open structure problems. In 1980, Bayliss and Turkel presented scattered-wave annihilating operators [115]. Later, Engquist and Majda derived a theory of one-way equations suitable for absorbing impinging scattered waves [116]. Based on this work, Mur developed a simple ABC which can effectively absorb normally incident waves [117]. The third thrust in ABC development in the 1970s and 1980s was originated by Liao in 1984 [118], which is called “multi-transmitting” theory. This approach can be understood as an extrapolation of the wave fields in space and time domain using a Newton backward-difference polynomial. The last approach to the ABC problem which was widely used in FDTD software during 1970s and 1980s is Mei-Fang’s *superabsorption* technique [119]. The concept of *superabsorption* is not an ABC itself, but rather a means to improve the performance of local ABCs via an error cancellation procedure.

In 1990s’, inspired by the anechoic chambers which can absorb effectively waves better than -70 dB, researchers had been trying to find numerical ABCs that simulates the anechoic chambers. In 1994, Berenger proposed a novel perfectly matched layers (PML) ABC for FDTD schemes in two dimensions with orders of improved performance compared to any earlier technique [120]. This approach is based on a splitting of electric or magnetic field components in predetermined lossy layers with the possibility of assigning losses to the individual split field components. In addition, there is impedance

match between the absorbing PML medium and the connecting FDTD mesh medium regardless of wave incident angles. With the confirmation of the remarkable properties of PML ABC by others [121] [122], the PML techniques have since been widely studied and used for analyzing open geometries and structures. The recently developed nonsplit PML ABCs, such as Uniaxial PML (UPML) [123], and Convolutional PML (CPML) [124] etc., extend the use of Berenger's PML with more Maxwellian like formulations.

In the following sections, more descriptions are given to the Mur and PML absorbing boundary conditions.

### 2.6.1 *Mur First-order Boundary Condition*

Mur ABC had been a primary absorbing boundary condition to truncate an FDTD domain prior to the development of PML ABC due to its simplicity and less requirements on computation resources.

Suppose the waves propagate in the  $z$ -direction and the computation domain is truncated at  $z=0$ . Then the one-way wave equation at the boundary  $z=0$ , that theoretically annihilate the waves propagating in the  $z$ -direction, can be written as:

$$\frac{\partial W}{\partial z} - \frac{1}{c} \frac{\partial W}{\partial t} = 0 \quad (2.15)$$

in which  $W$  denotes either  $E$  field or  $H$  field, and  $c$  is the wave propagation speed. In a numerical grid, let  $W^n(i, j, 0)$  represents a tangential field component of  $E$  or  $H$  located at  $z=0$ . By introducing an auxiliary grid point  $(i, j, 1/2) = (x=i\Delta x, y=j\Delta y, z=1/2\Delta z)$  and expanding the partial derivatives with central difference method, the partial differential terms in (2.16) at the auxiliary point can be written as:

$$\frac{\partial W^{n+1/2}}{\partial z} \left( i, j, \frac{1}{2} \right) = \left( \frac{W^{n+1}(i, j, 1) - W^{n+1}(i, j, 0) + W^n(i, j, 1) - W^n(i, j, 0)}{2\Delta z} \right) \quad (2.16a)$$

$$\frac{\partial W^{n+1/2}}{\partial t} \left( i, j, \frac{1}{2} \right) = \left( \frac{W^{n+1}(i, j, 1) - W^n(i, j, 1) + W^{n+1}(i, j, 0) - W^n(i, j, 0)}{2\Delta t} \right) \quad (2.16b)$$



Substituting (2.16) into (2.15), the following first-order time-stepping algorithm for the field components along  $z=0$  can be obtained:

$$W^{n+1}(i, j, 0) = W^n(i, j, 1) + \frac{c\Delta t - \Delta z}{c\Delta t + \Delta z} [W^{n+1}(i, j, 1) - W^n(i, j, 0)] \quad (2.17)$$

The first order Mur boundary condition can provide -30 dB to -45 dB absorbing performance. To obtain better performance, one can employ second-order Mur boundary condition to better absorb the outgoing waves.

### 2.6.2 Berenger's Perfectly Matched Layers (PML) Boundary Condition

The PML technique is a novel absorbing method. By splitting the field components in the discretized Maxwell's equations and adding the gradually changed lossy terms, the outgoing waves entering the PML layers with arbitrary incident angles are absorbed.

In the cylindrical coordinates, the field components in the PML region split as:

$$\begin{aligned} E_r &= E_{r\phi} + E_{rz} \\ E_\phi &= E_{\phi r} + E_{\phi z} \\ E_z &= E_{z\phi} + E_{zr} \\ H_r &= H_{r\phi} + H_{rz} \\ H_\phi &= H_{\phi r} + H_{\phi z} \\ H_z &= H_{zr} + H_{z\phi} \end{aligned} \quad (2.18)$$

The discretized PML equations in the cylindrical coordinates can then be expressed as:

$$\begin{aligned} H_{r\phi}^{n+\frac{1}{2}}(i, j + \frac{1}{2}, k + \frac{1}{2}) &= \frac{c_{\phi 1}^*(j+1)}{c_{\phi 2}^*(j+1)} H_{r\phi}^{n-\frac{1}{2}}(i, j + \frac{1}{2}, k + \frac{1}{2}) + \\ &\frac{\Delta t}{c_{\phi 2}^*(j+1)\mu r(i)\Delta\phi 2(j+1)} \left[ E_{zr}^n(i, j, k + \frac{1}{2}) - E_{zr}^n(i, j+1, k + \frac{1}{2}) \right. \\ &\quad \left. + E_{z\phi}^n(i, j, k + \frac{1}{2}) - E_{z\phi}^n(i, j+1, k + \frac{1}{2}) \right] \end{aligned} \quad (2.19a)$$

$$H_{r\phi}^{n+\frac{1}{2}}(i, j + \frac{1}{2}, k + \frac{1}{2}) = \frac{c_{\phi 1}^*(j+1)}{c_{\phi 2}^*(j+1)} H_{r\phi}^{n-\frac{1}{2}}(i, j + \frac{1}{2}, k + \frac{1}{2}) + \frac{\Delta t}{c_{\phi 2}^*(j+1)\mu r(i)\Delta\phi 2(j+1)} \left[ \begin{aligned} &E_{r\phi}^n(i, j, k + \frac{1}{2}) - E_{r\phi}^n(i, j+1, k + \frac{1}{2}) \\ &+ E_{z\phi}^n(i, j, k + \frac{1}{2}) - E_{z\phi}^n(i, j+1, k + \frac{1}{2}) \end{aligned} \right] \quad (2.19a)$$

$$H_{rz}^{n+\frac{1}{2}}(i, j + \frac{1}{2}, k + \frac{1}{2}) = \frac{c_{z1}^*(k+1)}{c_{z2}^*(k+1)} H_{rz}^{n-\frac{1}{2}}(i, j + \frac{1}{2}, k + \frac{1}{2}) + \frac{\Delta t}{c_{z2}^*(k+1)\mu\Delta z 2(k+1)} \left[ \begin{aligned} &E_{\phi r}^n(i, j + \frac{1}{2}, k+1) - E_{\phi r}^n(i, j + \frac{1}{2}, k) \\ &+ E_{\phi z}^n(i, j + \frac{1}{2}, k+1) - E_{\phi z}^n(i, j + \frac{1}{2}, k) \end{aligned} \right] \quad (2.19b)$$

$$H_{\phi z}^{n+\frac{1}{2}}(i + \frac{1}{2}, j, k + \frac{1}{2}) = \frac{c_{z1}^*(k+1)}{c_{z2}^*(k+1)} H_{\phi z}^{n-\frac{1}{2}}(i + \frac{1}{2}, j, k + \frac{1}{2}) + \frac{\Delta t}{c_{z2}^*(k+1)\mu\Delta z 2(k+1)} \left[ \begin{aligned} &E_{r\phi}^n(i + \frac{1}{2}, j, k) - E_{r\phi}^n(i + \frac{1}{2}, j, k+1) \\ &+ E_{rz}^n(i + \frac{1}{2}, j, k) - E_{rz}^n(i + \frac{1}{2}, j, k+1) \end{aligned} \right] \quad (2.19c)$$

$$H_{\phi r}^{n+\frac{1}{2}}(i + \frac{1}{2}, j, k + \frac{1}{2}) = \frac{c_{r1}^*(i+1)}{c_{r2}^*(i+1)} H_{\phi r}^{n-\frac{1}{2}}(i + \frac{1}{2}, j, k + \frac{1}{2}) + \frac{\Delta t}{c_{r2}^*(i+1)\mu\Delta r 2(i+1)} \left[ \begin{aligned} &E_{zr}^n(i+1, j, k + \frac{1}{2}) - E_{zr}^n(i, j, k + \frac{1}{2}) \\ &+ E_{z\phi}^n(i+1, j, k + \frac{1}{2}) - E_{z\phi}^n(i, j, k + \frac{1}{2}) \end{aligned} \right] \quad (2.19d)$$

$$H_{rz}^{n+\frac{1}{2}}(i + \frac{1}{2}, j + \frac{1}{2}, k) = \frac{c_{r1}^*(i+1)}{c_{r2}^*(i+1)} H_{rz}^{n-\frac{1}{2}}(i + \frac{1}{2}, j + \frac{1}{2}, k) + \frac{\Delta t}{c_{r2}^*(i+1)\mu\Delta r(i+1)r 2(i + \frac{1}{2})} \left[ \begin{aligned} &r(i)E_{\phi r}^n(i, j + \frac{1}{2}, k) - r(i+1)E_{\phi r}^n(i+1, j + \frac{1}{2}, k) \\ &+ r(i)E_{\phi z}^n(i, j + \frac{1}{2}, k) - r(i+1)E_{\phi z}^n(i+1, j + \frac{1}{2}, k) \end{aligned} \right] \quad (2.19e)$$

$$H_{z\phi}^{n+\frac{1}{2}}(i+\frac{1}{2}, j+\frac{1}{2}, k) = \frac{c_{\phi 1}^*(j+1)}{c_{\phi 2}^*(j+1)} H_{z\phi}^{n-\frac{1}{2}}(i+\frac{1}{2}, j+\frac{1}{2}, k) + \frac{\Delta t}{c_{\phi 2}^*(j+1)\mu\Delta\phi 2(j+1)r(i+\frac{1}{2})} \left[ E_{r\phi}^n(i+\frac{1}{2}, j+1, k) - E_{r\phi}^n(i+\frac{1}{2}, j, k) + E_{rz}^n(i+\frac{1}{2}, j+1, k) - E_{rz}^n(i+\frac{1}{2}, j, k) \right] \quad (2.19f)$$

$$E_{r\phi}^{n+1}(i+\frac{1}{2}, j, k) = \frac{c_{\phi 1}(j)}{c_{\phi 2}(j)} E_{r\phi}^n(i+\frac{1}{2}, j, k) + \frac{\Delta t}{c_{\phi 2}(j)\varepsilon r(i+\frac{1}{2})\Delta\phi 1(j)} \left[ H_{rz}^{n+\frac{1}{2}}(i+\frac{1}{2}, j+\frac{1}{2}, k) - H_{rz}^{n+\frac{1}{2}}(i+\frac{1}{2}, j-\frac{1}{2}, k) + H_{z\phi}^{n+\frac{1}{2}}(i+\frac{1}{2}, j+\frac{1}{2}, k) - H_{z\phi}^{n+\frac{1}{2}}(i+\frac{1}{2}, j-\frac{1}{2}, k) \right] \quad (2.20a)$$

$$E_{rz}^{n+1}(i+\frac{1}{2}, j, k) = \frac{c_{z1}(k)}{c_{z2}(k)} E_{rz}^n(i+\frac{1}{2}, j, k) + \frac{\Delta t}{c_{z2}(k)\varepsilon\Delta z 1(k)} \left[ H_{r\phi}^{n+\frac{1}{2}}(i+\frac{1}{2}, j, k-\frac{1}{2}) - H_{r\phi}^{n+\frac{1}{2}}(i+\frac{1}{2}, j, k+\frac{1}{2}) + H_{\phi z}^{n+\frac{1}{2}}(i+\frac{1}{2}, j, k-\frac{1}{2}) - H_{\phi z}^{n+\frac{1}{2}}(i+\frac{1}{2}, j, k+\frac{1}{2}) \right] \quad (2.20b)$$

$$E_{\phi z}^{n+1}(i, j+\frac{1}{2}, k) = \frac{c_{z1}(k)}{c_{z2}(k)} E_{\phi z}^n(i, j+\frac{1}{2}, k) + \frac{\Delta t}{c_{z2}(k)\varepsilon\Delta z 1(k)} \left[ H_{r\phi}^{n+\frac{1}{2}}(i, j+\frac{1}{2}, k+\frac{1}{2}) - H_{r\phi}^{n+\frac{1}{2}}(i, j+\frac{1}{2}, k-\frac{1}{2}) + H_{rz}^{n+\frac{1}{2}}(i, j+\frac{1}{2}, k+\frac{1}{2}) - H_{rz}^{n+\frac{1}{2}}(i, j+\frac{1}{2}, k-\frac{1}{2}) \right] \quad (2.20c)$$

$$E_{\phi r}^{n+1}(i, j+\frac{1}{2}, k) = \frac{c_{r1}(i)}{c_{r2}(i)} E_{\phi r}^n(i, j+\frac{1}{2}, k) + \frac{\Delta t}{c_{r2}(i)\varepsilon\Delta r 1(i)} \left[ H_{rz}^{n+\frac{1}{2}}(i-\frac{1}{2}, j+\frac{1}{2}, k) - H_{rz}^{n+\frac{1}{2}}(i+\frac{1}{2}, j+\frac{1}{2}, k) + H_{z\phi}^{n+\frac{1}{2}}(i-\frac{1}{2}, j+\frac{1}{2}, k) - H_{z\phi}^{n+\frac{1}{2}}(i+\frac{1}{2}, j+\frac{1}{2}, k) \right] \quad (2.20d)$$

$$E_{zr}^{n+1}(i, j, k + \frac{1}{2}) = \frac{c_{r1}(i)}{c_{r2}(i)} E_{zr}^n(i, j, k + \frac{1}{2}) + \frac{\Delta t}{c_{r2}(i)\epsilon\Delta r l(i)} \left[ r(i + \frac{1}{2}) H_{\phi}^{n+\frac{1}{2}}(i + \frac{1}{2}, j, k + \frac{1}{2}) - r(i - \frac{1}{2}) H_{\phi}^{n+\frac{1}{2}}(i - \frac{1}{2}, j, k + \frac{1}{2}) + r(i + \frac{1}{2}) H_{\phi}^{n+\frac{1}{2}}(i + \frac{1}{2}, j, k + \frac{1}{2}) - r(i - \frac{1}{2}) H_{\phi}^{n+\frac{1}{2}}(i - \frac{1}{2}, j, k + \frac{1}{2}) \right] \quad (2.20e)$$

$$E_{z\phi}^{n+1}(i, j, k + \frac{1}{2}) = \frac{c_{\phi1}(j)}{c_{\phi2}(j)} E_{z\phi}^n(i, j, k + \frac{1}{2}) + \frac{\Delta t}{c_{\phi2}(j)\epsilon\Delta\phi l(j)r(i)} \left[ H_{r\phi}^{n+\frac{1}{2}}(i, j - \frac{1}{2}, k + \frac{1}{2}) - H_{r\phi}^{n+\frac{1}{2}}(i, j + \frac{1}{2}, k + \frac{1}{2}) + H_{rz}^{n+\frac{1}{2}}(i, j - \frac{1}{2}, k + \frac{1}{2}) - H_{rz}^{n+\frac{1}{2}}(i, j + \frac{1}{2}, k + \frac{1}{2}) \right] \quad (2.20f)$$

in which:

$$\begin{aligned} c_{d1}(i + \frac{1}{2}, j, k) &= 1 - \frac{\Delta t \cdot \sigma_d(i + \frac{1}{2}, j, k)}{2\epsilon} \\ c_{d2}(i + \frac{1}{2}, j, k) &= 1 + \frac{\Delta t \cdot \sigma_d(i + \frac{1}{2}, j, k)}{2\epsilon} \quad (d=r, \phi, z) \\ c_{d1}^*(i + \frac{1}{2}, j, k) &= 1 - \frac{\Delta t \cdot \sigma_d^*(i + \frac{1}{2}, j, k)}{2\mu} \\ c_{d2}^*(i + \frac{1}{2}, j, k) &= 1 + \frac{\Delta t \cdot \sigma_d^*(i + \frac{1}{2}, j, k)}{2\mu} \end{aligned} \quad (2.21)$$

and  $\sigma_d(d=r, z)$  is the directional conductivity in the radial, azimuthal and axial direction.

In order to preserve the continuity across the interface between work domain and PML region, the electric and magnetic conductivity should be the same as those of the connected solution domains. The varying conductivities in PML region should be gradually increased in order to minimize the reflection errors. The conductivities can exponentially increase from the interface to the outer PEC boundary, using the following equation:

$$\sigma_d(x) = \sigma_m \left( \frac{x}{d} \right)^n \quad (2.22)$$

where  $x$  is the distance from the interface,  $d$  is the total thickness of the PML layer, and  $\sigma_m$  is the maximum value of the conductivity in the PML region.

In addition, in order to minimize the reflection from each layer of PML boundary, the impedance between the adjacent layers must be matched. This requires:

$$\frac{\sigma_i}{\varepsilon_1} = \frac{\sigma_i^*}{\mu_1} \quad (i=r, z) \quad (2.23)$$

in which  $\varepsilon_1$  and  $\mu_1$  are the permittivity and permeability of the work domain respectively. The directional conductivities in the PML region should also conform to the relationship in equation (2.22).

PML absorbing boundary condition outperforms all the previous ABCs by virtue of its omni directional absorbing ability. The previous study shows that the absorption can be as good as 50 to 70 dB for a 10-layer PML region [36] which has a performance similar to an anechoic chamber.

### 2.6.3 Stretched Coordinates PML Boundary Conditions

A more compact form of the nonsplit PML forms of (2.21) and (2.22) was introduced by Chew and Weedon [125] and independently by Rappaport [126]. By re-posing the split-field equations in a nonsplit form, the Maxwell's equations are mapped into a complex coordinate space. A specialized PML designed for the cylindrical-coordinate space was demonstrated by Maloney et al. [127] using a graphical solution and by Chew et al. using a stretched coordinate approach [128]. To this end, a cylindrical mapping into a complex space is introduced:

$$\begin{aligned} \hat{r} &\rightarrow r_0 + \int_0^r s_r(r') dr' & \hat{z} &\rightarrow z_0 + \int_{z_0}^z s_z(z') dz' \\ s_r &= 1 + \frac{\sigma_r(r)}{j\omega\varepsilon_0} & s_z &= 1 + \frac{\sigma_z(z)}{j\omega\varepsilon_0} \end{aligned} \quad (2.24)$$

in which  $\hat{r}$  and  $\hat{z}$  denote the cylindrical coordinates in the complex space in radial and axial directions respectively, and the corresponding partial differential operators in the complex space are:

$$\frac{\partial}{\partial \hat{r}} = \frac{1}{s_r} \frac{\partial}{\partial r}, \quad \frac{\partial}{\partial \hat{z}} = \frac{1}{s_z} \frac{\partial}{\partial z} \quad (2.25)$$

As a result, in the cylindrical coordinate complex space, the Maxwell's equations applied to uniaxial perfectly matched layers (UPML) can be expressed as:

$$j\omega\epsilon \cdot s_z \frac{\hat{r}}{r} E_r = \frac{\partial(s_z H_z)}{r \partial \phi} - \frac{\partial}{\partial z} \left( \frac{\hat{r}}{r} H_\phi \right) \quad (2.26a)$$

$$j\omega\epsilon \cdot s_z s_r E_\phi = \frac{\partial(s_r H_r)}{\partial z} - \frac{\partial(s_z H_z)}{\partial r} \quad (2.26b)$$

$$j\omega\epsilon \cdot s_r \frac{\hat{r}}{r} E_z = \frac{\partial(\hat{r} H_\phi)}{r \partial r} - \frac{\partial(s_r H_r)}{r \partial \phi} \quad (2.26c)$$

$$-j\omega\mu \cdot s_z \frac{\hat{r}}{r} H_r = \frac{\partial(s_z E_z)}{r \partial \phi} - \frac{\partial}{\partial z} \left( \frac{\hat{r}}{r} E_\phi \right) \quad (2.26d)$$

$$-j\omega\mu \cdot s_z s_r H_\phi = \frac{\partial(s_r E_r)}{\partial z} - \frac{\partial(s_z E_z)}{\partial r} \quad (2.26e)$$

$$-j\omega\mu \cdot s_r \frac{\hat{r}}{r} H_z = \frac{\partial(\hat{r} E_\phi)}{r \partial r} - \frac{\partial(s_r E_r)}{r \partial \phi} \quad (2.26f)$$

In a more compact form, the Maxwell's curl equations can be expressed as:

$$\begin{aligned} j\omega\epsilon \cdot \bar{s}_c \vec{E} &= \nabla \times \vec{H} \\ j\omega\epsilon \cdot \bar{s}_c \vec{H} &= \nabla \times \vec{E} \end{aligned} \quad (2.27)$$

where:

$$\bar{s}_c = \begin{vmatrix} \frac{s_z \hat{r}}{s_r r} & 0 & 0 \\ 0 & \frac{s_z s_r r}{\hat{r}} & 0 \\ 0 & 0 & \frac{s_r \hat{r}}{s_z r} \end{vmatrix} \quad (2.28)$$

By introducing the auxiliary field components that are located on the same positions of the corresponding  $E$  or  $H$  field components in the Yee's grid:

$$\begin{aligned} P_r &= \frac{\hat{r}}{s_r r} E_r & P_\phi &= \frac{s_z r}{\hat{r}} E_\phi & P_z &= \frac{\hat{r}}{s_z r} E_z \\ Q_r &= \frac{\hat{r}}{s_r r} H_r & Q_\phi &= \frac{s_z r}{\hat{r}} H_\phi & Q_z &= \frac{\hat{r}}{s_z r} H_z \end{aligned} \quad (2.29)$$

where:

$$s_r = \begin{cases} 1 & r < r_0 \\ 1 + \frac{\sigma_{\max}}{j\omega\epsilon_0} \left( \frac{r - r_0}{r_1 - r_0} \right)^m & r_0 < r < r_1 \end{cases} \quad (2.30)$$

$$\hat{r} = \begin{cases} r & r < r_0 \\ r + \frac{\sigma_{\max}}{j\omega(m+1)\epsilon_0} \frac{(r - r_0)^{m+1}}{(r_1 - r_0)^m} & r_0 < r < r_1 \end{cases}$$

and substituting the expressions of (2.30) into (2.29), the coupled set of time-dependent equations can be obtained:

$$\epsilon \frac{\partial P_r}{\partial t} + \sigma_z(z) P_r = \frac{\partial H_z}{r \partial \phi} - \frac{\partial H_\phi}{\partial z} \quad (2.31a)$$

$$\epsilon \frac{\partial P_\phi}{\partial t} + \sigma_r(r) P_\phi = \frac{\partial H_r}{\partial z} - \frac{\partial H_z}{\partial r} \quad (2.31b)$$

$$\epsilon \frac{\partial P_z}{\partial t} + \sigma_r(r) P_z = \frac{\partial (r H_\phi)}{r \partial r} - \frac{\partial H_r}{r \partial \phi} \quad (2.31c)$$

$$-\mu \frac{\partial Q_r}{\partial t} + \sigma_z(z) H_r = \frac{\partial E_z}{r \partial \phi} - \frac{\partial E_\phi}{\partial z} \quad (2.31d)$$

$$-\mu \frac{\partial Q_\phi}{\partial t} + \sigma_r(r) H_\phi = \frac{\partial E_r}{\partial z} - \frac{\partial E_z}{\partial r} \quad (2.31e)$$

$$-\mu \frac{\partial Q_z}{\partial t} + \sigma_r(r) H_z = \frac{\partial(r E_\phi)}{r \partial r} - \frac{\partial E_r}{r \partial \phi} \quad (2.31f)$$

By using central-differencing technique, the discretized recursive FDTD algorithm can be obtained for computer programming:

$$P_r^{n+1}(i + \frac{1}{2}, j, k) = \frac{l_{z1}(k)}{l_{z2}(k)} P_r^n(i + \frac{1}{2}, j, k) + \frac{\Delta t}{l_{z2}(k)} \left[ \frac{H_z^{n+\frac{1}{2}}(i + \frac{1}{2}, j + \frac{1}{2}, k) - H_z^{n+\frac{1}{2}}(i + \frac{1}{2}, j - \frac{1}{2}, k)}{\Delta \phi l(j) \cdot r(i + \frac{1}{2})} - \frac{H_\phi^{n+\frac{1}{2}}(i + \frac{1}{2}, j, k + \frac{1}{2}) - H_\phi^{n+\frac{1}{2}}(i + \frac{1}{2}, j, k - \frac{1}{2})}{\Delta z l(k)} \right] \quad (2.32a)$$

$$P_\phi^{n+1}(i, j + \frac{1}{2}, k) = \frac{l_{r1}(i)}{l_{r2}(i)} P_\phi^n(i, j + \frac{1}{2}, k) + \frac{\Delta t}{l_{r2}(i)} \left[ \frac{H_r^{n+\frac{1}{2}}(i, j + \frac{1}{2}, k + \frac{1}{2}) - H_r^{n+\frac{1}{2}}(i, j + \frac{1}{2}, k - \frac{1}{2})}{\Delta z l(k)} - \frac{H_z^{n+\frac{1}{2}}(i + \frac{1}{2}, j + \frac{1}{2}, k) - H_z^{n+\frac{1}{2}}(i - \frac{1}{2}, j + \frac{1}{2}, k)}{\Delta r l(i)} \right] \quad (2.32b)$$

$$P_z^{n+1}(i, j, k + \frac{1}{2}) = \frac{l_{r1}(i)}{l_{r2}(i)} P_z^n(i, j, k + \frac{1}{2}) + \frac{1}{l_{r2}(i) \cdot r(i)} \left[ \frac{(i + \frac{1}{2}) \cdot \Delta r \cdot H_\phi^{n+\frac{1}{2}}(i + \frac{1}{2}, j, k + \frac{1}{2}) - (i - \frac{1}{2}) \cdot \Delta r \cdot H_\phi^{n+\frac{1}{2}}(i - \frac{1}{2}, j, k + \frac{1}{2})}{\Delta r l(i)} - \frac{H_r^{n+\frac{1}{2}}(i, j + \frac{1}{2}, k + \frac{1}{2}) - H_r^{n+\frac{1}{2}}(i, j - \frac{1}{2}, k + \frac{1}{2})}{\Delta \phi l(j)} \right] \quad (2.32c)$$

$$E_r^{n+1}(i + \frac{1}{2}, j, k) = \frac{l_{r1}(i + \frac{1}{2})}{l_{r2}(i + \frac{1}{2})} E_r^n(i + \frac{1}{2}, j, k) + \frac{1}{l_{r2}(i + \frac{1}{2})} \left[ l_{r2}(i + \frac{1}{2}) P_r^{n+1}(i + \frac{1}{2}, j, k) - l_{r1}(i + \frac{1}{2}) P_r^n(i + \frac{1}{2}, j, k) \right] \quad (2.32d)$$



$$E_{\phi}^{n+1}(i, j + \frac{1}{2}, k) = \frac{l_{z1}(k)}{l_{z2}(k)} E_{\phi}^n(i, j + \frac{1}{2}, k) + \frac{1}{l_{z2}(k)} \left[ l_{r2}(i) P_{\phi}^{n+1}(i, j + \frac{1}{2}, k) - l_{r1}(i) P_{\phi}^n(i, j + \frac{1}{2}, k) \right] \quad (2.32e)$$

$$E_z^{n+1}(i, j, k + \frac{1}{2}) = \frac{l_{r1}(i)}{l_{r2}(i)} E_z^n(i, j, k + \frac{1}{2}) + \frac{1}{l_{r2}(i)} \left[ l_{z2}(k + \frac{1}{2}) P_z^{n+1}(i, j, k + \frac{1}{2}) - l_{z1}(k + \frac{1}{2}) P_z^n(i, j, k + \frac{1}{2}) \right] \quad (2.32f)$$

$$Q_r^{n+\frac{1}{2}}(i, j + \frac{1}{2}, k + \frac{1}{2}) = \frac{l_{z1}(k + \frac{1}{2})}{l_{z2}(k + \frac{1}{2})} Q_r^{n-\frac{1}{2}}(i, j + \frac{1}{2}, k + \frac{1}{2}) + \frac{1}{l_{z2}(k + \frac{1}{2})} \mu \left[ \frac{E_{\phi}^n(i, j + \frac{1}{2}, k + 1) - E_{\phi}^n(i, j + \frac{1}{2}, k)}{\Delta z 2(k + 1)} - \frac{E_z^n(i, j + 1, k + \frac{1}{2}) - E_z^n(i, j, k + \frac{1}{2})}{\Delta \phi 2(j + 1) \cdot r(i)} \right] \quad (2.33a)$$

$$Q_{\phi}^{n+\frac{1}{2}}(i + \frac{1}{2}, j, k + \frac{1}{2}) = \frac{l_{r1}(i + \frac{1}{2})}{l_{r2}(i + \frac{1}{2})} Q_{\phi}^{n-\frac{1}{2}}(i + \frac{1}{2}, j, k + \frac{1}{2}) + \frac{1}{l_{r2}(i + \frac{1}{2})} \mu \left[ \frac{E_z^n(i + 1, j, k + \frac{1}{2}) - E_z^n(i, j, k + \frac{1}{2})}{\Delta r 2(i + 1)} - \frac{E_r^n(i + \frac{1}{2}, j, k + 1) - E_r^n(i + \frac{1}{2}, j, k)}{\Delta z 2(k + 1)} \right] \quad (2.33b)$$

$$Q_z^{n+\frac{1}{2}}(i + \frac{1}{2}, j + \frac{1}{2}, k) = \frac{l_{r1}(i + \frac{1}{2})}{l_{r2}(i + \frac{1}{2})} Q_z^{n-\frac{1}{2}}(i + \frac{1}{2}, j + \frac{1}{2}, k) + \frac{1}{l_{r2}(i + \frac{1}{2})} \mu \cdot r(i + \frac{1}{2}) \left[ \frac{E_r^n(i + \frac{1}{2}, j + 1, k) - E_r^n(i + \frac{1}{2}, j, k)}{\Delta \phi 2(j + 1)} - \frac{(i + 1) \cdot \Delta r \cdot E_{\phi}^n(i + 1, j + \frac{1}{2}, k) - i \cdot \Delta r \cdot E_{\phi}^n(i, j + \frac{1}{2}, k)}{\Delta r 2(i + 1)} \right] \quad (2.33c)$$

$$H_r^{n+\frac{1}{2}}(i, j + \frac{1}{2}, k + \frac{1}{2}) = \frac{l_{r1}(i)}{l_{r2}(i)} H_r^{n-\frac{1}{2}}(i, j + \frac{1}{2}, k + \frac{1}{2}) + \frac{1}{l_{r2}(i)} \left[ l_{r2}(i) Q_r^{n+\frac{1}{2}}(i, j + \frac{1}{2}, k + \frac{1}{2}) - l_{r1}(i) Q_r^{n-\frac{1}{2}}(i, j + \frac{1}{2}, k + \frac{1}{2}) \right] \quad (2.33d)$$

$$H_{\phi}^{n+\frac{1}{2}}(i+\frac{1}{2}, j, k+\frac{1}{2}) = \frac{l_{z1}(k+\frac{1}{2})}{l_{z2}(k+\frac{1}{2})} H_{\phi}^{n-\frac{1}{2}}(i+\frac{1}{2}, j, k+\frac{1}{2}) + \frac{1}{l_{z2}(k+\frac{1}{2})} \left[ l_{r2}(i+\frac{1}{2}) Q_{\phi}^{n+\frac{1}{2}}(i+\frac{1}{2}, j, k+\frac{1}{2}) - l_{r1}(i+\frac{1}{2}) Q_{\phi}^{n-\frac{1}{2}}(i+\frac{1}{2}, j, k+\frac{1}{2}) \right] \quad (2.33e)$$

$$H_z^{n+\frac{1}{2}}(i+\frac{1}{2}, j+\frac{1}{2}, k) = \frac{l_{r1}(i+\frac{1}{2})}{l_{r2}(i+\frac{1}{2})} H_z^{n-\frac{1}{2}}(i+\frac{1}{2}, j+\frac{1}{2}, k) + \frac{1}{l_{r2}(i+\frac{1}{2})} \left[ l_{z2}(k) Q_z^{n+\frac{1}{2}}(i+\frac{1}{2}, j+\frac{1}{2}, k) - l_{z1}(k) Q_z^{n-\frac{1}{2}}(i+\frac{1}{2}, j+\frac{1}{2}, k) \right] \quad (2.33f)$$

in which:

$$\begin{aligned} l_{r1}(i+\frac{1}{2}, j, k) &= 1 - \frac{\Delta t \cdot \sigma_r(i+\frac{1}{2}, j, k)}{2\varepsilon} \\ l_{r2}(i+\frac{1}{2}, j, k) &= 1 + \frac{\Delta t \cdot \sigma_r(i+\frac{1}{2}, j, k)}{2\varepsilon} \\ l_{r1}(i+\frac{1}{2}, j, k) &= 1 - \frac{\Delta t \cdot \int_{r_0}^r \sigma_r(r) dr}{2\varepsilon} \end{aligned} \quad (2.34)$$

$$\begin{aligned} l_{r2}(i+\frac{1}{2}, j, k) &= 1 + \frac{\Delta t \cdot \int_{r_0}^r \sigma_r(r) dr}{2\varepsilon} \\ l_{z1}(i+\frac{1}{2}, j, k) &= 1 - \frac{\Delta t \cdot \sigma_z(i+\frac{1}{2}, j, k)}{2\varepsilon} \\ l_{z2}(i+\frac{1}{2}, j, k) &= 1 + \frac{\Delta t \cdot \sigma_z(i+\frac{1}{2}, j, k)}{2\varepsilon} \end{aligned}$$

The conductivity in the PML region must be scaled to reduce discretization error. One of the methods is spatial scaling, which scales the conductivity in terms of the distance from the interface between PML and work domain:

$$\sigma_r = \sigma_{max} \left( \frac{r - r_0}{r_1 - r_0} \right)^m \quad (2.35)$$

in which  $r_0$  is distance from the origin to the inner boundary of PML layer, and  $r_1$  is the distance from the origin to the outer boundary of PML layer. The maximum conductivity in PML region recommended is [36]:

$$\sigma_{max} = \sigma_{opt} = \frac{m + 1}{150 \pi \sqrt{\epsilon_r} \Delta d} \quad (2.36)$$

in which  $\epsilon_r$  denotes the permittivity of PML region, and  $\Delta d$  is the space increment in a certain direction.

The stretched coordinates PML boundary condition presents a more Maxwellian like the FDTD algorithm for absorbing outgoing waves. Due to this property and its easiness of incorporating other background material parameters, it is employed with the ADI-FDTD which will be derived in Chapter 6.

## 2.7 Conclusions

In this chapter, the fundamentals on FDTD algorithm are briefly reviewed. Yee's grid, the FDTD formulations in different coordinate systems, numerical dispersion, numerical stability, nonuniform mesh and commonly used absorbing boundary conditions are described. Due to the wide range of FDTD applications in electromagnetics, there are other considerations that should be taken into account for a specific problem. More detailed information can be found in [36]. In the following chapters, analogous analysis and discussions on ADI-FDTD algorithm are to be conducted in respect to the topics described in this chapter, in particular, numerical stability, modeling error and absorbing boundary conditions.

## CHAPTER 3    THE UNCONDITIONALLY STABLE ADI-FDTD METHOD FOR ELETROMAGNETIC MODELING

### 3.1        Introduction

The Alternating Direct Implicit (ADI) method was first introduced by Peaceman and Rachford in 1955 [129] to analyze elliptic and parabolic equations. In 1984, R. Holland introduced the ADI method into solving Maxwell's curl equations [79]. F. Zheng and Z. Chen then systematically developed the three dimensional ADI-FDTD algorithm in the cartesian coordinate system with a term-wise ADI scheme that is different from the one by Holland. Due to the removal of CFL condition, their method is unconditionally stable and has been applied for effectively and efficiently solving a variety of electromagnetic problems [83] [132].

In this chapter, the term-wise ADI-FDTD method is extended to the cylindrical coordinate system, which is different from the conventional ADI technique [129]. The algorithm is then validated by analyzing the resonant modes of a circular resonator. The discussions on the consumptions of computation resource, such as CPU time, memory usage, are also presented with comparison to the conventional FDTD method.

### 3.2        ADI Fundamentals

Consider solving the heat flow equation (3.1):

$$\frac{\partial u}{\partial t} = \frac{\partial^2 u}{\partial x^2} + \frac{\partial^2 u}{\partial y^2} \quad (3.1)$$

as a good example of parabolic differential equation, over the mesh superimposed on the rectangular region  $0 \leq x \leq a$ ,  $0 \leq y \leq b$ .

By using the same space-time notation as (2.4) in Chapter 2:

$$u^n(i, j) = u(x = i\Delta x, y = j\Delta y, t = n\Delta t) \quad (3.2)$$

a simple *explicit* finite-difference scheme for the solution may be written as:

$$\begin{aligned} \frac{u^{n+1}(i, j) - u^n(i, j)}{\Delta t} = & \frac{u^n(i+1, j) - 2u^n(i, j) + u^n(i-1, j)}{\Delta x^2} \\ & + \frac{u^n(i, j+1) - 2u^n(i, j) + u^n(i, j-1)}{\Delta y^2} \end{aligned} \quad (3.3)$$

The above explicit representation appears simple and straightforward for solutions. However, the method, where the field values at  $(n+1)$  time step  $u^{n+1}(i, j)$  can be recursively found from the field values  $u^n(i, j)$ , is constrained by the following CFL condition for stability:

$$\frac{1}{\Delta x^2} + \frac{1}{\Delta y^2} \leq \frac{1}{2\Delta t} \quad (3.4)$$

As a result,  $\Delta t$  has to be sufficiently small. It can make the method impractical since the marching iterations in time becomes too long for a solution to settle.

In the ADI approach, every time step is broken into two sub-steps, the  $(n+1/2)$ -th and the  $(n+1)$ -th steps. In the first half time step, the first second-order derivatives,  $\partial^2 u / \partial x^2$ , is approximated at the  $(n+1/2)$ -th iteration by the finite difference replacement and  $\partial^2 u / \partial y^2$  is replaced at the  $n$ -th iteration. In the second half time step, the second second-order derivatives,  $\partial^2 u / \partial y^2$ , is approximated at the  $(n+1)$ -th iteration by the finite difference replacement and  $\partial^2 u / \partial x^2$  is replaced at an intermediate  $(n+1/2)$ -th iteration. A set of simulation equations results. The equations are implicit in the  $x$ -direction at the  $(n+1/2)$ <sup>th</sup> time step, and in the  $y$ -direction at the  $(n+1)$ -th time step. More specifically, the two sub-computations are:

$$\frac{u^{n+\frac{1}{2}}(i,j) - u^n(i,j)}{\Delta t/2} = \frac{u^{n+\frac{1}{2}}(i+1,j) - 2u^{n+\frac{1}{2}}(i,j) + u^{n+\frac{1}{2}}(i-1,j)}{\Delta x^2} + \frac{u^n(i,j+1) - 2u^n(i,j) + u^n(i,j-1)}{\Delta y^2} \quad (3.5)$$

$$\frac{u^{n+1}(i,j) - u^{n+\frac{1}{2}}(i,j)}{\Delta t/2} = \frac{u^{n+\frac{1}{2}}(i+1,j) - 2u^{n+\frac{1}{2}}(i,j) + u^{n+\frac{1}{2}}(i-1,j)}{\Delta x^2} + \frac{u^{n+1}(i,j+1) - 2u^{n+1}(i,j) + u^{n+1}(i,j-1)}{\Delta y^2} \quad (3.6)$$

The above two sub-step computations are proven to be unconditionally stable with a procedure very similar to that used by O'Brien, Hyman, and Kaplan. The details can be found in reference [129].

By following the above procedure, the unconditionally stable ADI-FDTD algorithm in cartesian coordinate system was obtained, which was presented and numerically validated by analyzing a partially filled resonator in [130].

### 3.3 Development of the Cylindrical ADI-FDTD Algorithm

In order to broaden the applications of the ADI-FDTD method for efficient analysis of the non-rectangular electromagnetic structures and devices, the ADI-FDTD method is extended to the cylindrical coordinate system.

#### 3.3.1 Formulation of the Cylindrical ADI-FDTD Scheme

As stated in Chapter 2, in an isotropic source free medium of permittivity  $\varepsilon$ , and permeability  $\mu$ , the Maxwell's curl equations can be cast into six scalar partial differential equations in the cylindrical coordinates as shown in (3.7):

$$\varepsilon \frac{\partial E_r}{\partial t} = \frac{\partial H_z}{r \partial \phi} - \frac{\partial H_\phi}{\partial z} \quad (3.7a)$$

$$\varepsilon \frac{\partial E_\phi}{\partial t} = \frac{\partial H_r}{\partial z} - \frac{\partial H_z}{\partial r} \quad (3.7b)$$

$$\varepsilon \frac{\partial E_z}{\partial t} = \frac{\partial(rH_\phi)}{r\partial r} - \frac{\partial H_r}{r\partial \phi} \quad (3.7c)$$

$$-\mu \frac{\partial H_r}{\partial t} = \frac{\partial E_z}{r\partial \phi} - \frac{\partial E_\phi}{\partial z} \quad (3.7d)$$

$$-\mu \frac{\partial H_\phi}{\partial t} = \frac{\partial E_r}{\partial z} - \frac{\partial E_z}{\partial r} \quad (3.7e)$$

$$-\mu \frac{\partial H_z}{\partial t} = \frac{\partial(rE_\phi)}{r\partial r} - \frac{\partial E_r}{r\partial \phi} \quad (3.7f)$$

By applying the ADI principle to equation (3.7), the solution marching from the  $n$ -th time step to the  $(n+1)$ -th time step is broken up into two computational sub-advancements: the advancement from the  $n$ -th time step to the  $(n+1/2)$ -th time step and the advancement from the  $(n+1/2)$ -th time step to the  $(n+1)$ -th time step. For simplicity, take (3.7a) as an example. The two sub-step computations are:

- 1 at the  $(n+1/2)$ -th time step, the *first* partial derivative on the right-hand side of (3.7a),  $\partial H_z / (r\partial \phi)$ , is replaced with a difference approximation of its unknown pivotal values at the  $(n+1/2)$ th time step; while the *second* partial derivatives on the right-hand side,  $\partial H_\phi / \partial z$ , is replaced with a finite difference approximation in its known values at the previous  $n$ -th time step. In other words, equation (2.24a) becomes:

$$\frac{E_r^{n+1/2}(i+\frac{1}{2}, j, k) - E_r^n(i+\frac{1}{2}, j, k)}{\Delta t/2} = \frac{1}{\varepsilon} \left[ \frac{H_z^{n+1/2}(i+\frac{1}{2}, j+\frac{1}{2}, k) - H_z^{n+1/2}(i+\frac{1}{2}, j-\frac{1}{2}, k)}{\Delta \phi \cdot r(i+\frac{1}{2})} - \frac{H_\phi^n(i+\frac{1}{2}, j, k+\frac{1}{2}) - H_\phi^n(i+\frac{1}{2}, j, k-\frac{1}{2})}{\Delta z l(k)} \right] \quad (3.8)$$

- 2 at the  $(n+1)$ -th time step, the *second* term on the right-hand side,  $\partial H_\phi / \partial z$ , is replaced by a finite-difference approximation of its unknown pivotal values at  $(n+1)$ -th time step; while the *first* term,  $\partial H_z / (r\partial \phi)$ , is replaced with an explicit finite-difference approximation in its known values at the previous  $(n+1/2)$ -th time step. Similarly, equation (3.7a) becomes:

$$\frac{E_r^{n+1}(i+\frac{1}{2}, j, k) - E_r^{n+\frac{1}{2}}(i+\frac{1}{2}, j, k)}{\Delta t/2} = \frac{1}{\varepsilon} \left[ \frac{H_z^{n+\frac{1}{2}}(i+\frac{1}{2}, j+\frac{1}{2}, k) - H_z^{n+\frac{1}{2}}(i+\frac{1}{2}, j-\frac{1}{2}, k)}{\Delta \phi \cdot r(i+\frac{1}{2})} - \frac{H_\phi^{n+1}(i+\frac{1}{2}, j, k+\frac{1}{2}) - H_\phi^{n+1}(i+\frac{1}{2}, j, k-\frac{1}{2})}{\Delta z l(k)} \right] \quad (3.9)$$

Note that the above two sub-steps represent the alternations in the FDTD recursive computation directions in the sequence of the terms, the *first* and the *second* terms. They result in the implicit formulations as the right-hand sides of the equations now contain the field values which are unknown and need to be updated. The method is then termed “the Alternating Direction Implicit (ADI)” method.

Applying the same procedure to all the rest of the scalar differential equations as described in (2.25) and (2.26), one can obtain the complete set of the implicit unconditionally stable FDTD formula for general nonuniform grid, which is listed in Appendix A.

Note that the ADI-FDTD equations only consider nonuniform grid in  $r$  and  $z$  directions since all the structures analyzed in this thesis do not need nonuniform mesh in  $\phi$  direction. For the structures, such as radial waveguides, horn antennas, one may also take a nonuniform mesh in  $\phi$  direction if necessary. The medium parameters,  $\varepsilon$ ,  $\mu$  and  $\sigma$ , may also be replaced by  $\varepsilon(i, j, k)$ ,  $\mu(i, j, k)$  and  $\sigma(i, j, k)$  in case that the medium is not homogeneous in the computation domain.

Attention should be paid to the fact that there is no time-step difference (or lagging) between electric and magnetic field components in the formulations.

### 3.3.2 Advantages of the ADI Technique

The above ADI procedure is different from the conventional ADI procedure as appeared in [79-83]. In the conventional ADI procedure, the alternations in the computation direction are performed in each spatial coordinate direction, respectively. Therefore, the



computation for each temporal cycle (or each time step) is then broken into two sub-step computations in the two dimensional case [81]. In the three-dimensional case, the computation for each cycle is then broken up into three computational sub-steps [79] since there are three spatial coordinates,  $r$ ,  $\phi$  and  $z$ . In the proposed method, however, the number of the sub-steps is only *two* for each time step even in three dimensions. The reason is that in the proposed method, the ADI is applied in terms of the sequence of the terms on the right-hand side of the equations (the *first* and the *second* terms), rather than in terms of the coordinate directions. For instance, in equation (A-1a~A-1c), the magnetic field components  $H_z$ ,  $H_r$ , and  $H_\phi$ , which are involved in the first terms of the right-hand side, are implicitly computed in respect to the  $\phi$ ,  $z$  and  $r$  directions (mixed directions in the first sub-step), respectively, while the second terms of the right-hand side are all explicit for those equations. At the second sub-step, the first terms of the right-hand side in equation (3.11a-c),  $H_z$ ,  $H_r$ , and  $H_\phi$ , are computed explicitly while the second terms become implicit. The reduction in the number of the sub-steps certainly saves the computation time.

### 3.3.3 Efficient Computations of the ADI-FDTD Method

The unknown field components are coupled in equations (A-1)-(A-3) and are therefore, not easy to handle for computer programming. These equations may be rearranged more efficiently for computations. For instance, consider equation (A-1a) where both sides of the equations contain the unknown field components  $E_r^{n+\frac{1}{2}}$  and  $H_z^{n+\frac{1}{2}}$ . By substituting equation (A-1f) into equation (A-1a), one can obtain:

$$\begin{aligned}
& - \left( \frac{f}{\Delta \phi^2 r^2 (i + \frac{1}{2})} \right) E_r^{n+\frac{1}{2}}(i + \frac{1}{2}, j + 1, k) + \left( 1 + \frac{2f}{\Delta \phi^2 r^2 (i + \frac{1}{2})} \right) E_r^{n+\frac{1}{2}}(i + \frac{1}{2}, j, k) \\
& - \left( \frac{f}{\Delta \phi^2 r^2 (i + \frac{1}{2})} \right) E_r^{n+\frac{1}{2}}(i + \frac{1}{2}, j - 1, k) \\
& = E_r^n(i + \frac{1}{2}, j, k) + \frac{\Delta t}{2\varepsilon \Delta \phi r (i + \frac{1}{2})} \left[ H_z^n(i + \frac{1}{2}, j + \frac{1}{2}, k) - H_z^n(i + \frac{1}{2}, j - \frac{1}{2}, k) \right] \\
& - \frac{\Delta t}{2\varepsilon \Delta z l(k)} \left[ H_\phi^n(i + \frac{1}{2}, j, k + \frac{1}{2}) - H_\phi^n(i + \frac{1}{2}, j, k - \frac{1}{2}) \right] \\
& - \frac{f}{\Delta \phi r^2 (i + \frac{1}{2}) \Delta r 2(i + 1)} \left[ r(i + 1) (E_\phi^n(i + 1, j + \frac{1}{2}, k) - E_\phi^n(i + 1, j - \frac{1}{2}, k)) \right. \\
& \quad \left. - r(i) (E_\phi^n(i, j + \frac{1}{2}, k) - E_\phi^n(i, j - \frac{1}{2}, k)) \right] \tag{3.10}
\end{aligned}$$

In the above equation, all the field components on the right-hand side are of known values at the previous time steps, while the field components on the left-hand side are of the same field components,  $E_r$ , but at three adjacent grid points. The unknown variables are decoupled for computation.

The same decoupling procedures can be applied to equations (A-1)-(A-3) and similar equations can be obtained for the other field components. Full equations are listed in Appendix B.

The ADI implicit computation shown in (3.10) only applies to updating electric field components. The magnetic field components can be computed directly via (A-2d~A-2f) with the updated electric fields. This process can greatly save simulation time and memory consumption due to the reduced matrix calculation.

Equation (3.10) represents a system of linear equations with its coefficient matrix being a tridiagonal matrix. Therefore a special procedure can be applied. To be more general, equation (B-1a) can be written as:

$$-a_j u_{j-1} + b_j u_j - c_j u_{j+1} = d_j \tag{3.11}$$

where  $u_j$  represents  $E_r^{n+\frac{1}{2}}(i + \frac{1}{2}, j, k)$ ; a, b, c, and d represent corresponding known coefficient values in equation (B-1a).

Assume that  $j$  sweeps from 0 to  $N+1$ , and  $u_0 = 0$  and  $u_{N+1} = 0$  on the boundary. Application of equation (3.11) in the order of ascending  $j$  leads to a set of  $N$  simultaneous equations:

$$\left\{ \begin{array}{l} b_1 u_1 + c_1 u_2 = d_1 \\ a_2 u_1 + b_2 u_2 + c_2 u_3 = d_2 \\ \dots\dots\dots \\ a_r u_{r-1} + b_r u_r + c_r u_{r+1} = d_r \\ \dots\dots\dots \\ a_{N-1} u_{N-2} + b_{N-1} u_{N-1} + c_{N-1} u_N = d_{N-1} \\ a_N u_{N-1} + b_N u_N = d_N \end{array} \right. \quad (3.12)$$

from which  $N$  unknown values  $u_j$  ( $j = 1 \dots N$ ) can be determined.

The matrix expression of (3.12) can be given by

$$A u = d \quad (3.13)$$

where

$$A = \begin{bmatrix} b_1 & c_1 & 0 & \dots & 0 \\ a_2 & b_2 & c_2 & 0 & \dots & 0 \\ & & \dots & & & \\ & & a_r & b_r & c_r & \\ & & & \dots & & \\ 0 & \dots & 0 & a_{N-1} & b_{N-1} & c_{N-1} \\ 0 & \dots & & 0 & a_N & b_N \end{bmatrix}$$

$$u = [u_1 \quad u_2 \quad \dots \quad u_N]^T$$

$$d = [d_1 \quad d_2 \quad \dots \quad d_N]^T$$

Two different approaches can be used to solve the above equation:

#### A) Inverse matrix

The inverse matrix of  $\mathbf{A}$  can be directly obtained with many software packages. Once it is obtained, it may be used only once to get the field values at the left-most grid point, say  $u_1$ . Forward substitutions of  $u_1$  can then be applied in (3.12) to find the other components. More specifically, if  $u_1$  is found, then from (3.12):

$$u_2 = -\frac{1}{c_1}(d_1 - bu_1) \quad (3.14)$$

The rest of  $u$ 's can subsequently be calculated by applying (3.11):

$$u_{j+1} = -\frac{1}{c_j}(d_j - b_j u_j + a_j u_{j-1}) \quad (3.15)$$

with ascending  $j$  that allows one to find  $u_{j+1}$  from  $u_j$  and  $u_{j-1}$ . In such a way, for the most of the computations, we avoid the repetitive applications of  $\mathbf{A}^{-1}$ .

#### B) Direct Solution

Alternatively, by using the Gaussian elimination method,  $u$  can be obtained directly without involvement of  $\mathbf{A}^{-1}$ . Hence, time consuming calculation  $\mathbf{A}^{-1}$  can be totally avoided.

Our experiences show that, for a linear, lossless and isotropic medium, approach A) is more efficient because  $\mathbf{A}^{-1}$  is only calculated once and then used in each time step advance with only the first row of  $\mathbf{A}^{-1}$  is needed. However, method B) can be used when the matrix  $\mathbf{A}$  is too big to obtain its inverse matrix directly with software packages.

### **3.4 Numerical Verification of the ADI-FDTD Algorithm**

To demonstrate the validity of the proposed ADI-FDTD method, a simple cylindrical cavity resonator [130], as shown in Figure 3.1, is computed with both conventional

FDTD method and the cylindrical ADI-FDTD method. The radius of the cavity resonator is 3.995 centimeters and the height is 7.910 centimeters. The cavity is discretized with a uniform grid of  $16 \times 16 \times 15$  mesh along  $r$ ,  $\phi$  and  $z$ , respectively, for both conventional FDTD and the cylindrical ADI-FDTD method. The electric field  $E_z$  is recorded at the grid point (8,8,10) in both methods. By using equation (2.15), the maximum time step  $\Delta t_{\max}$  (or the CFL limit) was computed and found to be 2.2394 picoseconds for the conventional cylindrical FDTD method.

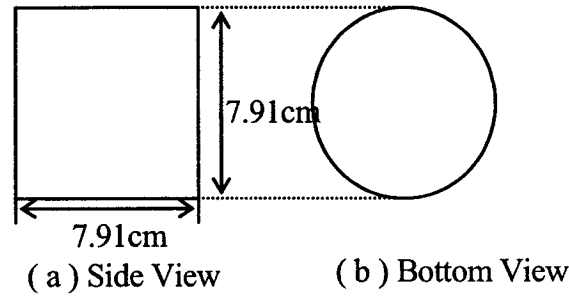


Figure 3.1 The geometry of the resonator cavity (dimensions in centimeter)

A time step  $\Delta t_{FDTD} = \Delta t_{\max} = 2.2394 ps$  and a larger time step  $\Delta t_{ADI-FDTD} = 4 \times \Delta t_{FDTD} = 8.9576 ps$  were chosen for FDTD and ADI-FDTD, respectively. The experiment was conducted on an AMD-Athlon 950 computer. To ensure that the same physical time is simulated, simulations were run of 20,000 iterations and of 5,000 iterations with FDTD and ADI-FDTD methods respectively, since the time step with the ADI-FDTD method is four times of that with FDTD method. Table 1 shows the resonant frequencies computed with both methods. It can be seen that the errors for both methods are comparable.

**Table 1 Resonant Frequencies Computed with the  
Conventional FDTD and the ADI-FDTD**

Analytical Results (GHz)	Conventional FDTD		Proposed ADI-FDTD Scheme	
	Simulation Results (GHz)	Relative Error (%)	Simulation Results (GHz)	Relative Error (%)
3.425	3.469	1.28	3.436	0.32
4.576	4.597	0.46	4.592	0.35
4.950	4.969	0.38	4.959	0.18
6.590	6.417	2.63	6.481	1.65

To further compare the cylindrical ADI-FDTD method with the conventional FDTD method, another experiment was executed by comparing the CPU time of the simulations and the memory consumption.

Since the Yee's grid is used with the ADI-FDTD method, the number of field components at all the grid points are the same as that with the conventional FDTD. However, due to the fact that  $E$  and  $H$  field components are not interlaced in time anymore, the memory requirement for storing the field components is almost double that for the conventional FDTD method as indicated in equations in Appendix B.

Since more components are involved in the recursive computation, the CPU time for each time step with the ADI-FDTD is then larger than that with the conventional FDTD method. However, because a larger time step can be used with the ADI-FDTD, the total number of iterations required with the ADI-FDTD could be reduced. In our case, the CPU time for the two methods is 205.72 seconds with conventional FDTD and 61.54 seconds with the proposed method. Roughly speaking that a saving factor of 3~4 was obtained with the proposed method in CPU time in this case.

### 3.5 Conclusions

In this Chapter, a new three-dimensional cylindrical ADI-FDTD free of the CFL stability condition is presented for solving electromagnetic problems. In the new scheme, the Yee's grid is used with the application of the alternative direction implicit technique in formulating the algorithm. As a result, the memory requirement is about twice that for the conventional FDTD while the time step is no longer restricted by the numerical stability. In comparison with earlier ADI work reported by reference [79], the proposed ADI-FDTD reduces the number of sub-steps by a factor of three to four, which means 33% time saving in a single run.

Numerical verifications are presented to demonstrate the validity of the proposed method without the CFL condition. Preliminary experiments indicated that with the same accuracy, the proposed method uses four times fewer of iterations and is 3.2 times faster

than the conventional FDTD. Parts of this chapter have been published in the technical journal [131].

## CHAPTER 4    A NOVEL METHOD FOR THE ANALYSIS OF NUMERICAL STABILITY

### 4.1 Introduction

For any time-stepping numerical method, stability is one of the important characteristics that need be taken into account. As stated in Chapter 2, the FDTD algorithm requires that the time step increment  $\Delta t$  be less than a specific upper bound defined by material properties and the space increments  $\Delta r$ ,  $\Delta \phi$ , and  $\Delta z$ . If the condition is not satisfied, the computed field values will eventually increase to infinity as an FDTD simulation recursively marches in time.

The proposed cylindrical ADI-FDTD algorithm in Chapter 3 has been numerically validated for its stability by taking larger time steps than CFL conditions of the conventional FDTD. A theoretical proof is needed to provide the rigorousness.

Although F. Zheng and Z. Chen have presented a technique to prove the stability by finding the eigenvalues of the matrix form of the ADI-FDTD [132], it is not always easy to evaluate the eigenvalues. For instance, in our case of the cylindrical ADI-FDTD, complex special functions, such as Bessel functions, are involved. In this chapter, a new method for analyzing the numerical stability is presented which circumvents the difficulty in obtaining the explicit expressions of the eigenvalues. The method utilizes the so called *SCHUR-COHN-FUJIWA* criterion. Details are provided in the following sections.

### 4.2        *SCHUR-COHN-FUJIWA* Criterion

In the 1910s, A.Cohn and I. Schur proposed a series of methods for solving the stability and root-clustering problems in terms of positive definite symmetric matrices [133][134]. Based on their work, H. Fujiwara presented SCF criterion in 1924 [135].



Consider an  $n^{\text{th}}$ -order polynomial expressed in the following form:

$$F(z) = \sum_{i=0}^n a_i z^i \quad a_n > 0 \quad (4.1)$$

with  $a_i$  being a real number. Then an associated  $n \times n$  symmetric matrix  $C = [\gamma_{ij}]$  can be constructed with the element:

$$\gamma_{ij} = \sum_{p=1}^{\min(i,j)} (a_{n-i+p} a_{n-j+p} - a_{i-p} a_{j-p}) \quad (4.2)$$

For instance:

$$F(z) = a_3 z^3 + a_2 z^2 + a_1 z + a_0 \quad a_n > 0 \quad (4.3)$$

the constructed symmetric matrix  $C$  is:

$$\begin{vmatrix} a_3^2 - a_0^2 & a_2 a_3 - a_1 a_0 & a_1 a_3 - a_2 a_0 \\ a_2 a_3 - a_1 a_0 & a_3^2 + a_2^2 - a_0^2 - a_1^2 & a_2 a_3 - a_1 a_0 \\ a_1 a_3 - a_2 a_0 & a_2 a_3 - a_1 a_0 & a_3^2 - a_0^2 \end{vmatrix} \quad (4.4)$$

the *SCHUR-COHN-FUJIWA* criterion states that the number of the roots of  $F(z)$  for which  $|z_i| < 1$  is equal to the number of positive eigenvalues of symmetric matrix  $C$ ; the number of the roots of  $F(z)$  for which  $|z_i| > 1$  is equal to the number of negative eigenvalues of symmetric matrix  $C$ ; the number of the roots of  $F(z)$  for which  $|z_i| = 1$  is equal to the number of zero eigenvalues of symmetric matrix  $C$ .

Note that the coefficients of the  $n^{\text{th}}$ -order polynomial should be strictly of real values and greater than zero. The constructed matrix has the symmetric property so that the properties of the  $n^{\text{th}}$ -order polynomial matrix can be obtained by analyzing the associated symmetric matrix. In cases where the explicit expressions of the roots of the  $n^{\text{th}}$ -order polynomial are not easy to be obtained, the criterion can effectively analyze the property of the roots by analyzing the associated symmetric matrix.

In the stability analysis of a certain dynamic system,  $F(z)$  normally represents the characteristic function of the system. The system is then stable if and only if all the roots of  $F(z)$  are inside the unit circle, correspondingly, all the eigenvalues of  $C$  should be all larger than or equal to zero.

### 4.3 Analytical Proof of the Unconditional Stability of the Cylindrical ADI-FDTD Method

With the *SCHUR-COHN-FUJIWA* criterion, the unconditional stability of the cylindrical ADI-FDTD can be proven as described below.

In the cylindrical coordinate system, the six electric and magnetic field components in an isotropic medium in the spatial spectral domain can always be expressed as [136]:

$$\begin{aligned} E_r \Big|_{i+\frac{1}{2},m,k}^n &= E_r^n B_p(k_r(i+\frac{1}{2})\Delta r) e^{jpm\Delta\phi} e^{jk_z k \Delta z} \\ E_\phi \Big|_{i,m+\frac{1}{2},k}^n &= E_\phi^n B_p(k_r i \Delta r) e^{jp(m+\frac{1}{2})\Delta\phi} e^{jk_z k \Delta z} \\ E_z \Big|_{i,m,k+\frac{1}{2}}^n &= E_z^n B_p(k_r i \Delta r) e^{jpm\Delta\phi} e^{jk_z(k+\frac{1}{2})\Delta z} \end{aligned} \quad (4.5a)$$

$$\begin{aligned} H_r \Big|_{i,m+\frac{1}{2},k+\frac{1}{2}}^n &= H_r^n B_p(k_r i \Delta r) e^{jp(m+\frac{1}{2})\Delta\phi} e^{jk_z(k+\frac{1}{2})\Delta z} \\ H_\phi \Big|_{i+\frac{1}{2},m,k+\frac{1}{2}}^n &= H_\phi^n B_p(k_r(i+\frac{1}{2})\Delta r) e^{jpm\Delta\phi} e^{jk_z(k+\frac{1}{2})\Delta z} \\ H_z \Big|_{i+\frac{1}{2},m+\frac{1}{2},k}^n &= H_z^n B_p(k_r(i+\frac{1}{2})\Delta r) e^{jp(m+\frac{1}{2})\Delta\phi} e^{jk_z \Delta z} \end{aligned} \quad (4.5b)$$

where  $B_p(k_r, r)$  is the appropriate  $p^{th}$  order Bessel function,  $\Delta r$ ,  $\Delta\phi$  and  $\Delta z$  are the space steps in radial, angular and z-direction, respectively.  $k_r$ ,  $k_z$  are the spectral frequencies in radial and axial directions, respectively.

Note that the mesh is assumed to be uniform for simplicity. By substituting the above expressions into the cylindrical ADI-FDTD equations in Appendix A, one can have two sets of matrix expression for each of the two sub time- steps respectively:

$$M_1 X^{n+\frac{1}{2}} = P_1 X^n \quad (4.6a)$$

$$M_2 X^{n+1} = P_2 X^{n+\frac{1}{2}} \quad (4.6b)$$

where:

$$X^n = \begin{bmatrix} E_r^n \\ E_\phi^n \\ E_z^n \\ H_r^n \\ H_\phi^n \\ H_z^n \end{bmatrix} \quad (4.7)$$

$$M_1 = \begin{bmatrix} 1 & 0 & 0 & 0 & 0 & -\frac{jW_\phi}{\varepsilon(i+\frac{1}{2})\Delta r} \\ 0 & 1 & 0 & -\frac{jW_z}{\varepsilon} & 0 & 0 \\ 0 & 0 & 1 & 0 & \frac{b_2}{\varepsilon} & 0 \\ 0 & -\frac{jW_z}{\mu} & 0 & 1 & 0 & 0 \\ 0 & 0 & -\frac{b_3}{\mu} & 0 & 1 & 0 \\ -\frac{jW_\phi}{\mu(i+\frac{1}{2})\Delta r} & 0 & 0 & 0 & 0 & 1 \end{bmatrix} \quad (4.8)$$

$$M_2 = \begin{bmatrix} 1 & 0 & 0 & 0 & \frac{jW_z}{\varepsilon} & 0 \\ 0 & 1 & 0 & -\frac{jW_z}{\varepsilon} & 0 & \frac{b_1}{\varepsilon} \\ 0 & 0 & 1 & \frac{jW_\phi}{\varepsilon i \Delta r} & 0 & 0 \\ 0 & 0 & \frac{jW_\phi}{\mu i \Delta r} & 1 & 0 & 0 \\ \frac{jW_z}{\mu} & 0 & 0 & 0 & 1 & 0 \\ 0 & -\frac{b_4}{\mu} & 0 & 0 & 0 & 1 \end{bmatrix} \quad (4.9)$$

$$P_1 = \begin{bmatrix} 1 & 0 & 0 & 0 & -\frac{jW_z}{\varepsilon} & 0 \\ 0 & 1 & 0 & -\frac{jW_z}{\varepsilon} & 0 & -\frac{b_1}{\varepsilon} \\ 0 & 0 & 1 & -\frac{jW_\phi}{\varepsilon i \Delta r} & 0 & 0 \\ 0 & 0 & -\frac{jW_\phi}{\mu i \Delta r} & 1 & 0 & 0 \\ -\frac{jW_z}{\mu} & 0 & 0 & 0 & 1 & 0 \\ 0 & \frac{b_4}{\mu} & 0 & 0 & 0 & 1 \end{bmatrix} \quad (4.10)$$

$$P_2 = \begin{bmatrix} 1 & 0 & 0 & 0 & 0 & \frac{jW_\phi}{\varepsilon(i + \frac{1}{2})\Delta r} \\ 0 & 1 & 0 & \frac{jW_z}{\varepsilon} & 0 & 0 \\ 0 & 0 & 1 & 0 & -\frac{b_2}{\varepsilon} & 0 \\ 0 & \frac{jW_z}{\mu} & 0 & 1 & 0 & 0 \\ 0 & 0 & \frac{b_3}{\mu} & 0 & 1 & 0 \\ \frac{jW_\phi}{\mu(i + \frac{1}{2})\Delta r} & 0 & 0 & 0 & 0 & 1 \end{bmatrix} \quad (4.11)$$

in which:

$$W_\phi = \frac{\Delta t \sin(n\Delta\phi)}{\Delta\phi}, W_z = \frac{\Delta t \sin(k_z \Delta z)}{\Delta z} \quad (4.12)$$

$$b1 = \frac{\Delta t \left[ B_n[k_r(i + \frac{1}{2})\Delta r] - B_n[k_r(i - \frac{1}{2})\Delta r] \right]}{2\Delta r B_n(k_r, i\Delta r)} \quad (4.13a)$$

$$b2 = \frac{\Delta t \left[ (i + \frac{1}{2})B_n[k_r(i + \frac{1}{2})\Delta r] - (i - \frac{1}{2})B_n[k_r(i - \frac{1}{2})\Delta r] \right]}{2\Delta r i B_n(k_r, i\Delta r)} \quad (4.13b)$$

$$b3 = \frac{\Delta t [B_n[k_r(i + 1)\Delta r] - B_n(k_r, i\Delta r)]}{2\Delta r B_n(k_r, (i + \frac{1}{2})\Delta r)} \quad (4.13c)$$

$$b4 = \frac{\Delta t [(i + 1)B_n[k_r(i + 1)\Delta r] - iB_n(k_r, i\Delta r)]}{2\Delta r (i + \frac{1}{2})B_n(k_r, i\Delta r)} \quad (4.13d)$$

By rearranging (4.6), the field components can be solved via:

$$X^{n+\frac{1}{2}} = M_1^{-1} P_1 X^n \quad (4.14a)$$

$$X^{n+1} = M_2^{-1} P_2 X^{n+\frac{1}{2}} \quad (4.14b)$$

or simply

$$X^{n+1} = \Lambda X^{n+\frac{1}{2}} \quad (4.15)$$

with  $\Lambda = M_2^{-1} P_2 M_1^{-1} P_1$ .

By checking the magnitudes of the eigenvalues of  $\Lambda$ , one can determine whether the proposed scheme is unconditionally stable or not: if the magnitudes of all the eigenvalues of  $\Lambda$  are equal to or less than unity, the proposed scheme is unconditionally stable, otherwise is potentially unstable.

The expression of  $\Lambda$  can be obtained by a mathematical software, such as Maple V used in our case. However, it is difficult to find the symbolic expressions of the eigenvalues of  $\Lambda$  directly. Therefore, *SCHUR-COHN-FUJIWA* criterion is employed here to analyze the roots of the characteristic function of  $\Lambda$ , which are the eigenvalues of  $\Lambda$ .

By using Maple V, the characteristic polynomial of  $\Lambda$  in our case can be found to be a 6<sup>th</sup>-order polynomial ( $n=6$ ):

$$Z^6 + B_5 Z^5 + B_4 Z^4 + B_3 Z^3 + B_2 Z^2 + B_1 Z + 1 = 0 \quad (4.16)$$

where  $B_3=A_3/A_6$ ,  $B_4=A_4/A_6$ ,  $B_5=A_5/A_6$ ,  $B_\alpha$  ( $\alpha=3,4,5$ ) is the coefficient of the characteristic polynomial. The expressions of  $A_3$ ,  $A_4$ ,  $A_5$  and  $A_6$  are shown in Appendix C.

To effect *SCHUR-COHN-FUJIWA* criterion, the coefficients  $B_\alpha$  ( $\alpha=3,4,5$ ) should be firstly proved to be of real values. By observing the symbolic expressions of the roots obtained by Maple V, it is found that all the roots can be expressed as:

$$B_\alpha = f(\varepsilon, \mu, W_\phi, W_z, b_1, b_2, b_3, b_4) \quad (4.17)$$

in which the expressions of all the parameters in function  $f$  are shown in (4.12)~(4.13).

In the above expressions, the only term that could be of complex values is Bessel function  $B_n$ .  $B_n$  can be the first, second, third and fourth kinds of the Bessel function depending on wave propagation direction. When it is the first or second kind of Bessel function,  $J_n$  (the first kind of Bessel function) or  $Y_n$  (the second kind of Bessel function), both functions are of real values when  $k_r$  is a real number. This can be easily seen from the series expansions of the two Bessel functions. When  $B_n$  is the third or fourth kind of Bessel function, or simply the first or second kind of Hankel function  $H_v^{(1)}(z)$ , or  $H_v^{(2)}(z)$ , they can be expressed as:

$$H_v^{(1)}(z) = \frac{J_{-v}(z) - e^{jv\pi} J_v(z)}{i \sin v\pi} \quad (4.18a)$$

$$H_v^{(2)}(z) = \frac{e^{jv\pi} J_v(z) - J_{-v}(z)}{j \sin v\pi} \quad (4.18b)$$

where  $v$  and  $z$  are both real number.  $v$  has to be an integer because electromagnetic fields in an isotropic medium has either  $\sin(n\phi)$  or  $\cos(n\phi)$  variations in the angular direction. Under this circumstance,  $J_{-n}(z)$  is equal to  $(-1)^n J_n(z)$  ( $n$  is an interger).

By substituting  $(-1)^n J_n(z)$  for  $J_{-n}(z)$  and replacing the Bessel function  $B_n$  in  $b1$ , for instance, with the first kind of Hankel function  $H_v^{(1)}(z)$ ,

$$\begin{aligned} b1 &= \lim_{v \rightarrow n} \frac{\Delta r \left[ \left( (-1)^n - e^{jn\pi} \right) J_v \left[ k_r \left( i + \frac{1}{2} \right) \Delta r \right] - \left( (-1)^n - e^{jn\pi} \right) J_v \left[ k_r \left( i - \frac{1}{2} \right) \Delta r \right] \right]}{2 \Delta r \left( (-1)^n - e^{jn\pi} \right) J_n(k_r i \Delta r)} \\ &= \frac{\Delta r \left[ J_n \left[ k_r \left( i + \frac{1}{2} \right) \Delta r \right] - J_n \left[ k_r \left( i - \frac{1}{2} \right) \Delta r \right] \right]}{2 \Delta r J_n(k_r i \Delta r)} \end{aligned} \quad (4.19a)$$

Similarly, expressions for  $b2$ ,  $b3$  and  $b4$  can be obtained as:

$$b_2 = \frac{\Delta t \left[ \left(i + \frac{1}{2}\right) J_n \left[ k_r \left(i + \frac{1}{2}\right) \Delta r \right] - \left(i - \frac{1}{2}\right) J_n \left[ k_r \left(i - \frac{1}{2}\right) \Delta r \right] \right]}{2 \Delta r i J_n(k_r i \Delta r)} \quad (4.19b)$$

$$b_3 = \frac{\Delta t \left[ J_n[k_r(i+1)\Delta r] - J_n(k_r i \Delta r) \right]}{2 \Delta r J_n \left( k_r \left(i + \frac{1}{2}\right) \Delta r \right)} \quad (4.19c)$$

$$b_4 = \frac{\Delta t \left[ (i+1) J_n[k_r(i+1)\Delta r] - i J_n(k_r i \Delta r) \right]}{2 \Delta r \left(i + \frac{1}{2}\right) J_n(k_r i \Delta r)} \quad (4.19d)$$

Obviously,  $b_1$ ,  $b_2$ ,  $b_3$  and  $b_4$  are of real value. The same conclusions can be drawn if the Bessel function  $B_n$  is the second kind of Hankel function  $H_v^{(2)}(z)$ .

Once  $b_1$ ,  $b_2$ ,  $b_3$  and  $b_4$  are shown to be of real value,  $A_\alpha$  ( $\alpha = 3, 4, 5, 6$ ), and therefore  $B_\alpha$  ( $\alpha = 3, 4, 5$ ) are of real values. In other words, the six coefficients of the characteristic polynomial are of real values no matter which kind of Bessel function is under consideration.

Equation (4.16) is a polynomial with coefficient symmetry: the coefficient for the 6<sup>th</sup>-order term is the same as that for the 0<sup>th</sup>-order term, the coefficient for the 5<sup>th</sup>-order term is the same as that for the 1<sup>st</sup>-order term, and the coefficient for the 4<sup>th</sup>-order term is the same as that for the 2<sup>nd</sup>-order term. By using equation (4.2) the corresponding C matrix can be found as:

$$C = \begin{bmatrix} 0 & 0 & 0 & 0 & 0 & 0 \\ 0 & 0 & 0 & 0 & 0 & 0 \\ 0 & 0 & 0 & 0 & 0 & 0 \\ 0 & 0 & 0 & 0 & 0 & 0 \\ 0 & 0 & 0 & 0 & 0 & 0 \\ 0 & 0 & 0 & 0 & 0 & 0 \end{bmatrix} \quad (4.20)$$

Obviously all the eigenvalues of C are then zeros. As stated in *Schur-Cohn-Fujiwa* criterion, it means that all the roots of (4.9), that are also the eigenvalues of  $\Lambda$ , reside on



the unit circle. Therefore, the magnitudes of all the roots or eigenvalues are equal to unity. In other words, the cylindrical ADI-FDTD proposed possesses to the unconditional stability regardless of the time step  $\Delta t$ . The CFL stability condition is thus removed.

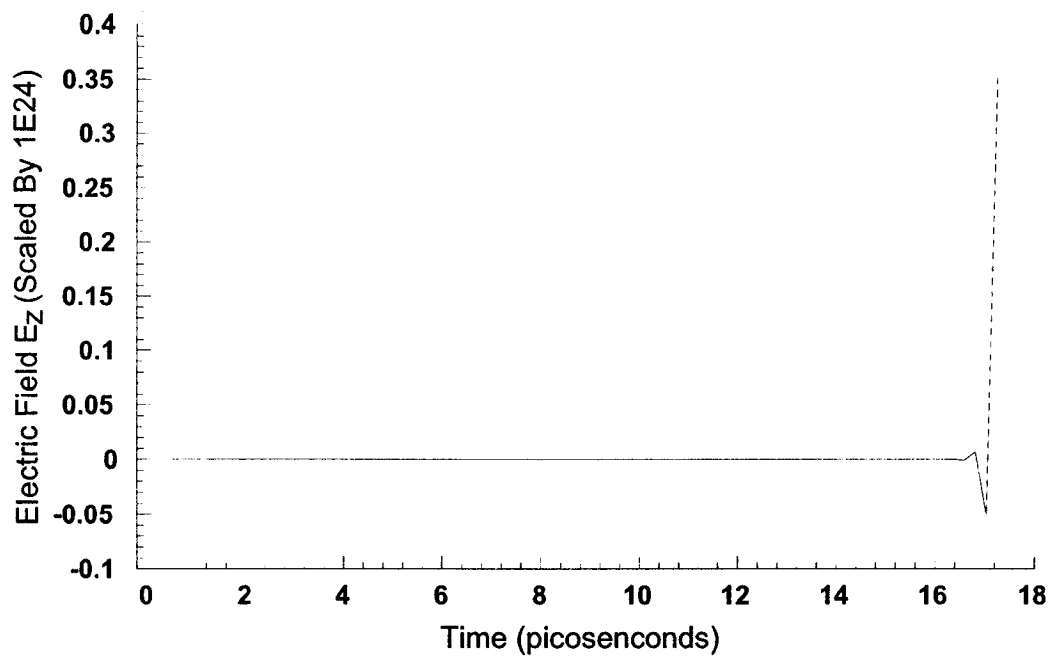
The above method may also be applied to the ADI-FDTD algorithms in the other coordinate systems as well as two dimensional cases with similar procedure. In addition, *Schur-Cohn-Fujiwa* criterion may also be employed to obtain the CFL condition with conventional FDTD by forcing all the eigenvalues residing in the unit circle.

#### 4.4 Numerical Experiments on Unconditional Stability

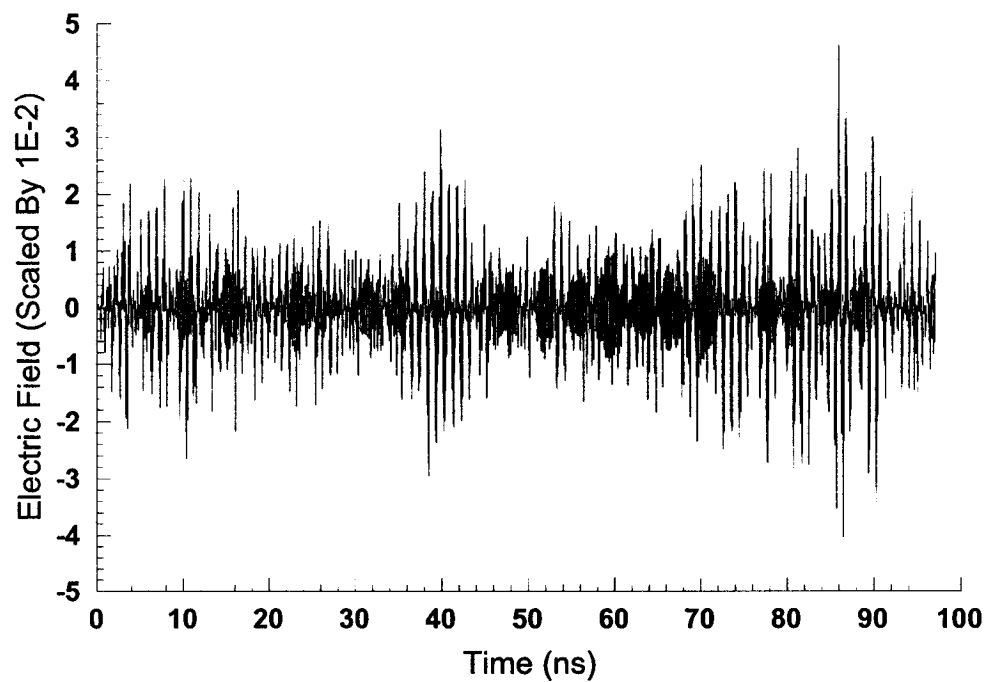
The ADI-FDTD is theoretically proven unconditionally stable in three-dimensional cylindrical coordinates. The CFL condition is completely removed. To further reinforce such a proof, numerical verification is carried out to confirm the result. In the following sections, the numerical validations are presented. A study on time step selection without CFL condition is also made with respect to the numerical errors. The preliminary error analysis shows that the time step in ADI-FDTD is now limited by modeling accuracy and the Nyquist sampling rate.

##### 4.4.1 Numerical Verification of the Unconditional Stability

Numerical experiments were run for the circular cavity again with both the conventional FDTD and the cylindrical ADI-FDTD having a time step that exceeds the limit  $\Delta t_{FDTDMAX}$ , defined by the CFL condition (2.14). The time step is chosen as  $1.5 \times \Delta t_{FDTDMAX}$  with the conventional cylindrical FDTD, which is  $\Delta t_{FDTDMAX} = 3.3591 ps$  and  $100 \times \Delta t_{FDTDMAX}$  with the proposed cylindrical ADI-FDTD, which is  $\Delta t_{ADI-FDTD} = 223.94 ps$ . Figure (4.1) shows the simulation results. As can be seen, solution of the conventional cylindrical FDTD explodes very quickly, while the solution of the cylindrical ADI-FDTD remains stable. Longer simulation periods with even larger time steps were taken as well, and no instability was observed. This shows numerically the proposed scheme is indeed unconditionally stable.



( a ) Conventional FDTD with the time step being 1.5 times of the CFL limit



( b ) ADI-FDTD with the time step being 100 times of the CFL limit

Figure 4.1 Electric field  $E_z$  recorded in time domain with the time steps larger than the CFL limit

#### 4.4.2 Numerical Accuracy with Different Time Steps

As shown by now, the time-step of cylindrical ADI-FDTD method is no longer restricted by the CFL condition. It should be determined only by the modeling accuracy. Therefore, it is useful to investigate the relation between the time step and the numerical accuracy.

Table 1 presents the simulation results for the  $TE_{011}$  mode of the cavity. With the increase of the time steps, relative computation error with the cylindrical ADI-FDTD increases. This property is also plotted in Figure 4.2.

**Table 1 Simulation Results with Different Time Steps**

Analytical Solution (GHz)	Simulation results with the proposed cylindrical ADI-FDTD scheme					
	$\Delta t=4\Delta t_{\max}$		$\Delta t=8\Delta t_{\max}$		$\Delta t=12\Delta t_{\max}$	
	Resonant frequency (GHz)	Relative error (%)	Resonant frequency (GHz)	Relative error (%)	Resonant frequency (GHz)	Relative error (%)
4.9497	4.960	+0.21	4.920	-0.60	4.916	-0.68

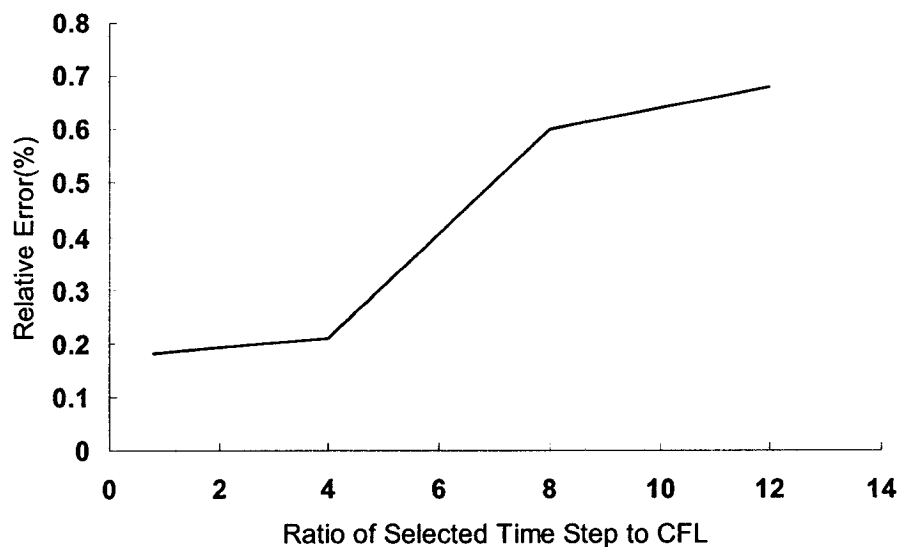


Figure 4.2 Relative error of the proposed scheme with various time steps

## 4.5 Conclusions

In this chapter, the unconditional stability of the proposed cylindrical ADI-FDTD has been proven analytically and illustrated numerically. A new method is firstly introduced into computational electromagnetics for stability analysis. Numerical results also show

that the proposed scheme is indeed stable even when a time step is a hundred times the CFL limit of the conventional FDTD. It can be expected that because of the removal of the CFL constraint on time step, various efficient modeling techniques, such as multigridding scheme, can be implemented in an easier way than before [64].

With the CFL limit removed in ADI-FDTD, the time step of ADI-FDTD is no longer restricted by the numerical stability but by the modeling accuracy of the algorithm and the Nyquist sampling limit.

As the cylindrical ADI-FDTD scheme has been validated, it is desired to apply the cylindrical ADI-FDTD algorithm to microwave structures. In the next two chapters, closed structures and open structures will be studied with the proposed method.

## **Chapter 5    ADI-FDTD MODELING OF CLOSED STRUCTURES**

### **5.1        Introduction**

The unconditional stability of the ADI-FDTD algorithm has been formulated and tested in the above chapters. The simple numerical experiments in chapter 4 show that the proposed method is suitable for analyzing microwave structures and devices with the advantages of less simulation time and free of CFL condition over the conventional FDTD method. In the following chapters, the applications of the ADI-FDTD methods to different microwave structures will be shown. The advantages of the proposed methods will be demonstrated.

In general, microwave structures and devices can be categorized into two primary types: closed structures and open structures. Closed structures refer to the structures enclosed by perfect electric conductor (PEC) walls, while open structures are the structures that are not enclosed by the PEC walls or partially enclosed by PEC walls. In this chapter, several selected closed structures, including a circular rod resonator, a circular disk resonator and a circular resonator filled with lossy dielectric material, are numerically analyzed with the cylindrical ADI-FDTD method. The highly conductive materials, which can not be well solved with the conventional FDTD method, are also analyzed with the proposed method. The advantages of ADI-FDTD method are then shown by analyzing these structures.

### **5.2        Approximation of Medium Parameters in ADI-FDTD Algorithm**

As shown in the Maxwell's curl equations, there are three medium parameters: permittivity  $\epsilon$ , permeability  $\mu$ , and conductivity  $\sigma$ . The conventional Yee's FDTD algorithm presented in the previous chapters is applicable to the arbitrary isotropic

inhomogeneous materials. However, it is desired to consider the inhomogeneous case to broaden the applicability of the cylindrical ADI-FDTD method.

Figure 5.1 illustrates a part of mesh including four nonuniform cells that are on the same surface of S. It is assumed that the primary edge passing through the centroid of S is tangential to the interface of a boundary shared by the four materials of  $\epsilon_1, \mu_1, \sigma_1$ ,  $\epsilon_2, \mu_2, \sigma_2$ ,  $\epsilon_3, \mu_3, \sigma_3$  and  $\epsilon_4, \mu_4, \sigma_4$ . The medium parameters in each cell remain constant. On the surface S, Ampere's Law can be expressed as:

$$\sum_{i=1}^4 \left( \frac{\partial}{\partial t} \iint_{S_i} \epsilon_i \vec{E} \cdot d\vec{s} + \iint_{S_i} \sigma_i \vec{E} \cdot d\vec{s} \right) = \sum_{i=1}^4 \left( \oint_{C_i} \vec{H} \cdot d\vec{l} \right) \quad (5.1)$$

where  $S_i$  is the surface of each cell that is bounded by the contour  $C_i$ . The integrals are then performed over each  $S_i$  and the bounding  $C_i$ . For example, in  $S_1$  we have:

$$\epsilon_1 A_1 \left( \frac{\vec{E}_1^{n+1} - \vec{E}_1^n}{\Delta t} \right) \cdot \hat{n} + \sigma_1 A_1 \left( \frac{\vec{E}_1^{n+1} + \vec{E}_1^n}{2} \right) \cdot \hat{n} = \left( l'_1 H_1^{n+\frac{1}{2}} - l'_{12} H_{12}^{n+\frac{1}{2}} - l'_{41} H_{41}^{n+\frac{1}{2}} + l'_4 H_4^{n+\frac{1}{2}} \right) \quad (5.2)$$

where  $\vec{E}_1$  is the electric field in  $S_1$ ,  $\hat{n}$  is the unit normal, and  $A_1$  is the area of  $S_1$ . Similar expressions can be derived for the remaining three regions.

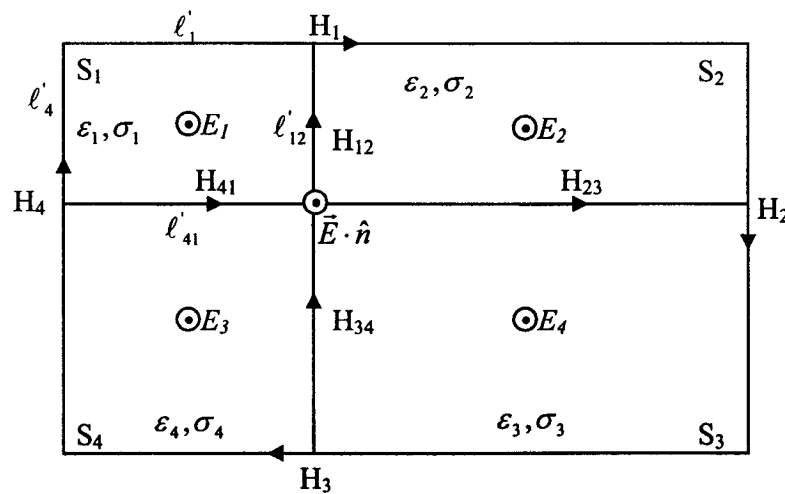


Figure 5.1 Interfaces of an inhomogeneous medium

With the assumption that  $\hat{n}$  is tangential to the boundary interface, the Maxwell boundary condition of continuity of the tangential electric field across an interface yields:

$$\vec{E}_1 \cdot \hat{n} \approx \vec{E}_2 \cdot \hat{n} \approx \vec{E}_3 \cdot \hat{n} \approx \vec{E}_4 \cdot \hat{n} \approx \vec{E} \cdot \hat{n} \quad (5.3)$$

Adding the four equations in (5.1) results in the expression:

$$\begin{aligned} & (\varepsilon_1 A_1 + \varepsilon_2 A_2 + \varepsilon_3 A_3 + \varepsilon_4 A_4) \left( \frac{\vec{E}^{n+1} - \vec{E}^n}{\Delta t} \right) \cdot \hat{n} \\ & + (\sigma_1 A_1 + \sigma_2 A_2 + \sigma_3 A_3 + \sigma_4 A_4) \left( \frac{\vec{E}^{n+1} + \vec{E}^n}{\Delta t} \right) \cdot \hat{n} \\ & = \left( \vec{l}_1 H_1^{n+\frac{1}{2}} + \vec{l}_2 H_2^{n+\frac{1}{2}} + \vec{l}_3 H_3^{n+\frac{1}{2}} + \vec{l}_4 H_4^{n+\frac{1}{2}} \right) \end{aligned} \quad (5.4)$$

This permits the definition of the weighted-average permittivity and conductivity:

$$\varepsilon_{avg} = \frac{\left( \sum_{i=1}^N A_i \varepsilon_i \right)}{\left( \sum_{i=1}^N A_i \right)}; \quad \sigma_{avg} = \frac{\left( \sum_{i=1}^N A_i \sigma_i \right)}{\left( \sum_{i=1}^N A_i \right)} \quad (5.5)$$

where  $A_i$  is the area of region  $S_i$ .

Equation (5.5) gives the effective permittivity and conductivity at inhomogeneous interfaces shown in Figure 5.1. Although this equation is derived using conventional FDTD, it is also applicable to ADI-FDTD method.

### 5.3 Modified ADI-FDTD Algorithm for Solving Highly Conductive Materials

It has been a great challenge to model the highly conductive materials at microwave frequencies with the conventional FDTD algorithm. The reason is that fine mesh should

be applied to highly conductive regions to track the fast field variation. The time step, which is related to the mesh cell size via the CFL condition, becomes extremely small. As a result, the total iteration number of a simulation is prohibitively huge. The approximate approaches, such as Surface Impedance Boundary Condition (SIBC) and perturbation techniques are used to circumvent the problem. But they were developed with the assumption of plane waves impinging on the conducting boundaries or unperturbed fields in the unperturbed regions [138]. These methods, though presenting good results in many cases, remain to be approximate in nature and fail in some special cases.

Due to the removal of the CFL condition, the proposed ADI-FDTD method presents a potential solution for simulating highly conductive media. The reason is that the ADI-FDTD method is unconditionally stable, and allows the independent selections of time step and space step. Consequently, the ADI-FDTD becomes very suitable for solving the structures in which fine mesh is indispensable [83]. An application of the ADI-FDTD based on this property was reported in [84] for computing shielding effectiveness of thin conductor structures but at low frequencies (10 MHz~1 GHz).

In the following paragraphs, the ADI-FDTD is modified for highly conductive materials.

Starting from Maxwell's equations, the relationship between electric field and magnetic field in the cylindrical coordinates in a lossy source free medium can be written as, for example:

$$\varepsilon \frac{\partial E_r}{\partial t} + \sigma E_r = \frac{\partial H_z}{r \partial \phi} - \frac{\partial H_\phi}{\partial z} \quad (5.6)$$

By applying the ADI-FDTD method to Maxwell's equations using central-differencing technique as described in 3.3, twelve equations can be obtained in two sub time steps respectively. For instance, the discretized form of equation (5.6) can be broken into two sub-step computation as in the following:

at the first half time step (i.e. at the  $(n+1/2)^{\text{th}}$  time step):



$$E_r^{n+1/2}(i+\frac{1}{2}, j, k) = \frac{1 - \frac{\sigma \cdot \Delta t}{4\epsilon}}{1 + \frac{\sigma \cdot \Delta t}{4\epsilon}} E_r^n(i+\frac{1}{2}, j, k) + \frac{\frac{\Delta t}{4\epsilon}}{1 + \frac{\sigma \cdot \Delta t}{4\epsilon}} \left[ \frac{H_z^{n+1/2}(i+\frac{1}{2}, j+\frac{1}{2}, k) - H_z^{n+1/2}(i+\frac{1}{2}, j-\frac{1}{2}, k)}{\Delta\phi \cdot r(i+\frac{1}{2})} - \frac{H_\phi^n(i+\frac{1}{2}, j, k+\frac{1}{2}) - H_\phi^n(i+\frac{1}{2}, j, k-\frac{1}{2})}{\Delta z l(k)} \right] \quad (5.7a)$$

at the second half time step (i.e. at the (n+1)<sup>th</sup> time step):

$$E_r^{n+1}(i+\frac{1}{2}, j, k) = \frac{1 - \frac{\sigma \cdot \Delta t}{4\epsilon}}{1 + \frac{\sigma \cdot \Delta t}{4\epsilon}} E_r^{n+1/2}(i+\frac{1}{2}, j, k) + \frac{\frac{\Delta t}{4\epsilon}}{1 + \frac{\sigma \cdot \Delta t}{4\epsilon}} \left[ \frac{H_z^{n+1/2}(i+\frac{1}{2}, j+\frac{1}{2}, k) - H_z^{n+1/2}(i+\frac{1}{2}, j-\frac{1}{2}, k)}{\Delta\phi \cdot r(i+\frac{1}{2})} - \frac{H_\phi^{n+1}(i+\frac{1}{2}, j, k+\frac{1}{2}) - H_\phi^{n+1}(i+\frac{1}{2}, j, k-\frac{1}{2})}{\Delta z l(k)} \right] \quad (5.7b)$$

However, in this form, the coefficient of the field value of the present time step can be zero when it reaches the threshold:

$$\sigma_0 = \frac{4\epsilon}{\Delta t} \quad (5.8)$$

Usually this threshold conductivity value is relatively low. For example, if  $\Delta r = \Delta z = 1$  cm,  $\Delta\phi = 2\pi/20$  rad, taking the Courant time step limit, the threshold conductivity is  $\sigma_0 = 6.9 \text{ s/m}$ . For greater conductivity values, the coefficient will become a negative value, which makes equations (5.7a) (5.7b) unusable. To overcome this problem, Lubbers et al. [138] suggested using the most recent value of electric field in computing conduction currents. In the ADI-FDTD algorithm, it turns out to be  $\sigma E = \sigma E^{n+1/2}$  for the first half time step and  $\sigma E = \sigma E^{n+1}$  for the second half time step. As a result, the revised ADI-FDTD equations of (2a) (2b) can be derived as:

$$E_r^{n+\frac{1}{2}}(i+\frac{1}{2}, j, k) = \frac{1}{1+\frac{\sigma \cdot \Delta t}{2\epsilon}} E_r^n(i+\frac{1}{2}, j, k) + \frac{\frac{\Delta t}{2\epsilon}}{1+\frac{\sigma \cdot \Delta t}{2\epsilon}} \left[ \frac{H_z^{n+\frac{1}{2}}(i+\frac{1}{2}, j+\frac{1}{2}, k) - H_z^{n+\frac{1}{2}}(i+\frac{1}{2}, j-\frac{1}{2}, k)}{\Delta\phi \cdot r(i+\frac{1}{2})} - \frac{H_\phi^n(i+\frac{1}{2}, j, k+\frac{1}{2}) - H_\phi^n(i+\frac{1}{2}, j, k-\frac{1}{2})}{\Delta z l(k)} \right] \quad (5.9a)$$

for the first half time step

$$E_r^{m+1}(i+\frac{1}{2}, j, k) = \frac{1}{1+\frac{\sigma \cdot \Delta t}{2\epsilon}} E_r^{m+\frac{1}{2}}(i+\frac{1}{2}, j, k) + \frac{\frac{\Delta t}{2\epsilon}}{1+\frac{\sigma \cdot \Delta t}{2\epsilon}} \left[ \frac{H_z^{m+\frac{1}{2}}(i+\frac{1}{2}, j+\frac{1}{2}, k) - H_z^{m+\frac{1}{2}}(i+\frac{1}{2}, j-\frac{1}{2}, k)}{\Delta\phi \cdot r(i+\frac{1}{2})} - \frac{H_\phi^{m+1}(i+\frac{1}{2}, j, k+\frac{1}{2}) - H_\phi^{m+1}(i+\frac{1}{2}, j, k-\frac{1}{2})}{\Delta z l(k)} \right] \quad (5.9b)$$

for the second half time step

Note the threshold conductivity disappears in the revised equations. In this way, the revised ADI-FDTD method can be applied to the materials with high conductivities.

The twelve equations for solving highly conductive materials can be obtained in a similar way, and they are shown in Appendix D.

By substituting and rearranging the field components, the computational efficiency realization for computer programming of equations (D-1) and (D-2) can be obtained as described in 3.3.3.

It should be pointed out that the above revised ADI-FDTD is also feasible for modeling the materials with low conductivities, which will be numerically verified in section 5.5 by analyzing a circular resonator filled with lossy dielectric material.

## 5.4 Padé Approximation

Time domain methods can provide the field behavior within a structure by recording the field signatures in time domain. However, it is always necessary to provide the frequency

domain information for spectrum analysis of a certain structure. The commonly used method is Discrete Fourier Transform (DFT) technique that is shown below:

$$F(\omega) = \int_{-\infty}^{\infty} f(t) e^{-j\omega t} dt \quad (5.10a)$$

or in discrete form:

$$F(\omega) = \sum_0^{N\Delta t} f(n\Delta t) e^{-jm\Delta\omega\Delta t} \Delta t \quad (5.10b)$$

in which  $\Delta t$  is the time step,  $N$  is the total number of iterations,  $\Delta\omega$  is the sampling radian frequency step and  $m$  is the frequency number.

It is shown in equation (5.10b) that in order to obtain the frequency resolution of  $\Delta\omega$ , the following relationship should be met:

$$\Delta t \leq \frac{1}{N\Delta\omega} \quad \text{or} \quad \Delta\omega \leq \frac{1}{N\Delta t} \quad (5.11)$$

As can be seen, the frequency resolution  $\Delta\omega$  is determined by the total available time domain data and the time step. In a simple term, one may take more iteration steps or/and decrease the time step to obtain higher frequency resolution. However, it may not be practical under some special circumstances. For instance, if the time step is a small number, the number of the iteration steps has to be large in order to obtain a small frequency resolution. As a result, the total number of iteration will be large and therefore the simulation time will be very long. In addition, the computer generated errors will also be accumulated from long iterations.

To resolve this problem, several mathematical methods have been developed to provide good frequency resolution with less time domain data, such as Prony's method [137], the generalized pencil-of-function method [138] and DFT/Padé method [139]. Since the first two methods are sensitive to the sampling condition, the DFT/Padé approximation is chosen to refine the DFT outputs in our experiments.

Suppose that there is a set of spectral data obtained from DFT/FFT process. The frequency response can be rewritten as a rational function:

$$P(\omega) = \frac{Q_N(\omega)}{D_M(\omega)} \quad (5.12)$$

where  $P(\omega)$  represents the DFT/FFT output. The numerator and the denominator polynomials  $Q_N(\omega)$  and  $D_M(\omega)$  are given by:

$$Q_N(\omega) = \sum_{i=0}^N \alpha_i \omega^i \quad (5.13a)$$

$$D_M(\omega) = \sum_{i=0}^M \beta_i \omega^i \quad (5.13b)$$

By substituting equation (5.13) into (5.12) and assuming  $\beta_0 = 1$ , one can get:

$$P(\omega_j) \cdot \sum_{i=1}^M \beta_i \omega_j^i - \sum_{i=0}^N \alpha_i \omega_j^i = -P(\omega_j) \quad j = 0 \dots S-1 \quad (5.14)$$

Equation (5.14) implies that the unknown coefficients of the Padé approximation can be obtained from a system of linear equations and the total number of samples (DFT/FFT output data samples) required is  $S \geq N + M + 1$ . Since the unknown coefficients are now the products of a sampled data and some power of the frequency, the dynamic range of the matrix elements is very large for large  $M$ 's and  $N$ 's. One way to avoid this problem is to scale the frequency. A typical scaling function is as follows:

$$\omega_0 = \frac{2\omega - (\omega_{\max} - \omega_{\min})}{\omega_{\max} + \omega_{\min}} \quad (5.15)$$

where  $\omega_{\max}$  and  $\omega_{\min}$  are the maximum and minimum angular frequency under interest. Once the coefficients are known, it is straightforward to interpolate the sampled data to obtain the desired resolution. In the application described in this thesis,  $N$  is chosen to be equal to  $M$  — known as the diagonal Padé approximation — which requires  $(2N+1)$  data

samples. The numerical experiments in this chapter will show that Padé approximation can provide greatly improved frequency resolution with very small number of DFT/FFT outputs, which results in fewer iteration steps. Detailed knowledge on Padé approximation can be found in [139].

## 5.5 Experiments on the Circular Resonators

To further investigate the ability of ADI-FDTD method for solving realistic EM problems, several experiments are carried out on selected typical microwave structures with closed PEC boundary. By incorporating the auxiliary techniques introduced in the above sections, it is found that the ADI-FDTD method can effectively and efficiently model the closed structures.

### (A) A circular dielectric rod resonator

The objective of this experiment is to test the ADI-FDTD method for solving the structures with nonuniform medium parameters which is discussed in section 5.2. The structure under consideration is shown in Figure 5.2. The time step is chosen to be 4 times of the CFL limit. The cavity is discretized with an  $80 \times 10 \times 10$  mesh and the time step is 58.14 picoseconds. By comparing the resonant frequency computed with different methods [140], the resonant frequency computed with the proposed ADI-FDTD scheme is found to agree well with the other methods (see Table 1). The differences among all the methods are less than 2%.

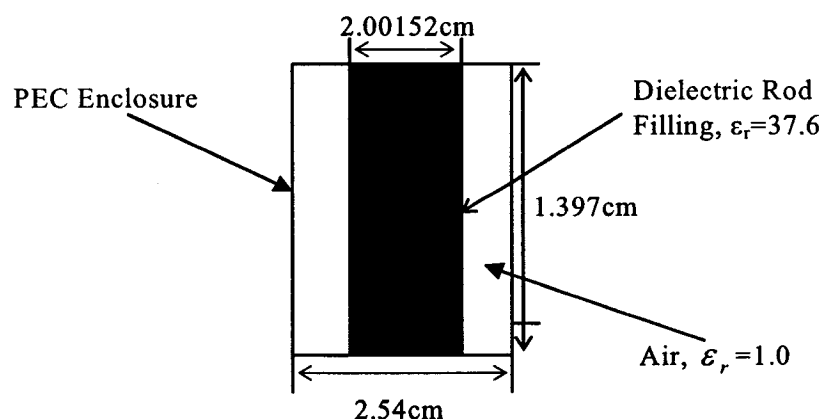


Figure 5.2 The geometry of a dielectric rod resonator

**Table 1 Resonant Frequencies of the Dielectric Rod Resonator Compared with Different Methods**

Conventional FDTD Method	Finite Element Method	Nonorthogonal FDTD Method	Proposed ADI-FDTD Method
1.47225 GHz	1.50 GHz	1.47 GHz	1.49675 GHz

As can be seen, by averaging the permittivity on the air-dielectric boundary introduced in section 5.2, the structures with nonuniform medium parameters can be effectively analyzed with the cylindrical ADI-FDTD method.

(B) *A circular dielectric disk resonator*

In FDTD modeling, sometimes a non-uniform mesh is introduced to account for the non-uniform field variations in a structure. The same applies to ADI-FDTD grid. To investigate the advantages of the non-uniform mesh with the ADI-FDTD method, a circular dielectric disk resonator is computed with both the conventional FDTD method and the ADI-FDTD method with uniform and non-uniform meshes. Figure 5.3 shows the geometry and parameters of a disk resonator.

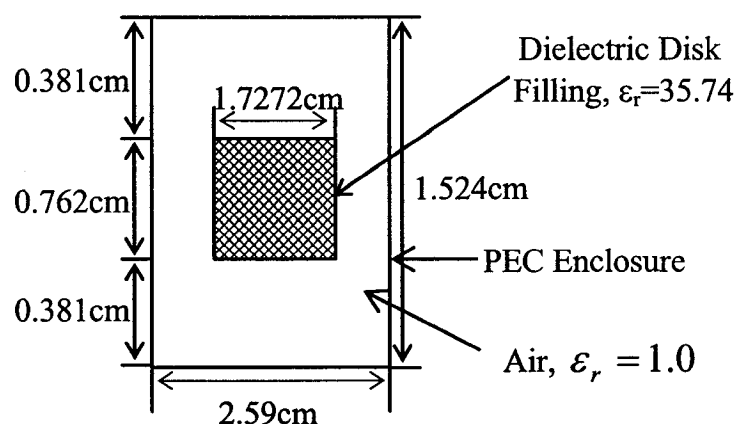


Figure 5.3 The geometry of the dielectric disk resonator (side view)

For the non-uniform grid, the whole area is discretized with a  $25 \times 16 \times 24$  grid. Because the field energy is mainly concentrated inside the dielectric, a denser mesh is applied to the dielectric region. 20 cells in the radial direction and 16 cells in the  $z$ -direction are assigned to the dielectric region (see Figure 5.4). In other words, the dense cell size is a

half of the coarse one, i.e.,  $\Delta r_{\text{dense}} = 0.5 \Delta r_{\text{coarse}}$ ,  $\Delta z_{\text{dense}} = 0.5 \Delta z_{\text{coarse}}$ . As a result, the whole area is divided into four different regions: (1)  $\Delta r_{\text{dense}}$  with  $\Delta z_{\text{dense}}$ , (2)  $\Delta r_{\text{coarse}}$  with  $\Delta z_{\text{dense}}$ , (3)  $\Delta r_{\text{dense}}$  with  $\Delta z_{\text{coarse}}$  and (4)  $\Delta r_{\text{coarse}}$  with  $\Delta z_{\text{coarse}}$ .

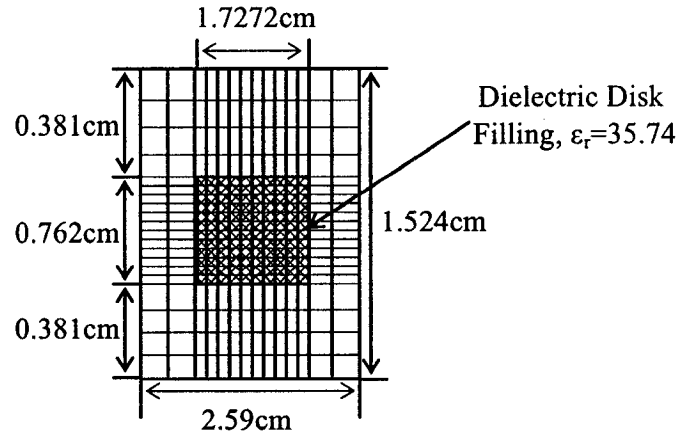


Figure 5.4 Discretization of the computation area

For the uniform mesh, a  $30 \times 32 \times 32$  grid is applied to the whole area. The cell sizes in the radial and  $z$ -direction are equal to  $\Delta r_{\text{dense}}$  and  $\Delta z_{\text{dense}}$  of the nonuniform case, respectively.

Different time steps of  $2 \Delta t_{\text{CFL}}$ ,  $4 \Delta t_{\text{CFL}}$ ,  $8 \Delta t_{\text{CFL}}$  and  $16 \Delta t_{\text{CFL}}$  were taken for the cylindrical ADI-FDTD method with the uniform and non-uniform grids, respectively. The results are shown in Figure 5.5.

### Comparison of Relative Error

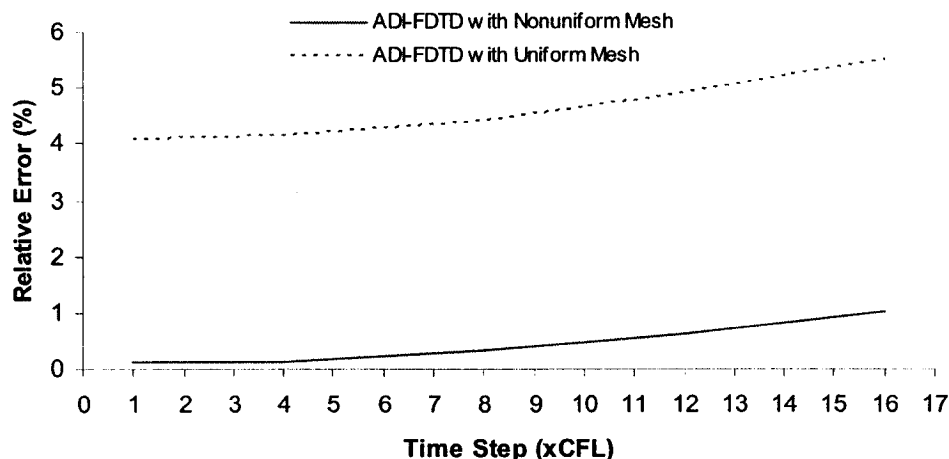


Figure 5.5 Computation errors of the cylindrical ADI-FDTD with the uniform and nonuniform grid

Although the computational errors increase with bigger  $\Delta t$  in a non-uniform grid, the computation error with a non-uniform grid is much lower than that with a uniform grid. Table 2 compares the resonant frequencies obtained with various methods. The cylindrical ADI-FDTD method with a nonuniform grid presents the best accuracy.

**Table 2 Resonant Frequencies of the Dielectric Resonator Computed with Different Methods ( $\Delta t=1.0\text{CFL}$  with the Proposed Method)**

Reference (GHz)	Conventional FDTD Method (Relative Error)	Finite Element Method (Relative Error)	Nonorthogonal FDTD Method (Relative Error)	Proposed ADI-FDTD Method (Relative Error)
4.60 GHz	4.73 GHz (2.83%)	4.54 GHz (1.304%)	4.62 GHz (0.435%)	4.594 GHz (0.130%)

Note that the results obtained with other techniques are cited from [140].

Due to the smaller grid size, the simulation time and the computation memory consumption with the ADI-FDTD is also smaller. To have certain references in assessing the CPU time and memory usages, three experiments are conducted: (1) the cylindrical ADI-FDTD with the non-uniform grid as described before but with a time step being  $4\Delta t_{\text{CFL}}$  (2) the cylindrical ADI-FDTD with a uniform grid whose cell size is equal to the dense mesh size of the non-uniform case and with its time step being  $4\Delta t_{\text{CFL}}$ , and (3) the



conventional FDTD with a uniform grid whose cell size is equal to the dense mesh size of the non-uniform case and with its time step being  $\Delta t_{CFL}$ . All the simulations were conducted on a Pentium 1.0 GHz computer. A physical time of 4.1321 microseconds were simulated, which means that the ADI-FDTD needs to run 1000 iterations while the conventional FDTD needs to run 4000 iterations. The CPU time was found to be 231.65 seconds with the non-uniform ADI-FDTD grid, 1667.73 seconds with the uniform ADI-FDTD grid, and 601.45 seconds with the conventional FDTD grid respectively. Consequently, it is concluded that the saving factor in computation time for the ADI-FDTD with a nonuniform grid is about 7 in comparison with the ADI-FDTD with a uniform grid and about 2.6 in comparison with the conventional FDTD.

For the memory consumption, it is directly related to the array size used for computation. Therefore, in our case, the memory consumption with nonuniform ADI-FDTD is about 0.3 of that with uniform ADI-FDTD ( $25 \times 16 \times 24 / 30 \times 32 \times 32$ )

## 5.6 Experiments on the Resonators with Lossy Materials

Conduction loss generated by conductive materials and the dielectric loss generated by lossy dielectric materials are two kinds of energy losses in a microwave structure. Specifically, the energy losses in resonant structures are described by *Quality Factors* (Q-factors) with respect to frequencies.

To model the lossy materials with the ADI-FDTD method, two sample structures are computed with the revised ADI-FDTD algorithm: one is a cylindrical cavity with copper enclosure and the other is a cylindrical cavity with lossless walls filled with a slightly lossy dielectric. Detailed comparisons of the resonant frequencies and Q-factors with the theoretical results are presented in the following sections.

### (A) Cylindrical cavity with high Conductivity walls

Fig. 5.6 shows the hollow cylindrical cavity with copper walls. There only exists conducting loss that needs to be taken into account for the computation of the Q-factors.

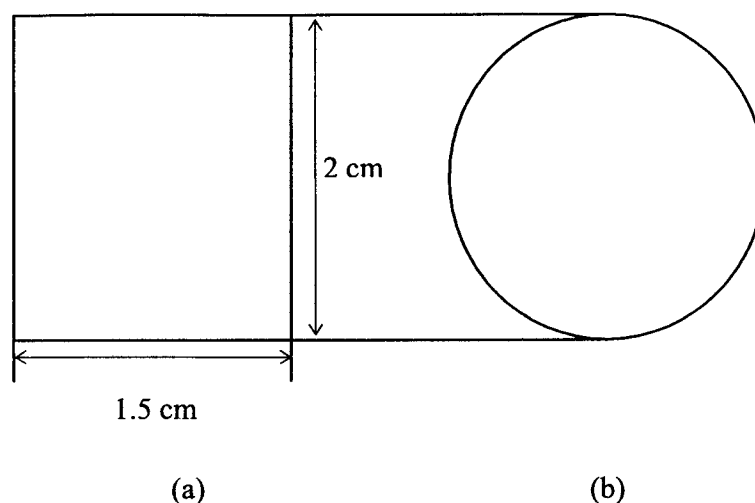


Figure 5.6 The geometry of the selected cylindrical cavity: (a) Side view (b) Bottom view

To affect the realistic computation without losing modeling accuracy, the thickness of the conducting wall should be finite. In our case, a conducting layer beneath the air-conductor interface with a thickness of several times of the skin depth is taken to represent the whole conducting wall in computations of conducting loss. The justification is that the fields further into the conductor are supposedly to be negligible small due to the strong skin depth effect at RF and microwave frequencies. In our case, we took a layer of three times of the skin depth computed with the lowest frequency under interest as the thickness of the conductor. For the sample structure, the lowest frequency is about 11 GHz and thus the skin depth is about  $0.63 \mu\text{m}$ . The thickness of the conductor was then taken to be  $2.0 \mu\text{m}$  (see Fig. 5.7).

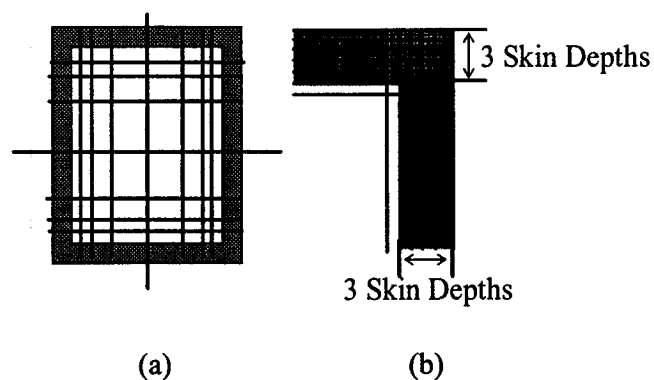


Figure 5.7 (a) Nonuniform mesh in the air-filled area (b) Uniform fine mesh inside the conducting walls

To reduce local numerical errors, a gradually decreased cell size is applied to the air-filled area, a uniform fine grid to the metal area in the radial direction and the  $z$ -direction, respectively (see Fig. 5.4). The minimum cell size in the air filled area is equal to the cell size in the conducting region. The adjacent cell sizes in the air-filled area have the following relationship [36]:

$$\begin{aligned} 0.5\Delta r_{i-1} &= \Delta r_i = 2\Delta r_{i+1} \\ 0.5\Delta z_{k-1} &= \Delta z_k = 2\Delta z_{k+1} \end{aligned} \quad (5.16)$$

Note that the first cell starts at the center of the cavity in the  $z$ -direction, and the relationship in (5.16) applies in both the radial and  $z$ -direction. In the angular direction, a uniform mesh is used due to its homogeneousness in the direction.

With the meshing method described above, a  $50 \times 8 \times 100$  grid was generated. By recording the time domain signature at a certain grid point in the structure and then using DFT, the mode frequencies can be obtained. The unloaded  $Q$ -factor of each mode can then be calculated with:

$$Q_0 = \frac{f_0}{\Delta f} \quad (5.17)$$

where  $f_0$  is a certain resonant frequency and  $\Delta f$  is the corresponding 3-dB bandwidth.

In order to get correct  $\Delta f$  in (5.17), an appropriate frequency resolution is required. In other words, sufficient simulation duration in time is necessary with the DFT method. For a high  $Q$  structure, the 3-dB bandwidth is usually very small compared to the center frequency. This means that a high number of iteration is required. For example, if we use conventional FDTD and applying the fine mesh described above, the time step is  $7.68 \times 10^{-5}$  picoseconds at most (due to the CFL limit). To get a 1 MHz frequency resolution, 1.3 billion iterations are required, which makes the conventional FDTD impractical for calculating the  $Q$ -factor. In addition, since too many iteration steps are needed to collect enough time domain information, the calculated  $Q$ -factor is

unrealistically high due to the computer-generated errors with conventional FDTD method [141].

With the unconditionally stable ADI-FDTD method the time step is only restricted by numerical accuracy. In our case the time step is taken to be 1.26 picoseconds, about 16380 times of that with the conventional FDTD. However, even with this large time step, it still needs 800,000 iterations to get the 1MHz frequency resolution. Therefore the DFT/Padé approximation, which is discussed in section 5.4, needs to be applied to process the DFT outputs.

Fig. 5.8 illustrates the improvement of FFT/Padé method compared to FFT method with only 4,096 time domain samples with the ADI-FDTD method. The original frequency resolution is 194 MHz. The greatly refined frequency resolution is 0.13 MHz. As a result, the Q-factors are obtainable with much fewer iteration steps. It should be noted that even with the FFT/Padé method, the conventional FDTD is difficult to implement since it still needs at least 1.2 million iterations.

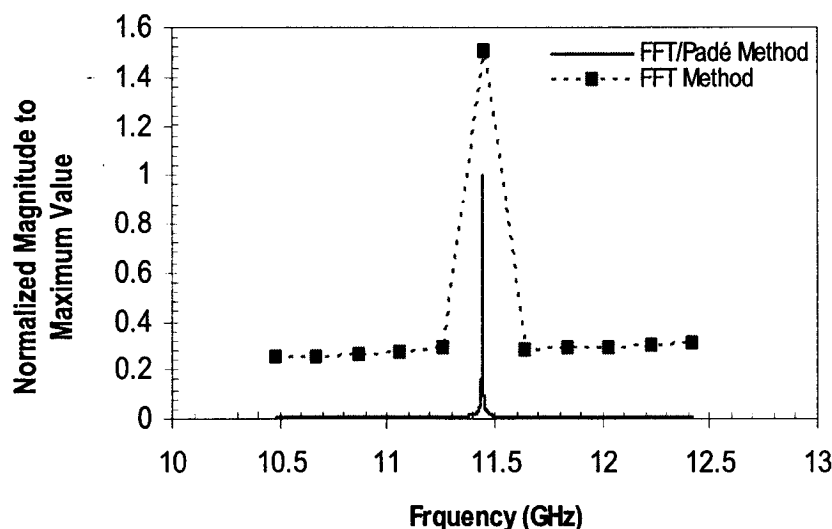


Figure 5.8 The comparison between DFT and DFT/Padé method for  $TM_{010}$  mode with the cylindrical ADI-FDTD method

Table 3 shows the computed resonant frequencies of a few modes and their comparisons with the theoretical values [141].

**Table 3 Resonant Frequencies with the Presented Methods**

Modes	In theory (GHz) (From [141])	This work (GHz)	Relative Difference (%)
TM <sub>010</sub>	11.483	11.442	+0.35
TE <sub>111</sub>	13.314	13.114	+1.50
TM <sub>011</sub>	15.227	15.185	+0.28
TM <sub>110</sub>	18.300	17.781	+2.84

Table 4 shows the Q-factor of each mode and the comparisons with the theoretical values. As can be seen, the computed results agree well with the theoretical ones.

**Table 4 Q-factor of Each Mode with the Presented Methods**

Modes	In theory [10]	This work	Relative Difference (%)
TM <sub>010</sub>	9729	9829	-1.03
TE <sub>111</sub>	10868	11152	-2.61
TM <sub>011</sub>	8002	8100	-1.22
TM <sub>110</sub>	12281	12571	-2.36

As can be seen from the simulation results, the modified ADI-FDTD method presents a remarkable suitability for modeling the highly conductive materials even though the material is in an electrically large structure. The efficient computation without losing modeling accuracy makes the proposed ADI-FDTD method excel over the conventional FDTD method.

*(B) Cylindrical cavity filled with lossy medium*

Dielectric loss is another kind of loss in a certain microwave structure where lossy dielectric materials exist in the structure. This kind of loss is caused by the effective conductivity of the dielectric material, which is related to the loss tangent through:

$$\sigma_{eff} = \omega \epsilon \tan \delta \quad (5.18)$$

Usually the effective conductivity of a lossy dielectric is of small value. For instance, the loss tangent of silicon at 10 GHz is 0.004. The effective conductivity is thus 0.0264 S/m obtained with (5.18).

To test the suitability of the proposed modified ADI-FDTD method for computing dielectric loss, an experiment is conducted for a cylindrical cavity of 210mm in diameter and 25.4mm in height with lossless walls, filled with a slightly lossy medium. The conductivity is  $\sigma = 0.001S/m$  at the resonant frequency.

Because the fine mesh is no longer necessary for computing this structure, a uniform  $16 \times 16 \times 15$  mesh is applied to the whole computation area. The time step is four times of the CFL limit, which is 13.0 picoseconds. Again DFT/Padé method is used to obtain frequency response as well as Q-factor. Table 5 shows the simulation results of  $TM_{010}$  mode. As can be seen, the revised ADI-FDTD method is also effective for computing the low conductivity materials.

**Table 5 Q-factor of  $TM_{010}$  Mode with the Presented Method**

	In theory [11]	This work	Relative Error
Q-factor	60.81	60.52	+0.47%
$f_o$ (MHz)	1093.6	1092.6	+0.09%

## 5.7 Conclusions

In this chapter, closed microwave structures are analyzed with the proposed unconditionally stable ADI-FDTD method. Other auxiliary numerical techniques, such as non-uniform gridding technique, gradually reduced cell size and DFT/Padé technique, are also discussed to facilitate the actual simulation for a certain structure. A revised ADI-FDTD method is developed for effectively modeling highly conductive materials. Combined with the DFT/Padé technique, the ADI-FDTD method is shown to be efficient and effective in computing the losses for both high conductivity materials and low conductivity materials.

It can be foreseen that the revised unconditionally stable ADI-FDTD method can be extended to predicting the conduction loss of more complex structures, such as highly conductive thin film structures and attenuation constant of transmission lines.

## CHAPTER 6    ADI-FDTD MODELING OF OPEN STRUCTURES

### 6.1      Introduction

A wide range of microwave structures are open or infinite at least in one of the three dimensions, such as antennas, guided-wave structures etc. To model these structures, an appropriate boundary condition should be applied to truncate the computation domain without incurring much error [36].

In this chapter, the widely used absorbing boundary conditions are incorporated into the unconditionally stable ADI-FDTD method. The resultant schemes are used to analyze open structures. A circular waveguide is analyzed as the example of modeling open structure. The conductive materials with arbitrary conductivities are also studied.

### 6.2      The Cylindrical ADI-FDTD Method with the Mur Boundary Condition

By following the method described in Chapter 2, Mur absorbing boundary condition can be incorporated into conventional FDTD algorithm for solving open structures. For instance, the radial electric field located on the Mur boundary can be computed with:

$$E_r^{n+1}(i+\frac{1}{2},j,0) = E_r^n(i+\frac{1}{2},j,1) + \frac{c\Delta t - \Delta z 2(1)}{c\Delta t + \Delta z 2(1)} \left[ E_r^{n+1}(i+\frac{1}{2},j,1) - E_r^n(i+\frac{1}{2},j,0) \right] \quad (6.1)$$

By applying the ADI technique to the Mur boundary described in Chapter 2, the following equations in the cylindrical coordinates can be obtained for the ADI form of the Mur boundary condition:

at the first sub time step:

$$E_r^{n+\frac{1}{2}}(i+\frac{1}{2},j,0) = E_r^n(i+\frac{1}{2},j,1) + \frac{c\Delta t - \Delta z 2(1)}{c\Delta t + \Delta z 2(1)} \left[ E_r^{n+\frac{1}{2}}(i+\frac{1}{2},j,1) - E_r^n(i+\frac{1}{2},j,0) \right] \quad (6.2a)$$

$$E_\phi^{n+\frac{1}{2}}(i,j+\frac{1}{2},0) = E_\phi^n(i,j+\frac{1}{2},1) + \frac{c\Delta t - \Delta z 2(1)}{c\Delta t + \Delta z 2(1)} \left[ E_\phi^{n+\frac{1}{2}}(i,j+\frac{1}{2},1) - E_\phi^n(i,j+\frac{1}{2},0) \right] \quad (6.2b)$$

at the second sub time step:

$$E_r^{n+1}(i+\frac{1}{2},j,0) = E_r^{n+\frac{1}{2}}(i+\frac{1}{2},j,1) + \frac{c\Delta t - \Delta z 2(1)}{c\Delta t + \Delta z 2(1)} \left[ E_r^{n+1}(i+\frac{1}{2},j,1) - E_r^{n+\frac{1}{2}}(i+\frac{1}{2},j,0) \right] \quad (6.3a)$$

$$E_\phi^{n+1}(i,j+\frac{1}{2},0) = E_\phi^{n+\frac{1}{2}}(i,j+\frac{1}{2},1) + \frac{c\Delta t - \Delta z 2(1)}{c\Delta t + \Delta z 2(1)} \left[ E_\phi^{n+1}(i,j+\frac{1}{2},1) - E_\phi^{n+\frac{1}{2}}(i,j+\frac{1}{2},0) \right] \quad (6.3b)$$

Note that here it is assumed that the waves propagate in the +z direction.

By incorporating the above equations into ADI-FDTD algorithm, the ADI-FDTD combined with Mur boundary condition is then obtained.

### 6.3 The Cylindrical ADI-FDTD Method with Uniaxial PML Boundary Condition

The UPML boundary condition is another absorbing boundary condition and has been proven effective for solving open structures with the conventional FDTD method in [143]. In this section, the UPML is adapted in the ADI-FDTD method with the consideration of nonuniform permittivity and conductivity.

In a source free UPML region with background medium parameters  $\varepsilon, \mu$  and  $\sigma$ , the normal UPML equations that are related to Ampere's law can be expressed as:



$$\varepsilon \frac{\partial P_r'}{\partial t} + \sigma P_r' = \frac{\partial H_z}{r \partial \phi} - \frac{\partial H_\phi}{\partial z} \quad (6.4a)$$

$$\varepsilon \frac{\partial P_\phi'}{\partial t} + \sigma P_\phi' = \frac{\partial H_r}{\partial z} - \frac{\partial H_z}{\partial r} \quad (6.4b)$$

$$\varepsilon \frac{\partial P_z'}{\partial t} + \sigma P_z' = \frac{\partial r H_\phi}{r \partial r} - \frac{\partial H_r}{r \partial \phi} \quad (6.4c)$$

$$\frac{\partial P_r'}{\partial t} = k_r \frac{\partial P_r}{\partial t} + \frac{\int_0^r \sigma_r(r') dr'}{\varepsilon_0(r-r_0)} P_r \quad (6.5a)$$

$$\frac{\partial P_\phi'}{\partial t} = k_z \frac{\partial P_\phi}{\partial t} + \frac{\sigma_z}{\varepsilon_0} P_\phi \quad (6.5b)$$

$$\frac{\partial P_z'}{\partial t} = k_r \frac{\partial P_z}{\partial t} + \frac{k_r}{\varepsilon_0 \sigma_r} P_z \quad (6.5c)$$

$$k_r \frac{\partial P_r}{\partial t} + \frac{\sigma_r}{\varepsilon_0} P_r = k_z \frac{\partial E_r}{\partial t} + \frac{\sigma_z}{\varepsilon_0} E_r \quad (6.6a)$$

$$k_r \frac{\partial P_\phi}{\partial t} + \frac{\int_0^r \sigma_r(r') dr'}{\varepsilon_0(r-r_0)} P_\phi = k_r \frac{\partial E_\phi}{\partial t} + \frac{\sigma_r}{\varepsilon_0} E_\phi \quad (6.6b)$$

$$k_z \frac{\partial P_z}{\partial t} + \frac{\sigma_z}{\varepsilon_0} P_z = k_r \frac{\partial E_z}{\partial t} + \frac{\int_0^r \sigma_r(r') dr'}{\varepsilon_0(r-r_0)} E_z \quad (6.6c)$$

in which  $P_r'$ ,  $P_\phi'$ ,  $P_z'$ ,  $P_r$ ,  $P_\phi$ ,  $P_z$  are auxiliary field components,  $\sigma_d(d=r, z)$  is the directional conductivity in PML region,  $k_d(d=r, z)$  can be treated as directional permittivity in PML region.  $\sigma_d(d=r, z)$  and  $k_d(d=r, z)$  should all be spatially scaled using polynomial scaling to eliminate possible numerical reflection error. For instance:

$$k_z = 1 + (k_{z\max} - 1) \left( \frac{z}{d} \right)^m \quad (6.7a)$$

$$\sigma_z = \sigma_{z\max} \left( \frac{z}{d} \right)^m \quad (6.7b)$$

in which  $\sigma_{z \max}$  and  $k_{z \max}$  are defined in the form of equation (2.37)

The UPML equations that relate to Faraday's law can be obtained by duality. By central-differencing equation (6.3) ~ (6.5) and applying the ADI technique, 20 equations can be obtained for the two sub time steps. For instance, for the  $E_z$  components on the  $z$ -axis, one can have:

at the first half time step:

$$\begin{aligned}
 E_r^{n+\frac{1}{2}}(i+\frac{1}{2}, j, k) = & \frac{czl(i+\frac{1}{2}, j, k)E_r^n(i+\frac{1}{2}, j, k) - crl(i+\frac{1}{2}, j, k)P_r^n(i+\frac{1}{2}, j, k)}{cz2(i+\frac{1}{2}, j, k)} \\
 & + \frac{cr2(i+\frac{1}{2}, j, k) \left[ crl1(i+\frac{1}{2}, j, k)P_r^n(i+\frac{1}{2}, j, k) - P_r^n(i+\frac{1}{2}, j, k) \right]}{cz2(i+\frac{1}{2}, j, k)crI2(i+\frac{1}{2}, j, k)} + \frac{cr2(i+\frac{1}{2}, j, k)P_r^n(i+\frac{1}{2}, j, k)}{cz2(i+\frac{1}{2}, j, k)crI2(i+\frac{1}{2}, j, k)cm(i+\frac{1}{2}, j, k)} \\
 & + \frac{\Delta t \cdot cr2(i+\frac{1}{2}, j, k)}{2\varepsilon \cdot cz2(i+\frac{1}{2}, j, k)crI2(i+\frac{1}{2}, j, k)cm(i+\frac{1}{2}, j, k)} \left[ \frac{H_z^{n+\frac{1}{2}}(i+\frac{1}{2}, j+\frac{1}{2}, k) - H_z^{n+\frac{1}{2}}(i+\frac{1}{2}, j-\frac{1}{2}, k)}{\Delta \phi \cdot (i+\frac{1}{2}) \cdot r(i+\frac{1}{2})} - \frac{H_\phi^n(i+\frac{1}{2}, j, k+\frac{1}{2}) - H_\phi^n(i+\frac{1}{2}, j, k-\frac{1}{2})}{\Delta z(i+\frac{1}{2}, j, k)} \right] \quad (6.8a) \\
 P_r^{n+\frac{1}{2}}(i+\frac{1}{2}, j, k) = & \frac{crl(i+\frac{1}{2}, j, k)}{cr2(i+\frac{1}{2}, j, k)} P_r^n(i+\frac{1}{2}, j, k) + \frac{cz2(i+\frac{1}{2}, j, k)E_r^{n+\frac{1}{2}}(i+\frac{1}{2}, j, k) - czl(i+\frac{1}{2}, j, k)E_r^n(i+\frac{1}{2}, j, k)}{cr2(i+\frac{1}{2}, j, k)} \\
 P_r^{n+\frac{1}{2}}(i+\frac{1}{2}, j, k) = & P_r^n(i+\frac{1}{2}, j, k) + \left[ crI2(i+\frac{1}{2}, j, k)P_r^{n+\frac{1}{2}}(i+\frac{1}{2}, j, k) - crI1(i+\frac{1}{2}, j, k)P_r^n(i+\frac{1}{2}, j, k) \right]
 \end{aligned}$$

at the second half time step:

$$\begin{aligned}
E_r^{n+1}(i+\frac{1}{2}, j, k) = & \frac{cz1(i+\frac{1}{2}, j, k)E_r^{n+\frac{1}{2}}(i+\frac{1}{2}, j, k) - cr1(i+\frac{1}{2}, j, k)P_r^{n+\frac{1}{2}}(i+\frac{1}{2}, j, k)}{cz2(i+\frac{1}{2}, j, k)} \\
& + \frac{cr2(i+\frac{1}{2}, j, k) \left[ cr1(i+\frac{1}{2}, j, k)P_r^{n+\frac{1}{2}}(i+\frac{1}{2}, j, k) - P_r^{n+\frac{1}{2}}(i+\frac{1}{2}, j, k) \right]}{cz2(i+\frac{1}{2}, j, k)cr12(i+\frac{1}{2}, j, k)} + \frac{cr2(i+\frac{1}{2}, j, k)P_r^{n+\frac{1}{2}}(i+\frac{1}{2}, j, k)}{cz2(i+\frac{1}{2}, j, k)cr12(i+\frac{1}{2}, j, k)cm(i+\frac{1}{2}, j, k)} \\
& + \frac{\Delta t \cdot cr2(i+\frac{1}{2}, j, k)}{2\varepsilon \cdot cz2(i+\frac{1}{2}, j, k)cr12(i+\frac{1}{2}, j, k)cm(i+\frac{1}{2}, j, k)} \left[ \frac{H_z^{n+\frac{1}{2}}(i+\frac{1}{2}, j+\frac{1}{2}, k) - H_z^{n+\frac{1}{2}}(i+\frac{1}{2}, j-\frac{1}{2}, k)}{\Delta \phi \cdot (i+\frac{1}{2}) \cdot r(i+\frac{1}{2})} - \frac{H_\phi^{n+1}(i+\frac{1}{2}, j, k+\frac{1}{2}) - H_\phi^{n+1}(i+\frac{1}{2}, j, k-\frac{1}{2})}{\Delta z(i+\frac{1}{2}, j, k)} \right] \quad (6.8b)
\end{aligned}$$

$$\begin{aligned}
P_r^{n+1}(i+\frac{1}{2}, j, k) = & \frac{cr1(i+\frac{1}{2}, j, k)}{cr2(i+\frac{1}{2}, j, k)} P_r^{n+\frac{1}{2}}(i+\frac{1}{2}, j, k) + \frac{cz2(i+\frac{1}{2}, j, k)E_r^{n+1}(i+\frac{1}{2}, j, k) - cz1(i+\frac{1}{2}, j, k)E_r^{n+\frac{1}{2}}(i+\frac{1}{2}, j, k)}{cr2(i+\frac{1}{2}, j, k)} \\
P_r^{n+1}(i+\frac{1}{2}, j, k) = & P_r^{n+\frac{1}{2}}(i+\frac{1}{2}, j, k) + \left[ cr12(i+\frac{1}{2}, j, k)P_r^{n+1}(i+\frac{1}{2}, j, k) - cr1(i+\frac{1}{2}, j, k)P_r^{n+\frac{1}{2}}(i+\frac{1}{2}, j, k) \right]
\end{aligned}$$

where:

$$\begin{aligned}
cr1(i+\frac{1}{2}, j, k) &= \kappa_r(i+\frac{1}{2}, j, k) - \frac{\Delta t \cdot \sigma_r(i+\frac{1}{2}, j, k)}{4\varepsilon} \\
cr2(i+\frac{1}{2}, j, k) &= \kappa_r(i+\frac{1}{2}, j, k) + \frac{\Delta t \cdot \sigma_r(i+\frac{1}{2}, j, k)}{4\varepsilon} \\
cr11(i+\frac{1}{2}, j, k) &= \kappa_r(i+\frac{1}{2}, j, k) - \frac{\Delta t \cdot \int_{r_0}^r \sigma_r(r) dr}{4\varepsilon} \\
cr12(i+\frac{1}{2}, j, k) &= \kappa_r(i+\frac{1}{2}, j, k) + \frac{\Delta t \cdot \int_{r_0}^r \sigma_r(r) dr}{4\varepsilon} \\
cz1(i+\frac{1}{2}, j, k) &= \kappa_z(i+\frac{1}{2}, j, k) - \frac{\Delta t \cdot \sigma_z(i+\frac{1}{2}, j, k)}{4\varepsilon} \\
cz2(i+\frac{1}{2}, j, k) &= \kappa_z(i+\frac{1}{2}, j, k) + \frac{\Delta t \cdot \sigma_z(i+\frac{1}{2}, j, k)}{4\varepsilon} \\
cm(i+\frac{1}{2}, j, k) &= 1 + \frac{\Delta t \cdot \sigma(i+\frac{1}{2}, j, k)}{2\varepsilon} \quad (6.9)
\end{aligned}$$

Note that the lossy terms of the fields are not averaged in time but use the most recent value of electric field in computing conduction currents. It is due to the effect of the

threshold conductivity as explained in Chapter 5. Other field components and the corresponding auxiliary components can be obtained in the similar way.

#### 6.4 Performance of the Absorbing Boundary Conditions

The numerical performance of a certain absorbing boundary condition can be measured by the reflection error caused by the unabsorbed waves. Quantitatively reflection error can be obtained by the following equation:

$$RE(f) = 20 \log \frac{S_{re}(f)}{S_{in}(f)} = 20 \log \frac{S_{mix}(f) - S_{in}(f)}{S_{in}(f)} \quad (\text{dB}) \quad (6.10)$$

where  $RE$  denotes the reflection error at a frequency  $f$ ,  $S_{re}$  denotes the reflected waves,  $S_{in}$  represents the incident waves, and  $S_{mix}$  is the total waves that is the summation of  $S_{re}$  and  $S_{in}$ .

To obtain the reflection error for both Mur and UPML boundary conditions, numerical experiments are conducted to measure the amount of nonphysical reflection that a given ABC produces as the waves propagate through it. Figure 6.1 illustrates the circular waveguide which is computed with ADI-FDTD method when the Mur boundary condition and PML boundary applied to the two terminals of the waveguide respectively.

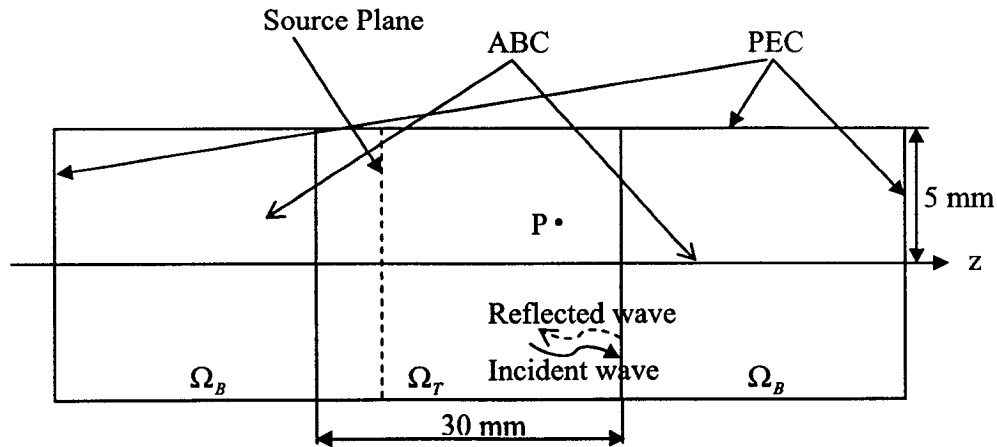


Figure 6.1 A circular waveguide terminated with ABCs

Note that there are two computation domains shown in Figure 6.1-  $\Omega_T$  and  $\Omega_B$  respectively. Domain  $\Omega_T$  is the solution domain of interest and is terminated with a certain absorbing boundary condition. Domain  $\Omega_T$  is of certain thickness when it is UPML boundary, while is a plane when it is Mur boundary condition. Domain  $\Omega_B$  at both terminals is terminated with PEC wall. The length of  $\Omega_B$  is much longer than  $\Omega_T$  so that the reflected waves from the two terminals of  $\Omega_B$  can not reach domain  $\Omega_T$ . The source plane launches a Gaussian pulse to excite TM waves propagating in the waveguide. To obtain  $S_{re}$  and  $S_{in}$ , two experiments are carried out on the two computation domains with Mur and UPML boundary conditions respectively.

A circular waveguide with a radius of 5.0 millimeters is chosen to be the subject under study (see Figure 6.2). The sidewall of the waveguide is assumed to be perfect conductor while the two ends of the waveguide are terminated with Mur boundary condition and UPML layers respectively. Based on the theory [130], the cutoff frequency for a certain mode is given by:

$$f_{c_{nm}} = \frac{p_{nm}}{2\pi a \sqrt{\mu\epsilon}} \quad (6.11)$$

where  $p_{nm}$  is the  $m$ th root of the  $n$ th-order Bessel function  $J_n(x)$  or its derivative.  $a$  is the radius, and  $\mu$  and  $\epsilon$  are the permeability and permittivity, respectively. Consider  $TM_{01}$  mode for our investigation. The theoretical cutoff frequency is then 22.97 GHz .

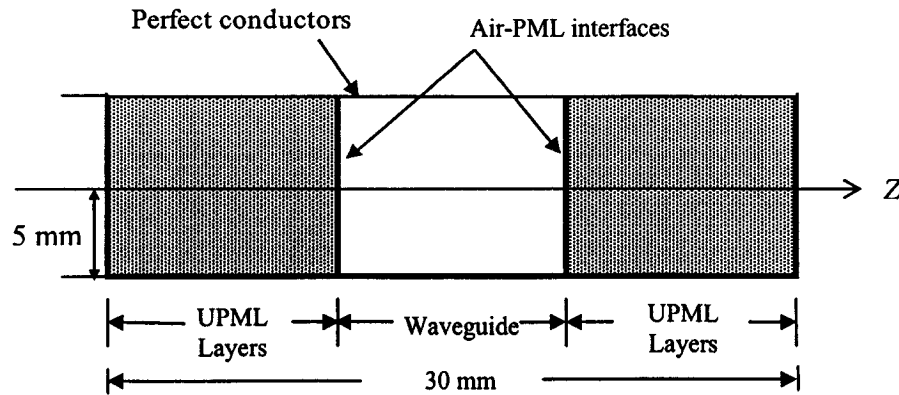


Figure 6.2 The perfect cylindrical waveguide terminated with UPML at both ends

With the UPML boundary condition, the entire computation domain is now divided into three sections: the guided wave section and the two UPML absorbing sections at the two ends of the waveguide (see Figure 6.2). The directional conductivity of  $\sigma_z$  in the UPML section is determined by [143]:

$$\sigma_z(z) = \sigma_{\max} \left( \frac{z}{\delta} \right)^m \quad (6.12)$$

where  $z$  is the distance from the air-UPML interface,  $\delta$  is the thickness of the UPML layer, and  $\sigma_{\max}$  is the maximum conductivity of the UPML layer which can be obtained by equation (2.37).

In order to enhance the UPML ability of absorbing the evanescent waves below the cutoff frequency, parameter  $\kappa_z$  is chosen from 1 to  $\kappa_{\max}$  from the interface [143].  $\kappa_z$  for each layer can be obtained with equation (6.7a)

To facilitate the comparisons with the theoretical solutions for  $TM_{01}$ , the ADI-FDTD grid is excited with the  $TM_{01}$  field distributions. The modulated Gaussian pulse with the space distribution of the mode is [144]:

$$E_r = J_1(p_{nm} r) e^{-\left(\frac{t-t_0}{T}\right)^2} \cos(2\pi f_m t) \quad (6.13)$$

where  $J_1$  is the first order Bessel function,  $p_{nm}$  is the  $m^{\text{th}}$  root of  $J_1(x)$ ,  $r$  is the distance from the axis of the waveguide,  $t_0$  is the time offset of the Gaussian pulse, and  $T$  is the width of the Gaussian pulse.  $f_m$  is the center frequency of the modulated Gaussian pulse. Based on [144],  $t_0$  and  $T$  can be chosen with a desired frequency bandwidth. In other words, the source is made to contain substantial frequency components below cutoff frequency so that degrees of absorption of evanescent modes can be observed.

The overall area is divided into a grid of 10 (in  $r$ ) $\times$ 15(in  $\phi$ ) $\times$ 60(in  $z$ ). The total length of the waveguide is 30 millimeters. The time step was chosen to be equal to the CFL limit. The source plane is placed at the middle of the waveguide.

For UPML layers, the parameters associated with the grid, the UPML layers and the source are as follows:

$$\begin{aligned}
 \Delta r &= 0.5 \text{ mm} , \Delta \phi = 0.42 \text{ rad} , \Delta z = 0.5 \text{ mm} \\
 \Delta t &= 0.635 \text{ ps} \\
 \sigma_{\max} &= 21.22 \text{ S/m} , \kappa_{\max} = 20 \\
 t_0 &= 0.1 \text{ ns} , T = 25 \text{ ps} \\
 f_m &= 40 \text{ GHz}
 \end{aligned} \tag{6.14}$$

Figure 6.3 shows the time domain signature and frequency response of  $E_r$  with 2,000 iterations at the grid point of (1,0,25) with UPML (which is five cells away from the source plane and five cells away from the UPML). As can be seen, the waves in the waveguide die down after 1000 iterations, which indicates that the waves are absorbed well by the UPML layers.

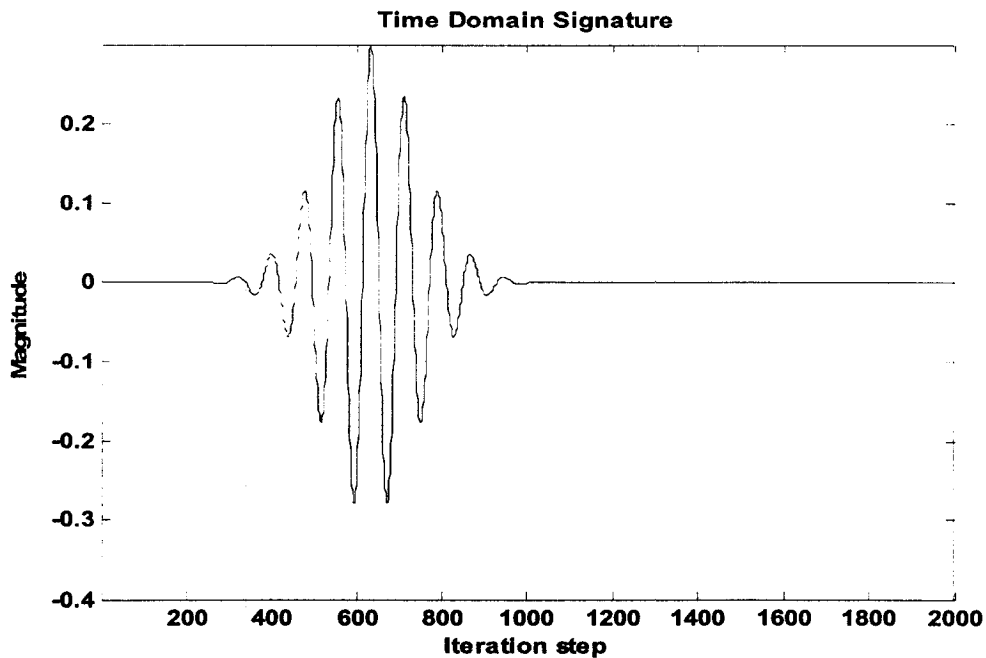


Figure 6.3 The  $E_r$  of 2000 iterations

Further quantitative measurements of the reflections of the 10- and 20-cell UPML are shown in Figure 6.4, and the PML absorptions are found to be better than -50dB in most cases even below the cutoff frequency. Thus we conclude that the UPML with the addition of non-unity  $k$  is very effective in absorbing cylindrical waves that include the evanescent modes.

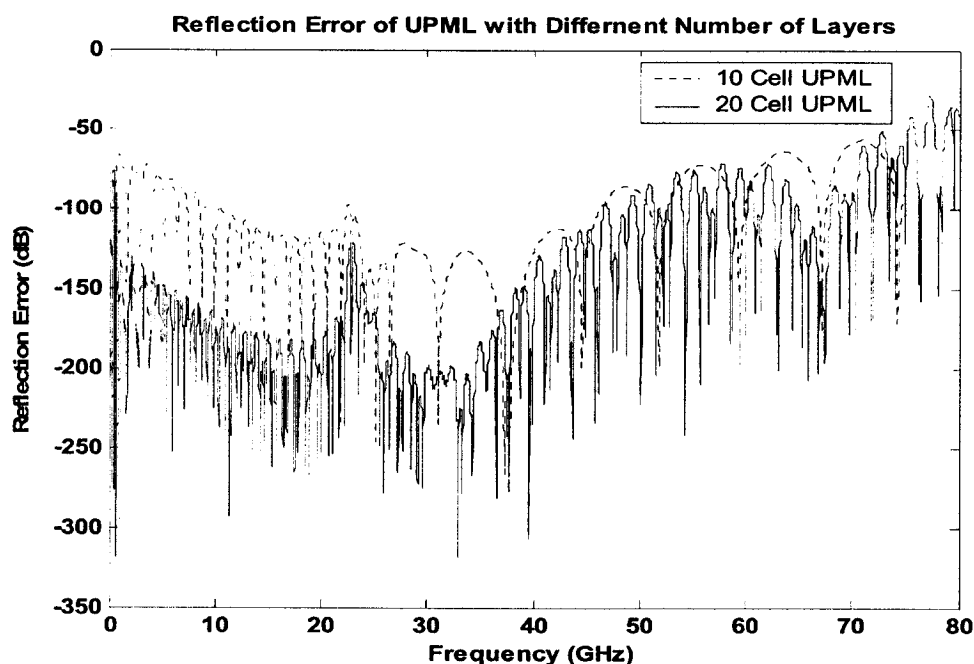


Figure 6.4 Numerical reflections from the UPML layers

Figure 6.5 shows the reflection error of Mur boundary condition in frequency domain. As can be seen, the overall performance of Mur boundary condition is much worse than UPML boundary condition, especially in the frequency range below the cutoff frequency. The reason is that Mur boundary condition can only be effective to the waves with normal incident angle. Therefore, UPML is much superior and is selected as the absorbing boundary condition in the following experiments.



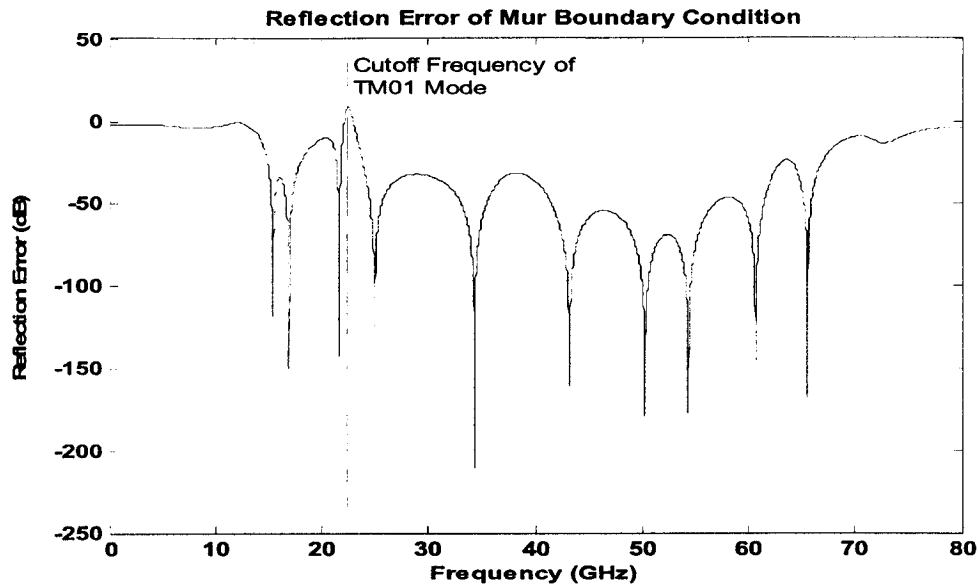


Figure 6.5 Reflection Error of Mur Boundary Condition

## 6.5 Numerical Simulations for Analyzing General Conductive Materials

One of the primary advantages of ADI-FDTD method is that it can solve problems where extremely fine meshes are involved, as has been shown in Chapter 5 that the ADI-FDTD method is suitable for obtaining the quality factors of the cavity resonators with highly conductive walls. In this section, we will show that the ADI-FDTD method combined with the cylindrical UPML boundary conditions is also effective for simulating open structures with conductive materials. The results obtained will then be compared with those obtained with the approximate Surface Impedance Boundary Condition (SIBC) approach [135], which so far is widely used for treating highly conductive materials with FDTD.

### 6.5.1 Experiments on Highly Conductive Materials

In this section, we will show that the ADI-FDTD method combined with the cylindrical UPML boundary conditions is effective for simulating the open structures containing conductive materials. Since few results are reported for exact computations of the cylindrical waveguide with a wall of finite conductivity, two additional sets of

simulations with other methods were also run and compared with the ADI-FDTD simulations. One is the conventional finite-difference time-domain method and the other one is approximate Surface Impedance Boundary Condition (SIBC) approach [138] (that is so far widely used for treating highly conductive materials with FDTD).

Consider the circular waveguide as described in Figure 6.2 but with a wall of a finite conductivity this time (see Figure 6.6). The meshing method is similar to the one used in [146]. In the radial direction  $r$ , gradually decreased cell sizes were applied to the air-filled area, and a fine uniform grid was used inside the conducting wall. The largest size  $\Delta r_{max}$  is 0.625 mm while the smallest size  $\Delta r_{min}$  (which is the cell size inside the conducting wall) was chosen to be one third of skin depth. For copper,  $\Delta r_{min} = 9.54 \text{ nm}$  at 40GHz. Therefore, the cell size ratio of the largest cell size to the smallest cell size is as large as 65513 in the  $r$  direction at 40GHz. In the azimuthal and  $z$  directions, uniform discretization was applied with  $\Delta\phi = 0.42 \text{ rad}$  and  $\Delta z = 0.5 \text{ mm}$ . Overall, a  $39 \times 15 \times 120$  mesh is generated for the whole computation domain. The thickness of the conductive wall is taken to be about 6 times of the skin depth, long enough for the fields to decay to a negligible level. Other simulation parameters remain the same as those used in section 6.4.

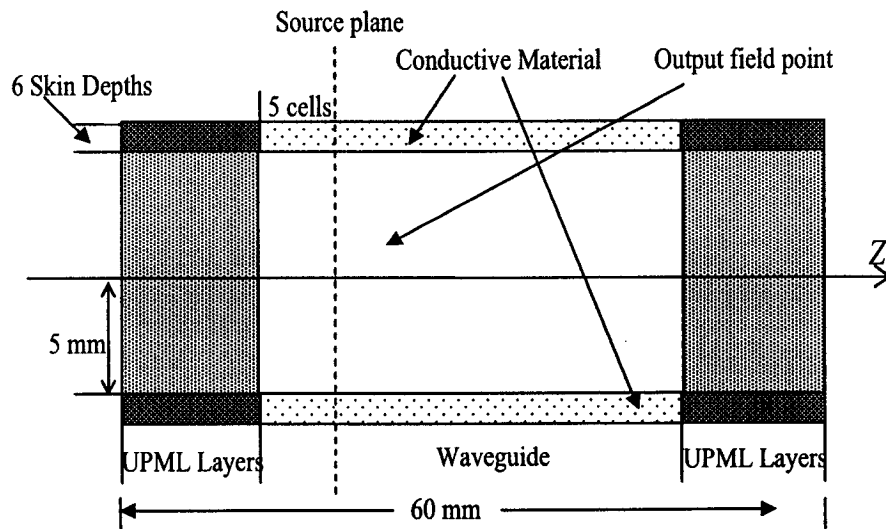


Figure 6.6 The non-perfect waveguide under study

The first two parameters under study are attenuation constant  $\alpha$  and phase shift constant  $\beta$ . The parameters were computed via:

$$\alpha = -\frac{1}{h} \ln \left| \frac{\Im(E_r(z+h, t))}{\Im(E_r(z, t))} \right| \quad (6.15)$$

$$\beta = \frac{1}{h} \text{Im} \left[ \ln \frac{\Im(E_r(z, t))}{\Im(E_r(z+h, t))} \right] \quad (6.16)$$

where  $\Im$  represents the Fourier transform at a selected frequency.  $z$  is taken to be at  $10 \Delta z$  away from the source and the distance  $h$  is  $10 \Delta z$ .  $\text{Im}$  is the operator that takes the imaginary part of a complex variable.

Tables 1 and 2 show the computed attenuation and phase-shift constants with different conductivities using different methods. In them, quantity  $p$  is introduced to represent the degree of conductivity of the walls.

$$p = \frac{\sigma}{\omega \epsilon} \quad (6.17)$$

The higher the value of  $p$ , the higher the conductive degree of the wall. In our simulations,  $p$  varies from 10 to  $10^5$  and  $2.62 \times 10^7$ . It corresponds to the conductivity of the wall varying from 22.22 to 22222.22 (s/m) and  $5.8 \times 10^7$  s/m (for copper) at 40 GHz.

**Table 1 Computed Attenuation Constants with Different Conductivities**

$p$	Attenuation constant (Nepers/m)				
	SIBC	ADI-FDTD	FDTD	Difference between FDTD and (%):	
				SIBC	ADI-FDTD
10	29.47	70.56	70.33	-58.10	+0.33
100	9.21	18.87	18.80	-51.01	+0.37
1000	3.02	5.79	5.78	-47.75	+0.17
10000	1.00	1.81	1.83	-45.36	-1.09
$2.62 \times 10^7$ (copper)	0.0136	0.1012	N/A	N/A	N/A

**Table 2 Computed Phase Shift Constants with Different Conductivities**

$p$	Phase shift constant (radian/m)				
	SIBC	ADI-FDTD	FDTD	Difference between FDTD and (%):	
				SIBC	ADI-FDTD
10	685.91	698.13	698.13	-1.75	0
100	685.91	698.13	698.13	-1.75	0
1000	685.91	698.13	698.13	-1.75	0
10000	685.91	698.13	698.13	-1.75	0
$2.62 \times 10^7$ (copper)	685.91	687.33	N/A	N/A	N/A

\*  $p = \frac{\sigma}{\omega\epsilon}$  is the measurement of the degree of conductivity.

From Tables 1 and 2, the following observations can be made:

- 1) The results obtained with the FDTD and the ADI-FDTD are very close to each other, and the differences are less than 0.5%. Since the FDTD is a well proven method, we conclude that the ADI-FDTD is valid and effective in computing conductive media, regardless of the values of conductivities. In other words, the accuracy of the ADI-FDTD is at the same level as that of the FDTD. The ADI-FDTD can be a substitute for the conventional FDTD whenever applicable
- 2) There exist quite large differences between the results obtained with the SIBC method and those obtained with the FDTD or ADI-FDTD methods. The smaller the  $p$  value, the larger the differences. That means that when the wall becomes less conductive, the SIBC method becomes less accurate. The reason is that the SIBC method is assumed of plane wave propagation in a conductive medium. In a medium of low or medium-high conductivities ( $p=10-10000$ ) or cylindrical structures, the assumption is no longer valid. Therefore the results obtained with the SIBC approach will be quite different and most likely inaccurate.
- 3) The phase shift constants do not change much with variations of the conductivities while the attenuation constants do. This reflects the fact that the variations of the wall conductivity have more impact on the attenuation constant of the fields than that on the phase shift constant, as the energy is absorbed by the lossy wall.

Note that in the above computations, the FDTD method is used for the purpose of validating the ADI-FDTD method. The computation time required for the FDTD

simulations is much higher than that for the ADI-FDTD because of the CFL stability condition. In fact, for the case of the copper wall, the FDTD computation time became so high that we were not able to complete the FDTD simulation in days (this is why in Tables 1 and 2, no results are shown with FDTD for the copper case). Table 3 gives the comparison of the time used by FDTD and ADI-FDTD methods.

**Table 3 Computation Time by FDTD and ADI-FDTD**

$p$	Time step $\Delta t$ (ps)			Simulation time T (s)		
	FDTD	ADI-FDTD	Ratio	FDTD	ADI-FDTD	Ratio
10	0.103	0.635	6.17	916.91	1329.98	0.69
100	$3.25 \times 10^{-2}$	0.635	19.54	4791.95	1467.19	3.27
1000	$1.03 \times 10^{-2}$	0.635	61.65	8724.17	1549.83	5.63
10000	$3.25 \times 10^{-3}$	0.635	195.38	31905.17	1637.13	19.49

As can be seen from Table 3, for the FDTD method, the total simulation time T tends to increase with higher conductivity because of the smaller time step. For the ADI-FDTD, the total simulation time just slightly increases with higher conductivity. Consequently, the higher the conductivity, the larger the savings with the ADI-FDTD method in simulation run time. When  $p$  is larger than 10000, the saving is more than 19 times.

Table 4 shows the memory used by the FDTD method and ADI-FDTD methods. The ADI-FDTD method requires about double the amount of memory required by the FDTD method due to the fact that more field components at each time step are computed with the ADI-FDTD. The detailed explanations were offered in [136].

**Table 4 Memory Usage by the FDTD and ADI-FDTD Methods**

$p$	FDTD (Mbytes)	ADI-FDTD (Mbytes)
10	12.6	27.1
100	13.1	29.5
1000	14.1	30.8
10000	15.6	32.1

To shed more light on the accuracy of the ADI-FDTD method (which can now be considered to produce the solutions almost the same as those from the FDTD), Figure 6.7 shows the wave impedance in the air-filled region with different conductivities in comparisons with the theoretical solutions.

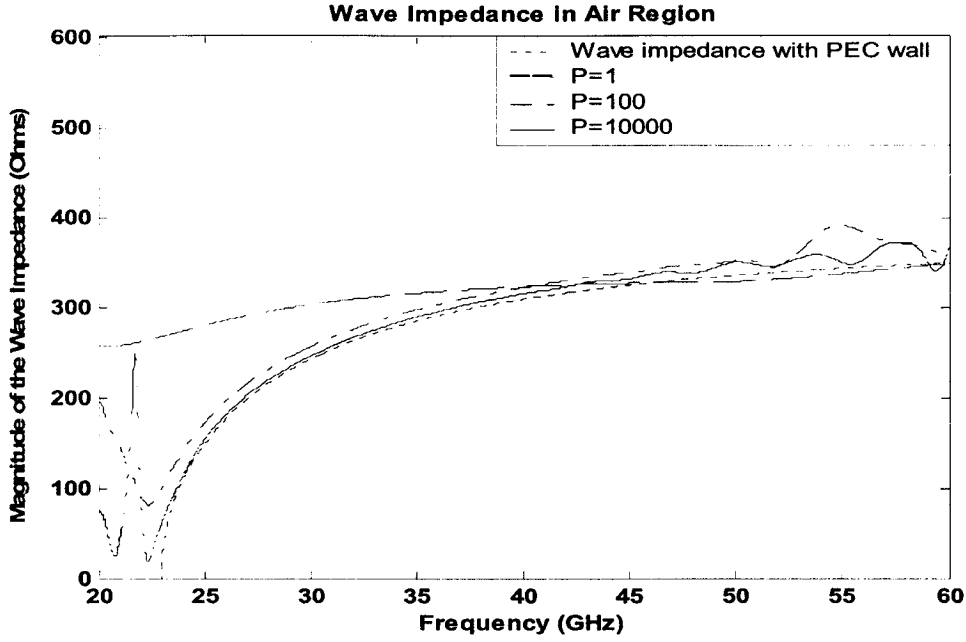


Figure 6.7 The z-directed wave impedance in the air-filled area with different conductivities

The wave impedance in the propagation direction in the air-filled region is defined as:

$$Z_{air \text{ } z - directed} = \left| \frac{\Im(E_r(z, t))}{\Im(H_\phi(z, t))} \right| \quad (6.18)$$

The theoretical impedance value is the wave impedance with a perfect conducting wall. As can be seen, the higher the  $p$  value, the closer the impedance computed with the ADI-FDTD is to the theoretical value with PEC. Consequently, the results obtained with the ADI-FDTD method are reasonably accurate. Ripples are observed at the higher end of the frequency range. We can not identify the exact cause. Our conjecture is that they are due to the dispersion error of the ADI-FDTD in a conducting medium at high frequencies. Further investigation along this line is currently under way.

### 6.5.2 Experiments on the Waveguide with Copper Wall

So far, we have shown that the ADI-FDTD can achieve the same accuracy as the FDTD with much less computation time in modeling conductive media. We then applied the ADI-FDD method to the copper wall which is more of a realistic problem.

The computed attenuation and phase shift constants were already shown in Table 1 and 2. The phase shift constant is very close to analytical solution with the perfect wall. The attenuation constants are, however, different from those obtained with the SIBC approach. Because the ADI-FDTD has been proven previously to be in a consistent agreement with the FDTD method, more confidence should be given to the ADI-FDTD results than to the SIBC results.

In the following paragraphs, other results, namely the field distributions and wave impedances, are shown. These results are presented simply because they can demonstrate that ADI-FDTD has not only the normal capability of the conventional FDTD and SIBC methods but also capabilities that the two methods do not have.

*a) Field distributions and wave impedance in the air-filled region*

Figure 6.8 shows the field attenuation along the  $z$  direction computed with the ADI-FDTD while Figure 6.9 is the phase of  $E_r$  at 40 GHz with the ADI-FDTD. From the two figures, one can see that the ADI-FDTD does pick up the field attenuation even it is small (as expected due to high conductivity of copper).

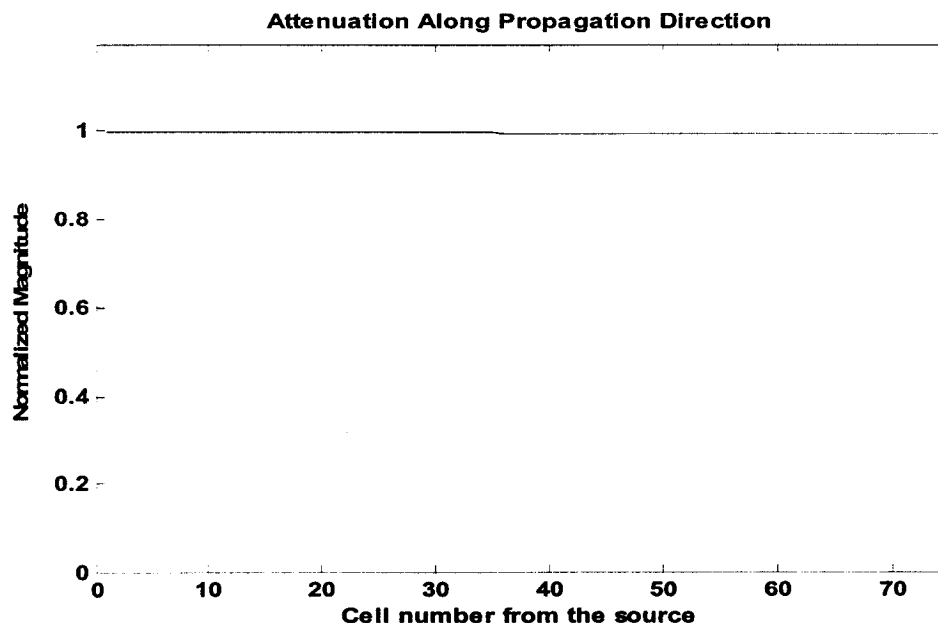


Figure 6.8 Field attenuation along propagation direction

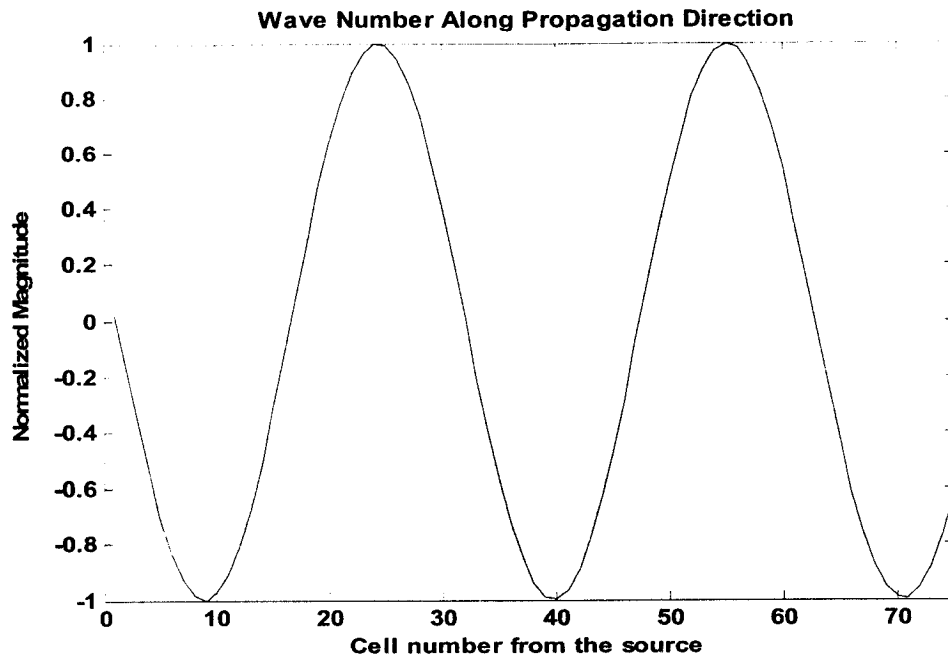


Figure 6.9 Wave number in the air-filled area in propagation direction

Figure 6.10 shows that the magnitude of the z-directed wave impedance simulated with the ADI-FDTD method as well as the analytical results with the assumption of the perfect electric conducting (PEC) wall. The impedance is computed with equation (6.18)

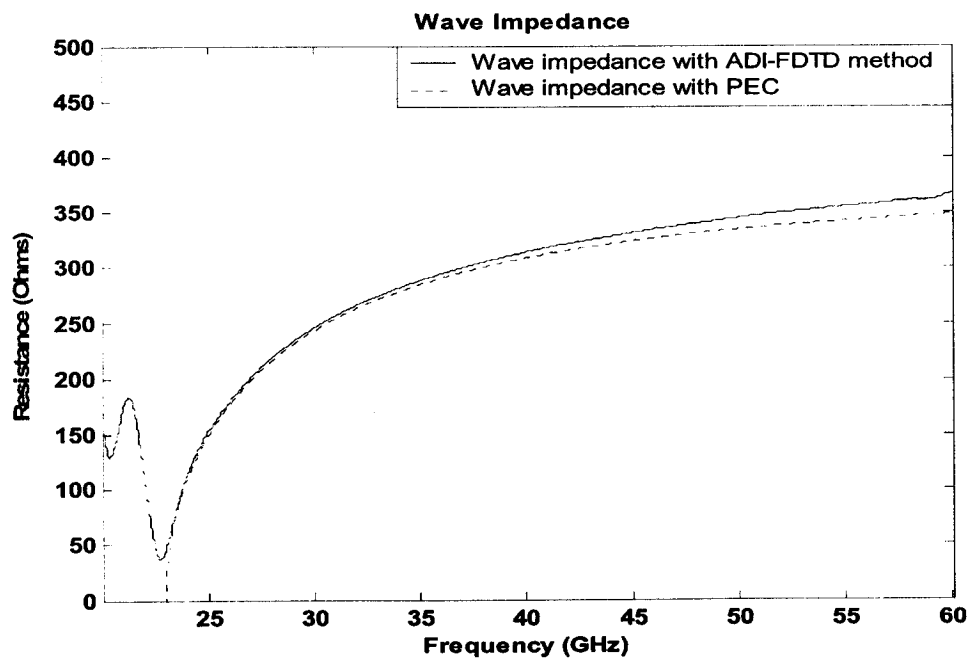


Figure 6.10 Wave impedance in the air-filled area



As can be seen, impedance calculated with the ADI-FDTD is very close to the theoretical result with PEC wall. The ripples at the very low frequencies may be attributed to the computer round-off errors since the field intensities below the cutoff frequency attenuate so much at the output points that the round-off errors simply override the real field values of small values below cutoff.

*b) Field distributions and wave impedance in the conducting wall*

Unlike the SIBC method that can not provide information on field distributions in the conductive region, the ADI-FDTD method is capable of simulating fields inside the conductive region. By recording time-domain field values at each grid point along a direction inside the wall, field distributions as well as the impedance in that direction can be obtained. Figure 6.11 (a) (b) and (c) show the field distribution inside the conductive region along the three respective directions.

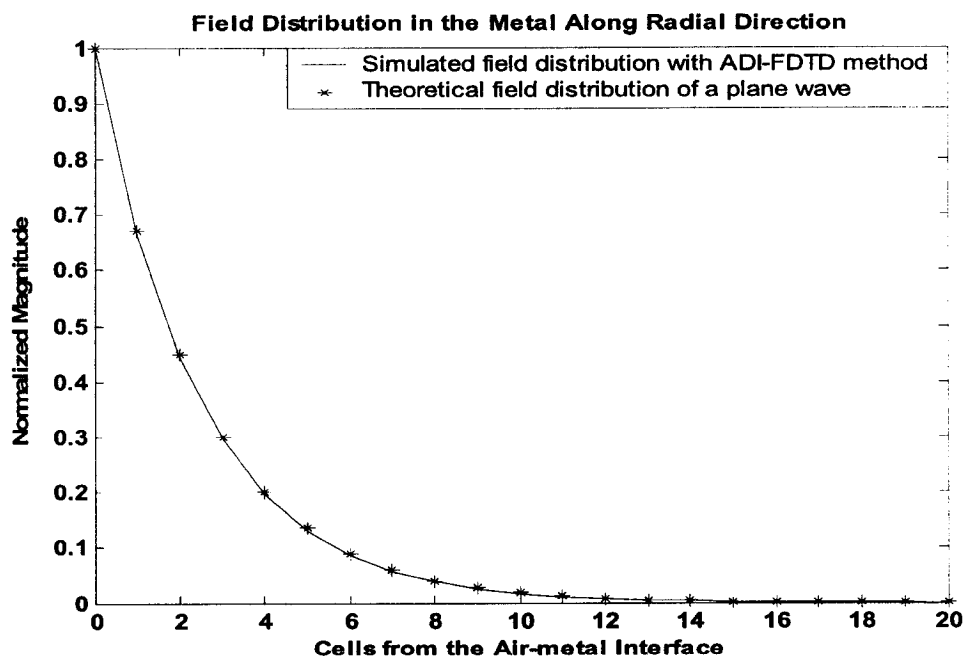


Figure 6.11(a) Field distribution in the conductive region in the radial direction at 40GHz

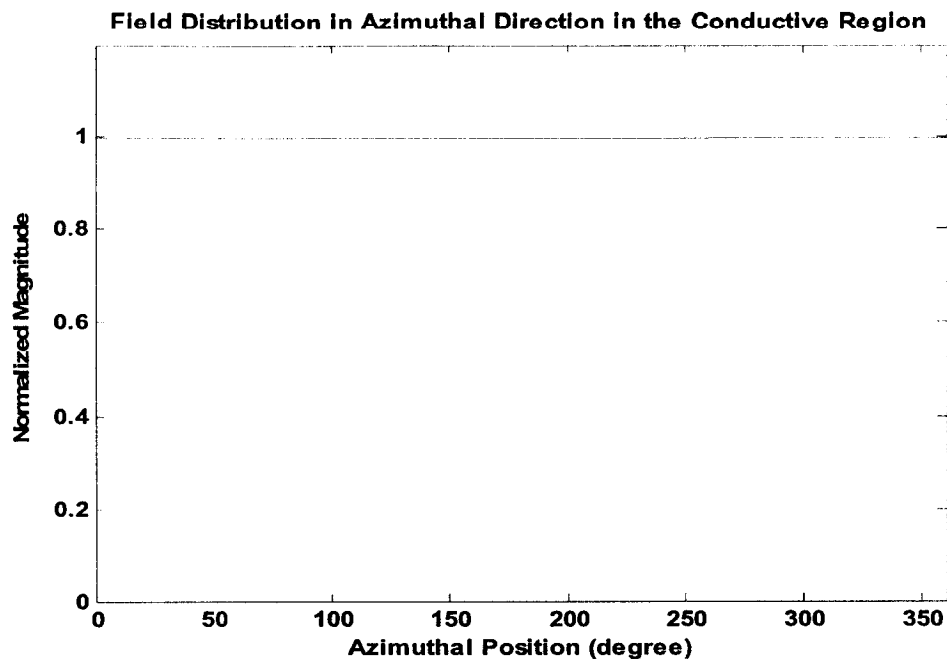


Figure 6.11(b) Field distribution in the conductive region in the azimuthal direction at 40GHz

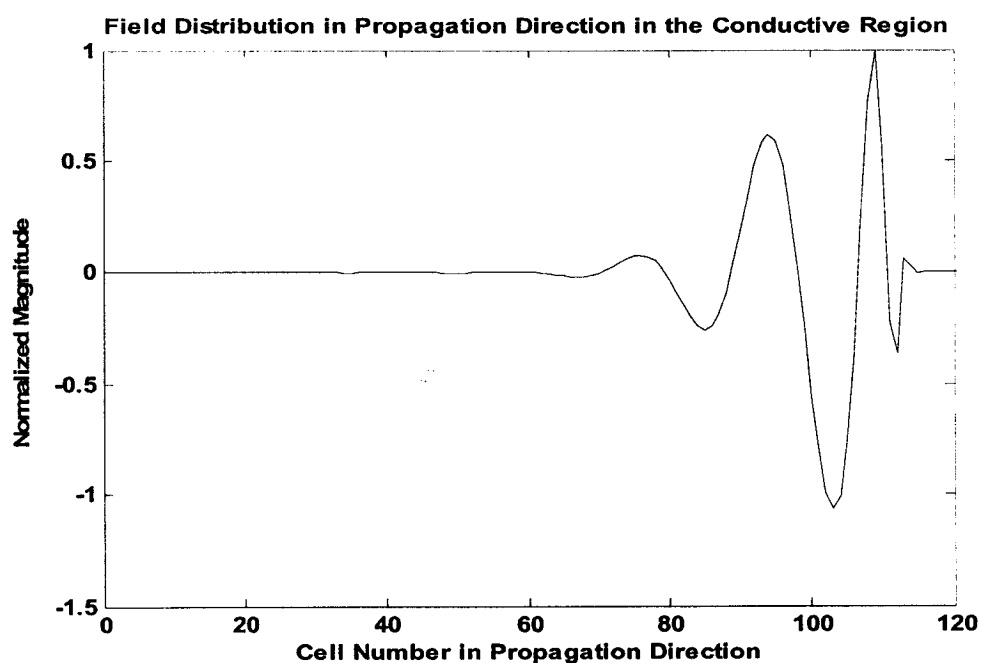


Figure 6.11(c) Field distribution in the conductive region in the propagation direction

From Figure 6.11(a), one can see that the field is attenuated in the radial direction. The theoretical distribution comes from the well-known case of the plane wave propagation in a conducting medium documented in most textbooks (where the field is attenuated with  $e^{-\frac{r}{\delta}}$  with  $\delta$  being the skin depth). The simulated and theoretical field distributions are

close to each other. It means that for highly conductive media, the field is attenuated as it is for a plane wave situation. However, this does not mean that the fields inside the conducting wall can be treated like a plane wave since the fields are distributed differently in the other directions. In the azimuthal and longitudinal directions (see Figure 11(b) and 11(c)), the fields are not attenuated with the factor of  $e^{-r/\delta}$ . Rather, they vary with the cylindrical mode field distributions like those in the air region. In our case, fields do not vary in the azimuthal direction but propagate in the longitudinal direction.

In correspondence to the field variations in the three directions inside the copper region, wave impedances on the surface of the copper wall along the three directions were also be computed via the following equations:

$$\begin{aligned} Z_r &= \frac{\Im(E_z(z, t))}{\Im(H_\phi(z, t))} \\ Z_\phi &= \frac{\Im(E_z(z, t))}{\Im(H_r(z, t))} \\ Z_z &= \frac{\Im(E_r(z, t))}{\Im(H_\phi(z, t))} \end{aligned} \quad (6.19)$$

Figure 6.12 shows the computed results. A particular attention should be paid to the impedance in the radial direction shown in Figure 6.12(a). It represents the surface impedance of the copper wall. As a reference, the surface impedance used with the SIBC approach is also shown in Figure 6.12(a). As seen, both impedances are close to each other, especially in a lower frequency range where  $p$  is larger. This validates the SIBC approach for modeling of highly conductive materials that are represented by large  $p$ . The impedances shown in Figure 6.12(b) and (c), however, are not associated with the surface impedance but the mode impedances. The z-directed wave impedance has a dip that corresponds to the cutoff frequency of  $TM_{01}$  mode. To the authors' best knowledge, values of these impedances in conducting media have not been reported so far in literature. This paper, for the first time, presents the results. This is significant in modeling of the highly conductive media with methods of the FDTD type.

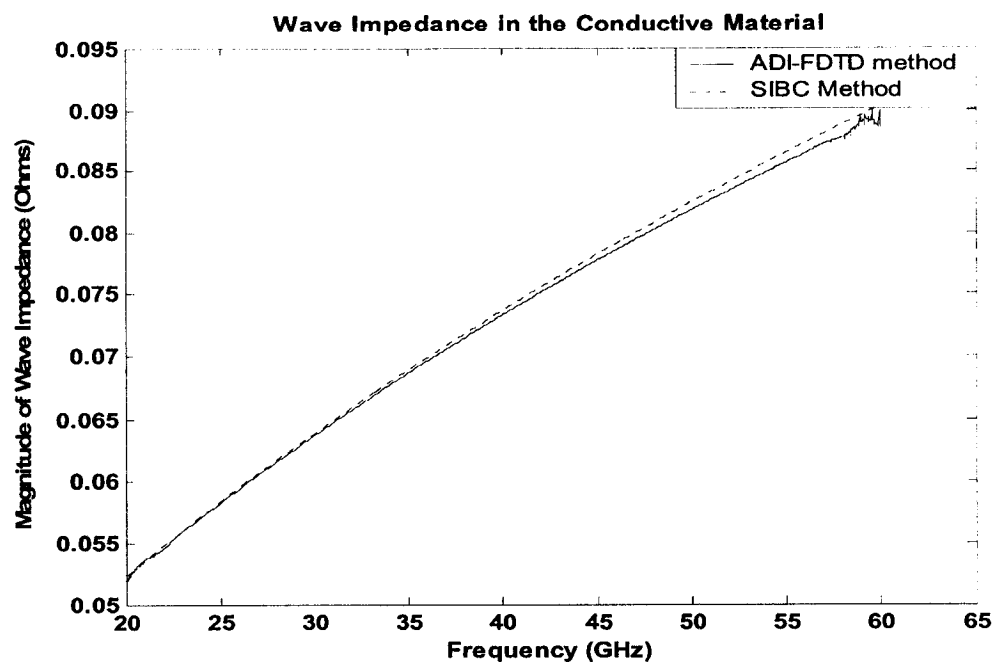


Figure 12(a) Wave impedance in the radial direction in the conductive area

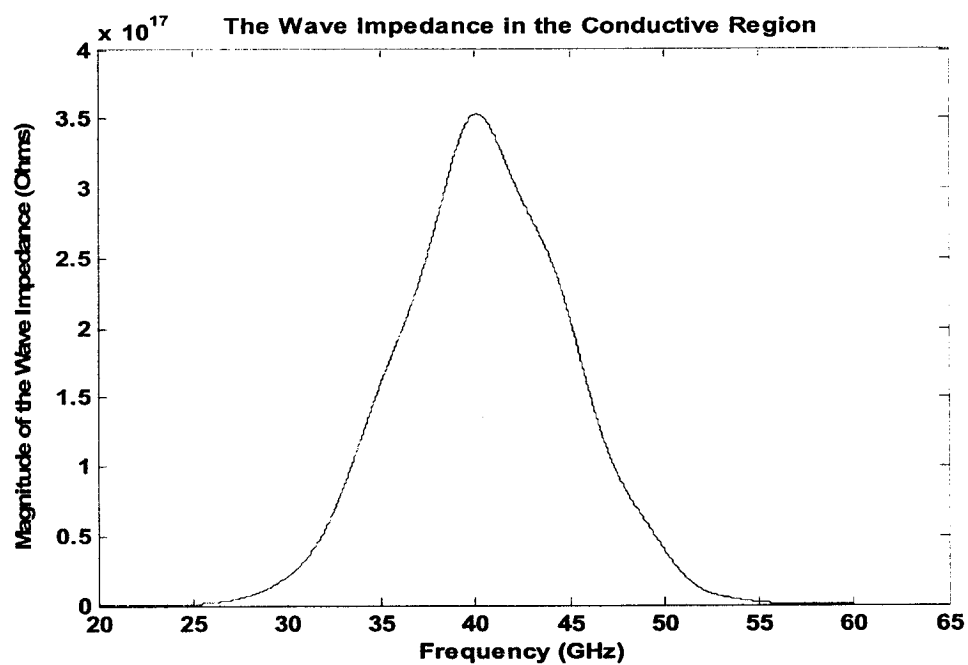


Figure 12(b) Wave impedance in the azimuthal direction in the conductive area

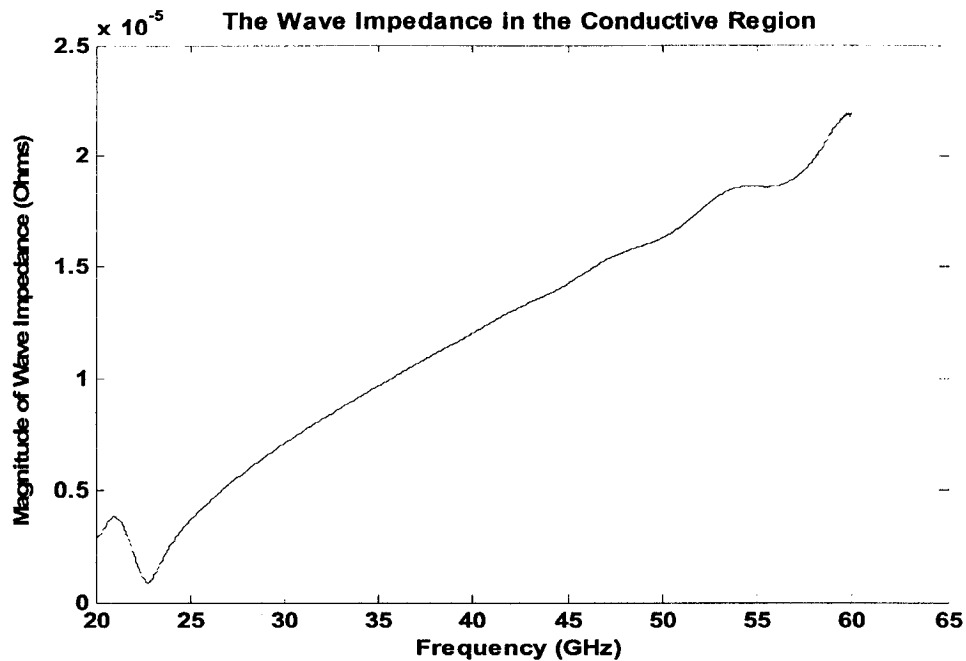


Figure 12(c) Wave impedance in the propagation direction in the conductive area

## 6.6 Conclusions

In this chapter, an extensive investigation on the application of ADI -FDTD to modeling open structures is presented. The unsplit uniaxial PML is also implemented into the cylindrical ADI-FDTD method for simulating structures that contain conductive medium with arbitrary conductivities. The performance comparison between Mur and UPML boundary conditions shows that UPML boundary condition is much more effective due to its omni direction wave-absorbing ability. The simulation results show that while the SIBC approach is valid for highly conductive media, the ADI-FDTD is an effective universal tool regardless of the degrees of medium conductivity. In comparison with the FDTD method, the ADI-FDTD can save significant amount of CPU time since it does not have the CFL condition.

## CHAPTER 7 SUMMARY AND FUTURE DIRECTIONS

### 7.1 Summary

Time-domain numerical techniques attract more and more research interest nowadays in computational electromagnetics for solving various electromagnetic problems. With the fast development of computer technologies, heavy CPU time requirements and large memory consumption are diminishing obstacles that limit the applications of time-domain techniques. Meanwhile more and more novel computation techniques are invented and introduced for efficient and accurate computation. Based on the knowledge of the numerical techniques, this thesis researches the existing numerical techniques, their advantages and disadvantages, their capabilities of solving various electromagnetic problems, and develops new time-domain schemes for improved computational efficiency and effectiveness.

Background knowledge of computational electromagnetics is reviewed in Chapter 1. The primary numerical techniques, including both frequency-domain and time-domain methods, are briefly discussed in this chapter. The newly developed time-domain techniques, such as PSTD and MRTD methods are also introduced in this chapter. As the basis of ADI-FDTD method, the basics of the conventional FDTD method are illustrated in Chapter 2. In Chapter 3, an unconditionally stable ADI-FDTD method in the cylindrical coordinate system is developed for effective and efficient modeling of microwave structures. Numerical simulation results are presented. Comparisons with the conventional FDTD method show that ADI-FDTD can use a large time step beyond CFL limits with acceptable modeling accuracy. In Chapter 4, the unconditional stability of the cylindrical ADI-FDTD is analytically proved with the use of *Schur-Cohn-Fujiwa* criterion, and further validated with numerical experiments. With the complete removal of CFL limit, the ADI-FDTD algorithm is then applied for solving closed type structures in Chapter 5. Various experiments are carried out for further testing the sustainability of the ADI-FDTD method. The structures with highly conductive enclosure, which have not been satisfactorily solved before with the conventional FDTD method, were simulated.

The simulation results show that ADI-FDTD method can effectively model the highly conductive materials. Applications of the ADI-FDTD method to open structures are presented in Chapter 6. Two popularly used boundary conditions-Mur and UPML ABCs-are successfully adapted and incorporated into the proposed ADI-FDTD method. The UPML-ADI-FDTD algorithm was formulated for modeling the open structures with arbitrary permittivity and conductivity. With the analysis of a circular waveguide with arbitrary conductive walls, it has been shown that the ADI-FDTD method presents much better numerical analysis than the approximated SIBC method. In other words, the ADI-FDTD presents a time-domain technique for modeling highly conductive materials, which has not been solved before with other time-domain methods.

In conclusion, while techniques such as MRTD and PSTD opened a way for reducing computation memory, the proposed ADI-FDTD presented a way to reduce the number of iterations which leads to less CPU time and provides the solution of a few problems previously untackled with other means. The work of this thesis has been published [131,145-147] and has led a new direction in the continuing effort of the electromagnetic modeling community towards improving computational efficiency of the FDTD algorithms.

## 7.2 Future Directions

The cylindrical ADI-FDTD method has been developed and investigated analytically and numerically, for numerical stability and computation efficiency. The typical closed and open structures with nonuniform medium parameters are also simulated. Nevertheless, there is still a wide range of topics yet to be researched.

### 1) *Dispersion Analysis of the Cylindrical ADI-FDTD Method*

As stated in 2.4.4, dispersion analysis is one of the most important aspects of any FDTD algorithm since dispersion contributes a major modeling error. As such, it is also desired to have the dispersion analysis for the ADI-FDTD algorithm. F. Zheng and Z. Chen have developed the dispersion analysis in the cartesian coordinate system [83]. In the cylindrical coordinate system, the dispersion error seems to be more difficult to evaluate

due to the varied cell sizes. As a result, the dispersion error produced from the inner cells would be different with that from the outer cells. The detailed analytical solution to the dispersion needs investigation.

## 2) *Modeling of Thin-Film Structures*

With the fast development of MMIC design, more and more thin-film structures appear and take the place of conventional microwave components and circuits. However, it is quite difficult to model thin-film structures at microwave frequencies, especially when they are placed in a relatively large structure. The reason is that fine mesh is required in the thin-film region for accurate modeling. The conventional FDTD has a hard time to deal with the fine mesh since fine mesh leads to small time step due to CFL condition. However, CFL condition is completely removed in the ADI-FDTD method. Therefore it is suitable for solving thin-film structures at microwave frequencies. The preliminary study on a cylindrical microstrip line [145] shows that the ADI-FDTD method is an effective and efficient tool to modeling this kind of structures. Nevertheless, extensive computations are needed to make solid conclusions.

## 3) *Combination with Other Numerical Method*

One possibility of having a more advanced ADI-FDTD model with smaller errors is to incorporate the MRTD principle into the proposed ADI-FDTD scheme. By doing so, it is expected that the time step can be further increased to a large value while the solution errors remain small because of the high accuracy of the MRTD model. In addition, since the MRTD allows the number of the grid points much smaller than that with the conventional FDTD, the combined saving in time could be very significant. Thus, incorporation of both techniques could well result in an efficient FDTD algorithm that can handle electrically large electromagnetic structures effectively.

## 4) *Applications to Optical Structures*

The cartesian ADI-FDTD method has been applied to a variety of microwave structures, especially planar type structures since it conforms the Yee's grid to the boundaries. However, optical structures usually appear in cylindrical shapes, such as optical fibers.



As a result, cylindrical ADI-FDTD method should be extended to analyzing the optical devices.

## Reference

- [1] G. D. Smith, *Numerical solution of partial differential equations*, Oxford, Oxford University Press, 1978.
- [2] G. E. Forsythe and W. R. Wasow, *Finite Difference Methods for Partial Differential Equations*, New York, Wiley, 1960.
- [3] P. F. Ryff, P. P. Biringer, P. E. Burke, "Calculation Methods for Current Distribution in Single Turn Coils of Arbitrary Cross Section," *IEEE Trans. on PAS*, 89(2), 228-232, 1967.
- [4] M. S. Sarma, "Potential Functions in Electromagnetic Field problems," *IEEE Trans. on Mag.*, 6(3), 513-518, 1970
- [5] R. Mitchell, D. F. Griffiths, *The Finite Difference Method in Partial Difference Equations*, Wiley, 1980.
- [6] E. Schweig, W. B. Bridges, "Computer Analysis of Dielectric Waveguides, A Finite Difference Method," *IEEE Trans. Microwave Theory and Techniques*, 32(5), 531-541, 1984.
- [7] J. L. Volakis, A. Chatterjee, and L. C. Kempel, *Finite Element Method for Electromagnetics*, IEEE Inc, 1998.
- [8] J. B. Davies, "Finite Element Analysis of Waveguides and Cavities – a Review," *IEEE Trans. Magnetism*, vol. 29, no. 2, Mar. 1993.
- [9] B. M. A. Rahman, F. A. Fernandez, and J. B. Davies, "Review of Finite Element Methods for Microwave and Optical Waveguides," in *Proc. IEEE*, vol. 79, No. 10, Oct. 1991.
- [10] Z. J. Cendes and P. Silverster, "Numerical Solution of Dielectric Loaded Waveguide: I – Finite Element Analysis," *IEEE Trans. Microwave Theory and Techniques*, pp. 1124-1131, 1970.
- [11] H. Whitney, *Geometric Integration Theory*, Princeton University. Press, NJ, 1957.
- [12] J. C. Nédélec, *Mixed Finite Elements in R<sup>3</sup>*, *Numerical Math.*, 35, pp. 315-341, 1980.
- [13] G. Mur and A. T. De Hoop, "A Finite Element Method for Computing Three-dimensional Electromagnetic Fields in Inhomogeneous Media," *IEEE Trans. Magnetism*, 21, pp. 2188-2191, Nov. 1985.

- [14] M. L. Barton and Z. J. Cendes, "New Vector Finite Elements for Three-Dimensional Magnetic Field Computation," *J. Appl. Phys*, 61(8), pp.3919-3921, Apr. 1987.
- [15] R. F. Harrington, *Field computation by Moment Methods*, Macmillan, 1968.
- [16] J. M. and J. L. Volakis, "A finite element-boundary integral formulation for scattering by three-dimensional cavity-backed apertures," *IEEE Trans. Antennas and Propagation*, vol. 39, pp.97-104, 1991.
- [17] Z. J. Cendes and P. Silverster, "Numerical solution of dielectric loaded waveguide: I – Finite element analysis," *IEEE Trans. Microwave Theory and Techniques*, pp. 1124-1131, 1970.
- [18] H. Whitney, *Geometric Integration Theory*, Princeton University. Press, NJ, 1957.
- [19] J. C. Nedelec, *Mixed finite elements in  $R^3$* , Numerical Math., 35, pp. 315-341, 1980.
- [20] M. L. Barton and Z. J. Cendes, "New vector finite elements for three-dimensional magnetic field computation," *J. Appl. Phys*, 61(8), pp.3919-3921, Apr. 1987.
- [21] V. N. Feddeeva, "An approximated method of lines applied to certain boundary value problems," *Tr. Mat. Inst. im V. A. Steklova Akad. Nauk SSSR*, 28, pp 73-103, 1949.
- [22] U. Schulz and R. Pregla, "A new technique for the analysis of plane waveguides and its application to microstrips with tuning septums," *Radio Sci.*, vol 16, pp. 1173-1178, 1981.
- [23] S. Worm and R. Pregla, "Hybrid-Mode Analysis of Arbitrarily Shaped Planar Microwave Structures by the Method of Lines," *IEEE Trans. Microwave Theory and Techniques*, vol. 32, no. 2, pp. 191-196, Feb. 1995.
- [24] P. Papachristoforos, "Method of lines for the calculation of excess capacitance for a cylindrical via in multilayer packaging," *IEE Proc. Microw. Antennas Propag.*, vol 146, no. 4, pp. 285-290, August 1999.
- [25] D. Argollo, H. Abdalla Jr., and A. Soares, "Method of Lines Applied to Broadside Suspended Stripline Coupler Design," *IEEE Trans. Magnetics*, vol. 31, no. 3, pp. 1634-1636, May 1995.

- [26] T. Itoh, "Analysis of Microstrip Resonators," *IEEE Trans. Microwave Theory and Techniques*, vol. 22, pp. 946-952, November 1974.
- [27] R. H. Jansen, "Unified User-oriented Computation of Shielded, Covered and Open Planar Microwave and Millimeter-wave Transmission-Line Characteristics," *IEE J. Microwaves, Opt. Acoust.*, vol. 3, pp. 14-22, January 1979.
- [28] L. P. Schmidt, T. Itoh, and H. Hofmann, "Characteristics of Unilateral Fin-line Structures and Arbitrarily Located Slots," *IEEE Trans. Microwave Theory and Techniques*, vol. 29, pp. 352-355, April 1981.
- [29] J. Boukamp and R. H. Jansen, "The High-frequency Behavior of Microstrip Open Ends in Microwave Integrated Circuits Including Energy Leakage," *14<sup>th</sup> Eur. Microwave Conf. Dig.*, pp. 142-147, September 1984.
- [30] T. Itoh, "Spectral Domain Immittance Approach for Dispersion Characteristics of Generalized Printed Transmission Lines," *IEEE Trans. Microwave Theory and Techniques*, vol. 28, pp. 733-736, July 1980.
- [31] K. S. Yee, "Numerical solution of initial boundary value problems involving Maxwell's equations in isotropic media," *IEEE Trans. Antennas and Propagation*, vol. 14, no. 3, pp. 302-307, May 1966.
- [32] K. L. Shlager and J. B. Scheider, "A Selective Survey of the Finite-Difference Time Domain Literature," *IEEE Antennas Propagation Mag.*, vol. 37, pp. 39-57, 1995.
- [33] P.B. Johns and R.L. Beurle, "Numerical Solution of Two-Dimensional Scattering Problems Using a Transmission Line Matrix," *Proc. IEEE*, vol. 118, Pt. H, pp. 1203-1208, 1971.
- [34] C. Cangellaris, C. Lin and K. K. Mei, "Point-Matched Time Domain Finite Element Methods for Electromagnetic Radiation and scattering," *IEEE Trans. on Antennas and Propagation*, vol. 35, No. 10, Oct. 1987.
- [35] S. Nam, H. Ling, and T. Itoh, "Characterization of Uniform Microstrip Line and Its Discontinuities Using the Time Domain Method of Lines," *IEEE Trans. Microwave Theory and Techniques*, vol. 37, pp. 2051-2057, 1989.
- [36] Allen Taflov, *Computational Electrodynamics: The Finite-Difference Time-Domain Method*, Artech House, 1995.

- [37] J. P. Berenger, "A Perfectly Matched Layer for the Absorption of Electromagnetic Waves", *J. Computational Physics*, vol. 114, pp. 185-200, 1994
- [38] Z. Ma, Y. Kobayashi "Analysis of Dielectric Resonators Using the FDTD Method Combined with the Padé Interpolation Technique," 1999 *Microwave Conference Asia Pacific*, vol. 2, pp. 401-404, September 1999.
- [39] J. Wang, O. Fujiwara, "FDTD computation of temperature rise in the human head for portable telephones," *IEEE Trans. Microwave Theory and Techniques*, vol. 47, no. 8, pp. 1528-1534, 1989
- [40] A. Taflove and M. E. Brodwin, "Numerical solution of steady-state electromagnetic scattering problems using the time-dependent Maxwell's equation," *IEEE Trans. Microwave Theory and Techniques*, vol. 23, pp. 623-630, Aug. 1975.
- [41] P.B. Johns and R.L. Beurle, "Numerical Solution of Two-Dimensional Scattering Problems Using a Transmission Line Matrix," *Proc. IEEE*, vol. 118, Pt. H, pp. 1203-1208, 1971.
- [42] P. B. Johns, "The solution of inhomogeneous waveguide problems using a transmission-line matrix," *IEEE Trans. Microwave Theory and Techniques*, vol. 22, pp. 209-215, Mar. 1974.
- [43] S. Akhtarzad, and P. B. Johns, "Numerical solution of lossy waveguides: TLM computer program," *Electron. Lett.*, vol. 10, no. 15, pp. 309-311, July, 1974.
- [44] S. Akhtarzad, and P. B. Johns, "Solution of 6-component electromagnetic fields in three space dimensions and time by the T. L. M. method," *Electron. Lett.*, vol. 10. no.25/26, pp. 535-537, Dec. 1974.
- [45] Z. Chen, M. M. Ney, and W.J.R. Hofer, "A New Finite-Difference Time Domain Formulation and Its Equivalence with the TLM Symmetrical Condensed Node," *IEEE MTT-S Trans.*, vol. 39, pp. 2160-2169, 1991.
- [46] J. Nelsen and W. Hoefer, " A complete dispersion analysis of the condensed node TLM mesh," *IEEE Trans. Magnetics*, vol. 27, pp. 3982-3985, Sept. 1991.
- [47] P. Berini and K. Wu, "A Comprehensive Study of Numerical Anisotropy and Dispersion in 3-D TLM Meshes," *IEEE Trans. Microwave Theory and Techniques*, vol. 43, no. 5, pp. 1173-1181, May 1995.

- [48] M. Krumpholz and P. Russer, "On the dispersion in TLM and FDTD," *IEEE Trans. Microwave Theory and Techniques*, vol. 42, pp. 1275-1279, July. 1994.
- [49] W.J.R. Hofer, "The Transmission-line Matrix Method—Theory and Applications," *IEEE Trans. Microwave Theory and Techniques*, vol. 33, pp. 882-893, 1985.
- [50] M. A. Kolbehdari, M. Srinivasan, M. Nakhla, Q. Zhang, R. Achar, "Simultaneous Time and Frequency Domain Solutions of EM problems Using Finite Element and CFH Techniques," *IEEE Trans. Microwave Theory and Techniques*, vol. 44, no.9, Sept. 1996.
- [51] J. F. Lee, R. Lee, and A. Cangellaris, "Time-Domain Finite-Element Methods," *IEEE Trans. Antennas and Propagation*, vol. 45, no. 3, pp. 430-442, Mar. 1997.
- [52] S. Gedney and U. Navasariwala, "An Unconditionally Stable Finite Element Time Domain Solution of the Vector Wave Equation," *IEEE Microwave Guided Wave Lett.*, vol. 5, pp. 332-334, October 1995.
- [53] M. F. Wong, O. Picon, and V. F. Hanna, "A Finite Element Method Based on Whitney forms to Solve Maxwell equations in the time domain," *IEEE Trans. Magnetics*, vol. 31, no. 5, pp. 1618-1621, May 1995.
- [54] S Chang, R. Coccioli, Y. Qian, and T. Itoh, "A global finite-element time-domain analysis of active nonlinear microwave circuits," *IEEE Trans. Microwave Theory and Techniques*, vol. 47, no. 12 , pp. 2410-2416 , Dec. 1999.
- [55] T. Yamada and K. Tani, "Finite element time domain method using hexahedral elements," *IEEE Trans. on Magnetics*, vol. 33, no. 2, pp. 1476 –1479, March 1997.
- [56] D. C. Dikken and R. Metaxas, "Time domain finite element analysis of multimode microwave applicators," *IEEE Trans. on Magnetics*, vol. 32, no. 3, pp. 942-945, May 1996.
- [57] M. Feliziani and F. Maradei, "Mixed finite-difference/Whitney-elements time domain (FD/WE-TD) method," *IEEE Trans. on Magnetics*, vol. 34, no. 5, pp. 3222-3227, Sept. 1998.

- [58] R. Wu, T. Itoh, "Hybrid finite-difference time-domain modeling of curved surfaces using tetrahedral edge elements," *IEEE Trans. Antennas and Propagation*, vol. 45, no. 8, pp. 1302-1309, Aug. 1997.
- [59] D. Koh, H. Lee, and T. Itoh, "A hybrid full-wave analysis of via-hole grounds using finite-difference and finite-element time-domain methods," *IEEE Trans. Microwave Theory and Techniques*, vol. 45, no. 12, pp. 2217-2223, Dec. 1997.
- [60] P. H. Aoyagi, J. F. Lee, and R. Mittra, "A Hybrid Yee algorithm/Scalarwave equation approach," *IEEE Trans. on Microwave Theory and Techniques*, vol. 41, no. 9, pp. 1593-1600, Sept. 1993.
- [61] M. Mrozowski, "A Hybrid PEE-FDTD algorithm for accelerated time domain analysis of electromagnetic wave in shielded structures," *IEEE Microwave Guided Wave Lett.*, vol. 4, no. 10, pp. 323-325, Oct. 1994.
- [62] S. Nam, S. El-Ghazaly, H. Ling and T. Itoh, "Time-domain Method of Lines Applied to a Partially Filled Waveguide," 1998 *IEEE International Symposium on Microwave Theory and Techniques* Dig., pp. 627-630.
- [63] S. Nam, H. Ling and T. Itoh, "Characterization of Uniform Microstrip Line and Its Discontinuities Using the Time-domain Method of Lines," *IEEE Trans. Microwave Theory and Techniques*, vol. 37, no. 12, pp. 2051-2057, Dec. 1989.
- [64] M. Krumpholz and L. P. B. Katehi, "MRTD: New Time-Domain Schemes Based on Multiresolution Analysis," *IEEE Trans. on Microwave Theory and Techniques*, vol. 44, no. 4, pp. 555-571, Apr. 1996.
- [65] M. Werthen and I. Wolff, "A novel wavelet based time domain simulation approach," *IEEE Microwave Guided Wave Letters*, vol. 6, pp. 438-440, Dec. 1996.
- [66] M. Fujii and W. J. R. Hoefer, "A Three-Dimensional Haar-Wavelet-Based Multiresolution Analysis Similar to the FDTD Method – Derivation and Application," *IEEE Trans. on Microwave Theory and Techniques*, vol. 46, no. 12, pp. 2463-2475, Dec. 1998.
- [67] K. Goverdhanam, L. P. B. Katehi, and A. Cangellaris, "Application of multiresolution based FDTD multigrid," in 1997 *IEEE MTT-S Int. Microwave Symp. Dig.*, pp. 333-336.

- [68] R. Robertson, E. Tentzeris, M. Krumpholz, and L. P. B. Katehi, "Application of MRTD analysis to dielectric cavity structures," in *Proc. Microwave Theory Tech. Soc.*, 1996, pp. 1840-1843.
- [69] K. Sabetfakhri and L. P. B. Katehi, "Analysis of integrated millimeterwave and submillimeter-wave waveguides using orthonormal wavelet expansions," *IEEE Trans. Microwave Theory and Techniques*, vol. 42, no. 12, pp. 2412-2422, Dec. 1994.
- [70] E. Tentzeris, R. Robertson, L. P. B. Katehi, and "Application of MRTD to printed transmission lines," in 1996 IEEE MTT-S Int. Microwave Symp. Dig. Pp. 573-577.
- [71] R. Robertson, E. M. Tentzeris, and L. P. B. Katehi, "Modeling of Membrane Patch Antennas Using MRTD Analysis," 1997 IEEE, pp.126-129.
- [72] M. Krumpholz, H. G. Winful, and L. P. B. Katehi, "Nonlinear Time-Domain Modeling by Multiresolution Time Domain (MRTD)," *IEEE Trans. Microwave Theory and Techniques*, vol. 45, no. 3, pp. 385-393, Mar. 1997.
- [73] K. L. Shlager and J. B. Schneider, "Analysis of the dispersion properties of the multiresolution time-domain method, " in *Proc. IEEE AP-S*, vol. 4, 1997, pp. 2144-2147.
- [74] Hong, N. Yoon, and H. Park, "Numerical dispersive characteristics and stability condition of the multiresolution time-domain (MRTD) method",
- [75] J. Zhang and Z. Chen, "Low dispersive super high order FDTD schemes," Digest of 2000 IEEE AP-S International Symposium and USNC/URSI National Radio Science Meeting, Salt Lake City, July 16-21, 2000, pp. 1510-1513.
- [76] Q. H. Liu, "The Pseudospectral Time-Domain (PSTD) method: a new algorithm for solution of Maxwell's equations," *IEEE Antennas and Propagation Society International Symposium*, vol. 1, pp. 122-125, 1997
- [77] Q. H. Liu, "The PSTD algorithm: A time-domain method requiring only two cells per wavelength," *Microwave and Optical Technology Letters*, vol. 15, no. 3, pp. 158-165, Mar. 1997.



- [78] Y. F. Leung and C. H. Chan, "Combining the FDTD and PSTD Method," *Microwave and Optical Technology Letters*, vol. 23, no. 4, pp. 249-254, Nov. 1999
- [79] R. Holland, "Implicit three-dimensional finite differencing of Maxwell's equations," *IEEE Trans. Nuclear Science*, Vol. NS-31, No. 6, pp. 1322-1326, 1984.
- [80] P. M. Goorjian, "Algorithm Development for Maxwell's Equations for Computational Electromagnetism," AIAA Paper 90-0251, American Institute of Aeronautics & Astronautics, 28<sup>th</sup> Aerospace Sciences Meeting, Reno, NV, January 8-11, 1990
- [81] T. Namiki and K. Ito, "A new FDTD algorithm free from the CFL condition restraint for a 2D-TE wave", *Digest of 1999 IEEE Antennas and Propagation Symposium*, Jul. 1999, Orlando, pp.192-195.
- [82] F. Zhen, Z. Chen, and J. Zhang, "Toward the Development of a Three-dimensional Unconditionally Stable Finite-difference Time-domain Method," *IEEE Trans. MTT.*, vol. 48, no. 9, pp. 1550-1558, September 2000.
- [83] F. H. Zheng and Z. Z. Chen, "Numerical dispersion analysis of the unconditionally stable 3-D ADI-FDTD method", *IEEE Trans. Microwave Theory Tech.*, vol.49,no 5,pp.1006-1009,May 2001.
- [84] T. Namiki,; K. Ito, "Numerical Simulation Using ADI-FDTD Method to Estimate Shielding Effectiveness of Thin Conductive Enclosures," *IEEE Trans. MTT.*, vol. 49, no. 6, pp. 1060-1066, June 2001.
- [85] X. Zhang and K. K. Mei, "Time domain finite difference approach for the calculation of the frequency-dependent characteristics of the microstrip discontinuities," *IEEE Trans. Microwave Theory and Techniques*, vol. 36, pp. 1775-1787, Dec. 1988.
- [86] Z. Bi, K. Wu, C. Wu, and J. Litva, "A dispersive boundary condition for microstrip component analysis using the FDTD method," *IEEE Trans. Microwave Theory and Techniques*, vol. 40, pp. 774-776, Aug. 1992.
- [87] J. A. Pereda, L. A. Viela, A. Vegas, and A. prieto, "A treatment of magnetized ferites using the FDTD method, " *IEEE Microwave and Guided Wave Letters*, vol. 3, 1993, pp. 136-138.

- [88] V. A. Thomas, M. E. Jones, M. J. Picket-May, A. Taflove, and E. Harrigan, "The use of SPICE lumped circuits as sub-grid models for high-speed electronic circuit design," *IEEE Microwave and Guided Wave Letters*, vol. 4, 1994, pp. 141-143.
- [89] D. M. Sheen, S. M. Ali, M. D. Abouzabra, and J. A. Kong, "Application of the three-dimensional finite-difference time-domain method to the analysis of planar microstrip circuits," *IEEE Trans. Microwave Theory and Techniques*, vol. 38, pp. 849-857, 1990.
- [90] P. Harms, J. Lee, and R. Mittra, "Characterizing the cylindrical via discontinuity," *IEEE Trans. Microwave Theory and Techniques*, vol. 41, no. 8, pp. 153-156, Aug. 1993.
- [91] L. W. Ko and R. Mittra, "A combination of FD-TD and Prony's methods for analyzing microwave integrated circuits," *IEEE Trans. Microwave Theory and Techniques*, vol. 39, no. 8, pp. 2176-2181, 1991.
- [92] S. Gedney, and F. Lansing, "A generalized Yee algorithm for the analysis of three-dimensional microwave circuit devices with planar symmetry," *IEEE Trans. Microwave Theory and Techniques*, vol. 42, no. 8, pp. 1514-1523, Aug. 1994.
- [93] E. Sano and T. Shibata, "Fullwave analysis of picosecond photoconductive switches," *IEEE J. Quantum Electronics*, vol. 26, 1990, pp. 372-377.
- [94] R. W. Ziolkowski and J. B. Judkins, "Full-wave vector Maxwell's equations modeling of self-focusing of ultra-short optical pulses in a nonlinear Kerr medium exhibiting a finite response time," *J. Optical Society of America B*, vol. 10, 1993, pp. 186-198.
- [95] R. M. Joseph and A. Taflove, "Spatial soliton deflection mechanism indicated by FDTD Maxwell's equation modeling," *IEEE Photonics Technology Letters*, 1994, pp. 1251-1254.
- [96] N. M. Potheary and C. J. Railton, "Analysis of Cross-Talk on High-Speed Digital Circuits Using the Finite Difference Time-Domain Method," *International Journal of Numerical Modeling*, 1991.
- [97] M. Rittweger, M. Werthen, and I. Wolff, "FDTD Simulation for Microwave Packages and Interconnects," *Proceeding of Workshop WSFC: EM Modeling of Microwave Packages and Interconnects*, IEEE Microwave

Theory and Techniques Society International Microwave Symposium Digest, May 1993.

- [98] M. J. Piket-May, A. Taflove, and J. Baron, "FD-TD modeling of digital signal propagation in 3-D circuits with passive and active loads," *IEEE Trans. Microwave Theory and Techniques*, vol. 42, no. 8, pp. 1514-1523, Aug. 1994.
- [99] W. D. Becker, P. H. Harms, and R. Mittra, "Time-Domain electromagnetic analysis of interconnects in a computer chip package," *IEEE Trans. Microwave Theory and Techniques*, vol. 40, no. 8, pp. 430-451, 1992.
- [100] Reineix and B. Jecko, "Analysis of microstrip patch antennas using finite difference time domain method," *IEEE Trans. Antennas and Propagation*, vol. 37, pp. 1361-1369, 1989.
- [101] J. G. Maloney, G. S. Smith, and W. R. Scoot, "Accurate computation of the radiation from simple antenna using the finite-difference time-domain method," *IEEE Trans. Antennas and Propagation*, vol. 38, pp. 1059-1068, 1990.
- [102] P. A. Tirkas, and C. A. Balanis, "Finite-difference time-domain method for antenna radiation," *IEEE Trans. Antennas and Propagation*, vol. 40, pp. 334-340, 1992.
- [103] D. M. Sullivan, O. P. Gandhi, and A. Taflove, "Use of the Finite-Difference Time-Domain Method in Calculating EM absorbtion human models," *IEEE Trans. Biomedical Engineering*, vol. 35, pp. 179-186, 1988.
- [104] M. J. Piket-May, A. Taflove, W. C. Lin, D. S. Katz, V. Sathiaselalan, and B. B. Mittal, "Initial results for automated computational modeling of patient-specific electromagnetic hyperthermia," *IEEE Trans. Biomedical Engineering*, vol. 39, pp. 226-237, 1992.
- [105] M. E. Bialkowski and S. S. Stuchly, "A study of handset antenna and human body interaction," *IEEE Trans. Microwave Theory and Techniques*, vol. 44, no. 8, pp. 1855-1864, 1994.
- [106] D. Sheen, Numerical modeling of microstrip circuits and antennas, *Ph. D. Dissertation, Massachusetts Institute of Technology, Cambridge, MA*, June 1991

- [107] T. G. Jurgens, A. Taflove, K. Umashankar, and T. G. Moore, "Finite-difference time-domain modeling of curved surfaces," *IEEE Trans. Antennas and Propagation*, vol. 40, pp. 357-366, 1992
- [108] R. Holland, "Finite-difference solution of Maxwell's equations in generalized nonorthogonal coordinates," *IEEE Trans. Nuclear Science*, vol. NS-30, pp. 4589-4591, 1983
- [109] J. -F. Lee, R. Palendech, and R. Mittra, "Modeling three-dimensional discontinuities in waveguides using nonorthogonal FD-TD algorithm," *IEEE Trans. Microwave Theory and Techniques*, vol. 40, pp. 346-352, 1992
- [110] N. Madsen, "Divergence preserving discrete surface integral methods for Maxwell's equations using nonorthogonal unstructured grids," Technical Report UCRL-JC-109787, LLNL, 1992
- [111] P. Monk, and E. Suli, "A convergence analysis of Yee's scheme on nonuniform grids," *SIAM J. Numerical Analysis*, vol. 31, pp. 393-412, 1994
- [112] P. Monk, "Error estimates for Yee's method on nonuniform grids," *IEEE Trans. Magnetics*, vol. 30, pp. 3200-3203, 1994
- [113] L. Paul and Z. Skvor, "Stability of FDTD in curvilinear coordinates," *IEEE EUROCON'2001, Trends in Communications*, vol. 2, pp. 314-317, 2001
- [114] H. Chen and K. Wong, "Characterization of cylindrical microstrip gap discontinuities," *Microwave Optical Tech. Lett.*, pp. 260-263, 1995
- [115] Bayliss and E. Turkel, "Radiation boundary conditions for wave-like equations," *Comm. Pure Appl. Math.*, vol. 23, pp. 707-725, 1980
- [116] Enquist and A. Majda, "Absorbing boundary conditions for the numerical simulation of waves," *Mathematics of Computation*, vol. 31, pp. 629-651, 1977
- [117] G. Mur, "Absorbing boundary conditions for the finite-difference approximation of the time-domain electromagnetic equations," *IEEE Trans. Electromagnetic Compatibility*, vol. 23, pp. 377-382, 1981
- [118] Z. P. Liao, H. L. Wong, B. P. Yang, and Y. F. Yuan, "A transmitting boundary condition for transient wave analyses," *Scientia Sinica (series A)*, vol. XXVII, pp. 1063-1076, 1984

- [119] K. K. Mei and J. Fang, "Superabsorption- a method to improve absorbing boundary conditions," *IEEE Trans. Antennas and Propagation*, vol. 40, pp. 1001-1010, 1992
- [120] J.-P. Berenger, "A perfectly matched layer for the absorption of electromagnetic waves," *J. Computational Physics*, vol. 114, pp. 185-200, 1994
- [121] S. Katz, E. T. Thiele, and A. Taflove, "Validation and extension to three dimensions of the Berenger PML absorbing boundary condition for FD-TD meshes," *IEEE Microwave and Guided Wave Letters*, vol. 4, pp. 268-270, 1994
- [122] J.-P. Berenger, "A perfectly matched layer for free-space simulation in finite-difference computer codes," *presentation at EUROEM'94*, France, 1994
- [123] Z. S. Sacks, D. M. Kingsland, R. Lee, and J. F. Lee, "A perfectly matched anisotropic absorber for use as an absorbing boundary condition," *IEEE Trans. Antennas and Propagations*, vol. 43, pp. 1460-1463, 1995
- [124] J. A. Roden and S. D. Gedney, "Convolutional PML (CPML): An efficient FDTD implementation of the CFS-PML for arbitrary media," *Microwave and Optical Technology Letters*, vol. 27, pp. 334-339, 2000
- [125] W. C. Chew and W. H. Weedon, "A 3D perfectly matched medium from modified Maxwell's equations with stretched coordinates," *IEEE Microwave and Guided Wave Letters*, vol. 7, pp. 599-604, 1994
- [126] M. Rappaport, "Perfectly matched absorbing boundary conditions based on anisotropic lossy mapping of space," *IEEE Microwave and Guided Wave Letters*, vol. 5 pp. 90-92, 1995
- [127] W. C. Chew, J. M. Jin, and E. Michielssen, "Complex coordinate stretching as a generalized absorbing boundary condition," *Microwave and Optical Technology Letters*, vol. 15, pp. 363-369, 1997
- [128] J. Maloney, M. Kesler, and G. Smith, "Generalization of PML to cylindrical geometries," *Proc. 13<sup>th</sup> Annual Review of Progress in Applied Computational Electromagnetics*, vol. 2, pp. 900-908, 1997
- [129] D. W. Peaceman and H. H. Rachford, "The Numerical Solution of Parabolic and Elliptic Differential Equations," *J. Soc. Indust. Appl. Math.*, vol. 42, no. 3, pp. 28-41, 1955

- [130] D. M. Pozar, *Microwave Engineering*, Addison Wesley, 1990, ISBN 0201504189
- [131] C. Yuan, Z. Chen, "A three dimensional unconditionally stable ADI-FDTD method in the cylindrical coordinate system", *IEEE Trans. Microwave Theory Techniques.*, vol. 50, no. 10, pp. 2401-2405, October 2002.
- [132] F. Zhen, Z. Chen, and J. Zhang, "Toward the Development of a Three-dimensional Unconditionally Stable Finite-difference Time-domain Method," *IEEE Trans. MTT.*, vol. 48, no. 9, pp. 1550-1558, September 2000.
- [133] I. SCHUR, "Über Potenzreihen, die in Innern des Einheitskreises beschränkt sind," *J. F}r Math.*, 147,205-232, 1917.
- [134] A. COHN, "Über die Anzahl der Wurzeln einer algebraischen Gleichung in einem Kreise," *Math. Z.*, 14-15, 110-148, 1914.
- [135] H. FUJIWARA, "Über die algebraischen Gleichungen, deren Wurzeln einem Kreise oder in eine liegen," *Math. Z.*, 24, 160-169, 1926.
- [136] F. Zheng, Z. Chen and J. Zhang, "Towards the development of a three-dimensional unconditionally stable finite-difference time-domain method", *IEEE Trans. Microwave Technology and Techniques*, vol. 48, no. 9, pp. 1550-1558, 2000
- [137] R. F. Harrington, *Time-harmonic Electromagnetic Fields*, McGraw-Hill Book Company, ISBN39361010240951,1961.
- [138] C. Wang, B. Q. Gao, and C. P. Deng, "Accurate Study of Q-Factor of Resonator by a Finite-Difference Time-Domain Method," *IEEE Trans.MTT.*, vol. 43, no. 7, pp. 1524-1528, July 1995
- [136] R. J. Lubbers, and F. Hunsberger, and K. S. Kunz, "Application of a New FDTD Formulation to Highly Conductive Materials," *Proc.URSI Nat. Radio Sci. Meet.*, San Jose, CA, June 1995.
- [137] J. A. Pereda, L. A. Vielva, A. Vegas, and A. Prieto, "Computation of resonant frequencies and quality factors by the combination of the finite-difference time-domain and Prony's methods," *IEEE Guided Wave Lett.*, vol.2, no. 11, pp. 431-433, Nov. 1992

- [138] Monorchio, and R. Mittra, "A hybrid finite-element finite-difference time-domain (FE/FDTD) technique for solving complex electromagnetic problems," *IEEE Guided Wave Lett.* vol. 8, pp. 93-95, Feb. 1998
- [139] Z. Ma,; Y. Kobayashi "Analysis of Dielectric Resonators Using the FDTD Method Combined with the Padé Interpolation Technique," 1999 *Microwave Conference Asia Pacific*, vol. 2, pp. 401-404, September 1999.
- [140] P. H. Harms, J.-F. Lee, and R. Mittra, "A Study of Nonorthogonal FDTD Method Versus the Conventional FDTD Technique for Computing Resonant Frequencies of Cylindrical Cavities", *IEEE Trans. MTT*, vol. 41, no. 5, pp.668-676, May 1993
- [141] K. Chamberlin, and L. Gordon, "Modeling Good Conductors Using the Finite-Difference Time-Domain Technique" *IEEE Trans. Electromagnetic Compatibility*, vol. 37, pp. 210-216, May 1995.
- [142] Y. Gao, and C. J. Railton, "Efficient Determination of Q Factor by Structured Nonorthogonal FDTD Method," *Electronics Lett.*, vol. 34, no. 19, pp. 1834-1836, September 1998.
- [143] Allen Taflove, *Advances in Computational Electrodynamics: The Finite-Difference Time-Domain Method*, Artech House, 1998.
- [144] C-S. Shin, R. Nevels, "Optimizing the Gaussian Excitation Function in the Finite Difference Time Domain Method ", *IEEE Tans. on Education*, vol. 45, no. 13, pp. 15-18, February 2002.
- [145] C. Yuan and Zhizhang Chen, "Efficient Computation of Thin-layer Structures with the Unconditionally Stable ADI-FDTD Method", *IEEE 2003 International Symposium on Microwave Theory and Techniques*, vol. 2, pp.1133-1136, June 2003
- [146] C. Yuan and Zhizhang Chen, "Towards Accurate Simulation of Highly onductive Materials", *IEEE International Symposium on Microwave Theory and Techniques*, vol.2, Seattle USA, June 2002
- [147] C. Yuan and Zhizhang Chen, "On the Modeling of Conducting Materials with the Unconditionally Stable ADI-FDTD Method", *IEEE Transaction on Microwave Theory and Techniques*, vol. 51, no. 8, pp. 1929-1938, August 2003

## Appendix A      Equations of the Cylindrical ADI-FDTD Algorithm

For the advancement from the  $n$ th time step to the  $(n+1/2)$ th time step:

$$E_r^{n+\frac{1}{2}}(i+\frac{1}{2}, j, k) = E_r^n(i+\frac{1}{2}, j, k) + \frac{\Delta t}{2\varepsilon} \left[ \frac{H_z^{n+\frac{1}{2}}(i+\frac{1}{2}, j+\frac{1}{2}, k) - H_z^{n+\frac{1}{2}}(i+\frac{1}{2}, j-\frac{1}{2}, k)}{\Delta\phi r(i+\frac{1}{2})} - \frac{H_\phi^n(i+\frac{1}{2}, j, k+\frac{1}{2}) - H_\phi^n(i+\frac{1}{2}, j, k-\frac{1}{2})}{\Delta z l(k)} \right] \quad (\text{A-1a})$$

$$E_\phi^{n+\frac{1}{2}}(i, j+\frac{1}{2}, k) = E_\phi^n(i, j+\frac{1}{2}, k) + \frac{\Delta t}{2\varepsilon} \left[ \frac{H_r^{n+\frac{1}{2}}(i, j+\frac{1}{2}, k+\frac{1}{2}) - H_r^{n+\frac{1}{2}}(i, j+\frac{1}{2}, k-\frac{1}{2})}{\Delta z l(k)} - \frac{H_z^n(i+\frac{1}{2}, j+\frac{1}{2}, k) - H_z^n(i-\frac{1}{2}, j+\frac{1}{2}, k)}{\Delta r l(i)} \right] \quad (\text{A-1b})$$

$$E_z^{n+\frac{1}{2}}(i, j, k+\frac{1}{2}) = E_z^n(i, j, k+\frac{1}{2}) + \frac{\Delta t}{2 \cdot \varepsilon \cdot r(i)} \left[ \frac{r(i+\frac{1}{2}) \cdot H_\phi^{n+\frac{1}{2}}(i+\frac{1}{2}, j, k+\frac{1}{2}) - r(i-\frac{1}{2}) \cdot H_\phi^{n+\frac{1}{2}}(i-\frac{1}{2}, j, k+\frac{1}{2})}{\Delta r l(i)} - \frac{H_r^n(i, j+\frac{1}{2}, k+\frac{1}{2}) - H_r^n(i, j-\frac{1}{2}, k+\frac{1}{2})}{\Delta\phi} \right] \quad (\text{A-1c})$$



$$H_r^{n+\frac{1}{2}}(i, j + \frac{1}{2}, k + \frac{1}{2}) = H_r^n(i, j + \frac{1}{2}, k + \frac{1}{2}) + \frac{\Delta t}{2\mu} \left[ \frac{E_\phi^{n+\frac{1}{2}}(i, j + \frac{1}{2}, k + 1) - E_\phi^{n+\frac{1}{2}}(i, j + \frac{1}{2}, k)}{\Delta z 2(k + 1)} - \frac{E_z^n(i, j + 1, k + \frac{1}{2}) - E_z^n(i, j, k + \frac{1}{2})}{\Delta \phi r(i)} \right] \quad (\text{A-1d})$$

$$H_\phi^{n+\frac{1}{2}}(i + \frac{1}{2}, j, k + \frac{1}{2}) = H_\phi^n(i + \frac{1}{2}, j, k + \frac{1}{2}) + \frac{\Delta t}{2\mu} \left[ \frac{E_z^{n+\frac{1}{2}}(i + 1, j, k + \frac{1}{2}) - E_z^{n+\frac{1}{2}}(i, j, k + \frac{1}{2})}{\Delta r 2(i + 1)} - \frac{E_r^n(i + \frac{1}{2}, j, k + 1) - E_r^n(i + \frac{1}{2}, j, k)}{\Delta z 2(k + 1)} \right] \quad (\text{A-1e})$$

$$H_z^{n+\frac{1}{2}}(i + \frac{1}{2}, j + \frac{1}{2}, k) = H_z^n(i + \frac{1}{2}, j + \frac{1}{2}, k) + \frac{\Delta t}{2\mu \cdot r(i + \frac{1}{2})} \left[ \frac{E_r^{n+\frac{1}{2}}(i + \frac{1}{2}, j + 1, k) - E_r^{n+\frac{1}{2}}(i + \frac{1}{2}, j, k)}{\Delta \phi} - \frac{r(i + 1) \cdot E_\phi^n(i + 1, j + \frac{1}{2}, k) - r(i) \cdot E_\phi^n(i, j + \frac{1}{2}, k)}{\Delta r 2(i + 1)} \right] \quad (\text{A-1f})$$

For the advancement from the  $(n+1/2)$ th to the  $(n+1)$ th time step

$$E_r^{n+1}(i + \frac{1}{2}, j, k) = E_r^{n+\frac{1}{2}}(i + \frac{1}{2}, j, k) + \frac{\Delta t}{2\varepsilon} \left[ \frac{H_z^{n+\frac{1}{2}}(i + \frac{1}{2}, j + \frac{1}{2}, k) - H_z^{n+\frac{1}{2}}(i + \frac{1}{2}, j - \frac{1}{2}, k)}{\Delta \phi r(i + \frac{1}{2})} - \frac{H_\phi^{n+1}(i + \frac{1}{2}, j, k + \frac{1}{2}) - H_\phi^{n+1}(i + \frac{1}{2}, j, k - \frac{1}{2})}{\Delta z 1(k)} \right] \quad (\text{A-2a})$$

$$E_{\phi}^{n+1}(i, j + \frac{1}{2}, k) = E_{\phi}^{n+\frac{1}{2}}(i, j + \frac{1}{2}, k) + \frac{\Delta t}{2\varepsilon} \left[ \frac{H_r^{n+\frac{1}{2}}(i, j + \frac{1}{2}, k + \frac{1}{2}) - H_r^{n+\frac{1}{2}}(i, j + \frac{1}{2}, k - \frac{1}{2})}{\Delta z1(k)} - \frac{H_z^{n+1}(i + \frac{1}{2}, j + \frac{1}{2}, k) - H_z^{n+1}(i - \frac{1}{2}, j + \frac{1}{2}, k)}{\Delta r1(i)} \right] \quad (\text{A-2b})$$

$$E_z^{n+1}(i, j, k + \frac{1}{2}) = E_z^{n+\frac{1}{2}}(i, j, k + \frac{1}{2}) + \frac{\Delta t}{2\varepsilon \cdot r(i)} \left[ \frac{(i + \frac{1}{2}) \cdot \Delta r \cdot H_{\phi}^{n+\frac{1}{2}}(i + \frac{1}{2}, j, k + \frac{1}{2}) - (i - \frac{1}{2}) \cdot \Delta r \cdot H_{\phi}^{n+\frac{1}{2}}(i - \frac{1}{2}, j, k + \frac{1}{2})}{\Delta r1(i)} - \frac{H_r^{n+1}(i, j + \frac{1}{2}, k + \frac{1}{2}) - H_r^{n+1}(i, j - \frac{1}{2}, k + \frac{1}{2})}{\Delta \phi} \right] \quad (\text{A-2c})$$

$$H_r^{n+1}(i, j + \frac{1}{2}, k + \frac{1}{2}) = H_r^{n+\frac{1}{2}}(i, j + \frac{1}{2}, k + \frac{1}{2}) + \frac{\Delta t}{2\mu} \left[ \frac{E_{\phi}^{n+\frac{1}{2}}(i, j + \frac{1}{2}, k + 1) - E_{\phi}^{n+\frac{1}{2}}(i, j + \frac{1}{2}, k)}{\Delta z2(k + 1)} - \frac{E_z^{n+1}(i, j + 1, k + \frac{1}{2}) - E_z^{n+1}(i, j, k + \frac{1}{2})}{\Delta \phi r(i)} \right] \quad (\text{A-2d})$$

$$H_{\phi}^{n+1}(i + \frac{1}{2}, j, k + \frac{1}{2}) = H_{\phi}^{n+\frac{1}{2}}(i + \frac{1}{2}, j, k + \frac{1}{2}) + \frac{\Delta t}{2\mu} \left[ \frac{E_z^{n+\frac{1}{2}}(i + 1, j, k + \frac{1}{2}) - E_z^{n+\frac{1}{2}}(i, j, k + \frac{1}{2})}{\Delta r2(i + 1)} - \frac{E_r^{n+1}(i + \frac{1}{2}, j, k + 1) - E_r^{n+1}(i + \frac{1}{2}, j, k)}{\Delta z2(k + 1)} \right] \quad (\text{A-2e})$$

$$H_z^{n+1}(i + \frac{1}{2}, j + \frac{1}{2}, k) = H_z^{n+\frac{1}{2}}(i + \frac{1}{2}, j + \frac{1}{2}, k) + \frac{\Delta t}{2\mu \cdot r(i + \frac{1}{2})} \left[ \frac{E_r^{n+\frac{1}{2}}(i + \frac{1}{2}, j + 1, k) - E_r^{n+\frac{1}{2}}(i + \frac{1}{2}, j, k)}{\Delta \phi} - \frac{r(i + 1) \cdot E_\phi^{n+1}(i + 1, j + \frac{1}{2}, k) - r(i) \cdot E_\phi^{n+1}(i, j + \frac{1}{2}, k)}{\Delta r 2(i + 1)} \right] \quad (\text{A-2f})$$

As stated in 2.3.1, the field components located on the z-axis need a special treatment. To obtain the corresponding unconditionally stable scheme, the ADI is applied. As a result, the following two equations are obtained for the two sub-time steps computations:

$$E_z^{n+\frac{1}{2}}(0, j, k + \frac{1}{2}) = E_z^n(0, j, k + \frac{1}{2}) + \frac{4\Delta t}{\varepsilon \cdot \Delta r 2(1)} H_\phi^{n+\frac{1}{2}}(\frac{1}{2}, j, k + \frac{1}{2}) \quad (\text{A-3a})$$

for the first sub time-step and

$$E_z^{n+1}(0, j, k + \frac{1}{2}) = E_z^{n+\frac{1}{2}}(0, j, k + \frac{1}{2}) + \frac{4\Delta t}{\varepsilon \cdot \Delta r 2(1)} H_\phi^{n+\frac{1}{2}}(\frac{1}{2}, j, k + \frac{1}{2}) \quad (\text{A-3b})$$

for the second sub time-step.

The notations  $E_\alpha^n(i, j, k)$  and  $H_\alpha^n(i, j, k)$  with  $\alpha = r, \phi, z$  are the field components with their grid positions being the same as those with the conventional FDTD of the Yee's scheme.

## Appendix B      Rearranged Equations of ADI-FDTD Equations for Computer Programming

for the first sub-step:

$$\begin{aligned}
 & - \left( \frac{f}{\Delta \phi^2 r^2 (i + \frac{1}{2})} \right) E_r^{n+\frac{1}{2}}(i + \frac{1}{2}, j + 1, k) + \left( 1 + \frac{2f}{\Delta \phi^2 r^2 (i + \frac{1}{2})} \right) E_r^{n+\frac{1}{2}}(i + \frac{1}{2}, j, k) \\
 & - \left( \frac{f}{\Delta \phi^2 r^2 (i + \frac{1}{2})} \right) E_r^{n+\frac{1}{2}}(i + \frac{1}{2}, j - 1, k) \\
 & = E_r^n(i + \frac{1}{2}, j, k) + \frac{\Delta t}{2\varepsilon \Delta \phi r (i + \frac{1}{2})} \left[ H_z^n(i + \frac{1}{2}, j + \frac{1}{2}, k) - H_z^n(i + \frac{1}{2}, j - \frac{1}{2}, k) \right] \\
 & - \frac{\Delta t}{2\varepsilon \Delta z l(k)} \left[ H_\phi^n(i + \frac{1}{2}, j, k + \frac{1}{2}) - H_\phi^n(i + \frac{1}{2}, j, k - \frac{1}{2}) \right] \\
 & - \frac{f}{\Delta \phi r^2 (i + \frac{1}{2}) \Delta r 2(i + 1)} \left[ \begin{aligned} & r(i + 1) (E_\phi^n(i + 1, j + \frac{1}{2}, k) - E_\phi^n(i + 1, j - \frac{1}{2}, k)) \\ & - r(i) (E_\phi^n(i, j + \frac{1}{2}, k) - E_\phi^n(i, j - \frac{1}{2}, k)) \end{aligned} \right] \tag{B-1a}
 \end{aligned}$$

$$\begin{aligned}
 & - \left( \frac{f}{\Delta z l(k) \Delta z 2(k + 1)} \right) E_\phi^{n+\frac{1}{2}}(i, j + \frac{1}{2}, k + 1) + \left[ 1 + \frac{f}{\Delta z l(k)} \left( \frac{1}{\Delta z 2(k + 1)} + \frac{1}{\Delta z 2(k)} \right) \right] E_\phi^{n+\frac{1}{2}}(i, j + \frac{1}{2}, k) \\
 & - \left( \frac{f}{\Delta z l(k) \Delta z 2(k)} \right) E_\phi^{n+\frac{1}{2}}(i, j + \frac{1}{2}, k - 1) \\
 & = E_\phi^n(i, j + \frac{1}{2}, k) + \frac{\Delta t}{2\varepsilon \Delta z l(k)} [H_r^n(i, j + \frac{1}{2}, k + \frac{1}{2}) - H_r^n(i, j + \frac{1}{2}, k - \frac{1}{2})] \\
 & - \frac{\Delta t}{2\varepsilon \Delta r l(i)} [H_z^n(i + \frac{1}{2}, j + \frac{1}{2}, k) - H_z^n(i - \frac{1}{2}, j + \frac{1}{2}, k)] \\
 & - \frac{f}{\Delta \phi \cdot r(i) \Delta z l(k)} \left[ \begin{aligned} & E_z^n(i, j + 1, k + \frac{1}{2}) - E_z^n(i, j, k + \frac{1}{2}) \\ & - E_z^n(i, j + 1, k - \frac{1}{2}) + E_z^n(i, j, k - \frac{1}{2}) \end{aligned} \right] \tag{B-1b}
 \end{aligned}$$

$$\begin{aligned}
& -\left(\frac{f \cdot r(i+\frac{1}{2})}{r(i)\Delta r1(i)\Delta r2(i+1)}\right)E_z^{n+\frac{1}{2}}(i+1, j, k+\frac{1}{2}) + \left[1 + \frac{f}{r(i)\Delta r1(i)}\left(\frac{r(i+\frac{1}{2})}{\Delta r2(i+1)} + \frac{r(i-\frac{1}{2})}{\Delta r2(i)}\right)\right]E_z^{n+\frac{1}{2}}(i, j, k+\frac{1}{2}) \\
& -\left(\frac{f \cdot r(i-\frac{1}{2})}{r(i)\Delta r1(i)\Delta r2(i)}\right)E_z^{n+\frac{1}{2}}(i-1, j, k+\frac{1}{2}) \\
& = E_z^n(i, j, k+\frac{1}{2}) \\
& + \frac{\Delta t}{2\sigma(i)\Delta r1(i)}\left[r(i+\frac{1}{2})H_\phi^n(i+\frac{1}{2}, j, k+\frac{1}{2}) - r(i-\frac{1}{2})H_\phi^n(i-\frac{1}{2}, j, k+\frac{1}{2})\right] \\
& - \frac{\Delta t}{2\sigma(i)\Delta\phi}\left[H_r^n(i, j+\frac{1}{2}, k+\frac{1}{2}) - H_r^n(i, j-\frac{1}{2}, k+\frac{1}{2})\right] \\
& - \frac{f}{r(i)\Delta r1(i)\Delta z2(k+1)}\left[r(i+\frac{1}{2})\left(E_r^n(i+\frac{1}{2}, j, k+1) - E_r^n(i+\frac{1}{2}, j, k)\right)\right. \\
& \quad \left.- r(i-\frac{1}{2})\left(E_r^n(i-\frac{1}{2}, j, k+1) - E_r^n(i-\frac{1}{2}, j, k)\right)\right] \tag{B-1c}
\end{aligned}$$

$$\begin{aligned}
& -\frac{4f}{\Delta r2(1)^2}E_z^{n+\frac{1}{2}}(1, j, k+\frac{1}{2}) + \left(1 + \frac{4f}{\Delta r2^2(1)}\right)E_z^{n+\frac{1}{2}}(0, j, k+\frac{1}{2}) \\
& = \frac{c1}{c2}E_z^n(0, j, k+\frac{1}{2}) + \frac{\Delta t}{\varepsilon \cdot \Delta r2(1)}H_\phi^n(\frac{1}{2}, j, k+\frac{1}{2}) \\
& - \frac{4f}{\Delta r2(1) \cdot \Delta z2(k+1)}[E_r(0, j, k+1) - E_r(0, j, k)] \tag{B-1d}
\end{aligned}$$

$$\begin{aligned}
H_r^{n+\frac{1}{2}}(i, j+\frac{1}{2}, k+\frac{1}{2}) & = H_r^n(i, j+\frac{1}{2}, k+\frac{1}{2}) + \\
& \frac{\Delta t}{2\mu}\left[\frac{E_\phi^{n+\frac{1}{2}}(i, j+\frac{1}{2}, k+1) - E_\phi^{n+\frac{1}{2}}(i, j+\frac{1}{2}, k)}{\Delta z2(k+1)}\right. \\
& \quad \left.- \frac{E_z^n(i, j+1, k+\frac{1}{2}) - E_z^n(i, j, k+\frac{1}{2})}{\Delta\phi \cdot r(i)}\right] \tag{B-1e}
\end{aligned}$$

$$\begin{aligned}
H_\phi^{n+\frac{1}{2}}(i+\frac{1}{2}, j, k+\frac{1}{2}) & = H_\phi^n(i+\frac{1}{2}, j, k+\frac{1}{2}) + \\
& \frac{\Delta t}{2\mu}\left[\frac{E_z^{n+\frac{1}{2}}(i+1, j, k+\frac{1}{2}) - E_z^{n+\frac{1}{2}}(i, j, k+\frac{1}{2})}{\Delta r2(i+1)}\right. \\
& \quad \left.- \frac{E_r^n(i+\frac{1}{2}, j, k+1) - E_r^n(i+\frac{1}{2}, j, k)}{\Delta z2(k+1)}\right] \tag{B-1f}
\end{aligned}$$

$$\begin{aligned}
H_z^{n+\frac{1}{2}}(i+\frac{1}{2}, j+\frac{1}{2}, k) &= H_z^n(i+\frac{1}{2}, j+\frac{1}{2}, k) + \\
&\frac{\Delta t}{2\mu \cdot r(i+\frac{1}{2})} \left[ \frac{E_r^{n+\frac{1}{2}}(i+\frac{1}{2}, j+1, k) - E_r^{n+\frac{1}{2}}(i+\frac{1}{2}, j, k)}{\Delta \phi} \right. \\
&\quad \left. - \frac{r(i+1) \cdot E_\phi^n(i+1, j+\frac{1}{2}, k) - r(i) \cdot E_\phi^n(i, j+\frac{1}{2}, k)}{\Delta r 2(i+1)} \right] \quad (B-1g)
\end{aligned}$$

For the second sub-step:

$$\begin{aligned}
& - \left( \frac{f}{\Delta z 1(k) \Delta z 2(k+1)} \right) E_r^{n+1}(i+\frac{1}{2}, j, k+1) + \left[ 1 + \frac{f}{\Delta z 1(k)} \left( \frac{1}{\Delta z 2(k+1)} + \frac{1}{\Delta z 2(k)} \right) \right] E_r^{n+1}(i+\frac{1}{2}, j, k) \\
& - \left( \frac{f}{\Delta z 1(k) \Delta z 2(k)} \right) E_r^{n+\frac{1}{2}}(i+\frac{1}{2}, j, k-1) \\
& = E_r^{n+\frac{1}{2}}(i+\frac{1}{2}, j, k) + \frac{\Delta t}{2\epsilon \Delta \phi r(i+\frac{1}{2})} \left[ H_z^{n+\frac{1}{2}}(i+\frac{1}{2}, j+\frac{1}{2}, k) - H_z^{n+\frac{1}{2}}(i+\frac{1}{2}, j-\frac{1}{2}, k) \right] \\
& - \frac{\Delta t}{2\epsilon \Delta z 1(k)} \left[ H_\phi^{n+\frac{1}{2}}(i+\frac{1}{2}, j, k+\frac{1}{2}) - H_\phi^{n+\frac{1}{2}}(i+\frac{1}{2}, j, k-\frac{1}{2}) \right] \\
& - \frac{f}{\Delta z 1(k) \Delta r 2(i+1)} \left[ \begin{aligned} & E_z^{n+\frac{1}{2}}(i+1, j, k+\frac{1}{2}) - E_z^{n+\frac{1}{2}}(i, j, k+\frac{1}{2}) \\ & - E_z^{n+\frac{1}{2}}(i+1, j, k-\frac{1}{2}) - E_z^{n+\frac{1}{2}}(i, j, k-\frac{1}{2}) \end{aligned} \right] \quad (B-2a)
\end{aligned}$$

$$\begin{aligned}
& -\left(\frac{f \cdot r(i+1)}{\Delta r(i) \Delta r 2(i+1) r(i+\frac{1}{2})}\right) E_{\phi}^{n+1}(i+1, j+\frac{1}{2}, k) + \left[1 + \frac{f \cdot r(i)}{\Delta r(i)} \left(\frac{1}{r(i+\frac{1}{2}) \Delta r 2(i+1)} + \frac{1}{r(i-\frac{1}{2}) \Delta r 2(i)}\right)\right] E_{\phi}^{n+1}(i, j+\frac{1}{2}, k) \\
& -\left(\frac{f \cdot r(i-1)}{\Delta r(i) \Delta r 2(i) r(i-\frac{1}{2})}\right) E_{\phi}^{n+1}(i-1, j+\frac{1}{2}, k) \\
& = E_{\phi}^{n+\frac{1}{2}}(i, j+\frac{1}{2}, k) + \frac{\Delta r}{2 \varepsilon \Delta z l(k)} [H_r^{n+\frac{1}{2}}(i, j+\frac{1}{2}, k+\frac{1}{2}) - H_r^{n+\frac{1}{2}}(i, j+\frac{1}{2}, k-\frac{1}{2})] \\
& - \frac{\Delta r}{2 \varepsilon \Delta r l(i)} [H_z^{n+\frac{1}{2}}(i+\frac{1}{2}, j+\frac{1}{2}, k) - H_z^{n+\frac{1}{2}}(i-\frac{1}{2}, j+\frac{1}{2}, k)] \\
& - \frac{f}{\Delta \phi \cdot \Delta r l(i)} \left[ \frac{E_r^{n+\frac{1}{2}}(i+\frac{1}{2}, j+1, k) - E_r^{n+\frac{1}{2}}(i+\frac{1}{2}, j, k)}{r(i+\frac{1}{2})} \right. \\
& \quad \left. \frac{E_r^{n+\frac{1}{2}}(i-\frac{1}{2}, j+1, k) - E_r^{n+\frac{1}{2}}(i-\frac{1}{2}, j, k)}{r(i-\frac{1}{2})} \right] \tag{B-2b}
\end{aligned}$$

$$\begin{aligned}
& -\left(\frac{f}{\Delta \phi^2 r^2(i)}\right) E_z^{n+1}(i, j+1, k+\frac{1}{2}) + \left(1 + \frac{2f}{\Delta \phi^2 r^2(i)}\right) E_z^{n+1}(i, j, k+\frac{1}{2}) \\
& -\left(\frac{f}{\Delta \phi^2 r^2(i)}\right) E_z^{n+1}(i, j-1, k+\frac{1}{2}) \\
& = E_z^{n+\frac{1}{2}}(i, j, k+\frac{1}{2}) \\
& + \frac{\Delta t}{2 \varepsilon r(i) \Delta r l(i)} \left[ r(i+\frac{1}{2}) H_{\phi}^{n+\frac{1}{2}}(i+\frac{1}{2}, j, k+\frac{1}{2}) - r(i-\frac{1}{2}) H_{\phi}^{n+\frac{1}{2}}(i-\frac{1}{2}, j, k+\frac{1}{2}) \right] \tag{B-2c} \\
& - \frac{\Delta t}{2 \varepsilon r(i) \Delta \phi} \left[ H_r^{n+\frac{1}{2}}(i, j+\frac{1}{2}, k+\frac{1}{2}) - H_r^n(i, j-\frac{1}{2}, k+\frac{1}{2}) \right] \\
& - \frac{f}{r(i) \Delta \phi \Delta z 2(k+1) r(i)} \left[ \frac{E_{\phi}^{n+\frac{1}{2}}(i, j+\frac{1}{2}, k+1) - E_{\phi}^{n+\frac{1}{2}}(i, j+\frac{1}{2}, k)}{r(i+\frac{1}{2})} \right. \\
& \quad \left. - \frac{E_{\phi}^{n+\frac{1}{2}}(i, j-\frac{1}{2}, k+1) + E_{\phi}^{n+\frac{1}{2}}(i, j-\frac{1}{2}, k)}{r(i-\frac{1}{2})} \right]
\end{aligned}$$

$$E_z^{n+1}(0, j, k+\frac{1}{2}) = E_z^{n+\frac{1}{2}}(0, j, k+\frac{1}{2}) + \frac{4 \Delta t}{\varepsilon \cdot \Delta r 2(1)} H_{\phi}^{n+\frac{1}{2}}(\frac{1}{2}, j, k+\frac{1}{2}) \tag{B-2d}$$

$$H_r^{n+1}(i, j + \frac{1}{2}, k + \frac{1}{2}) = H_r^{n+\frac{1}{2}}(i, j + \frac{1}{2}, k + \frac{1}{2}) + \frac{\Delta t}{2\mu} \left[ \frac{E_\phi^{n+\frac{1}{2}}(i, j + \frac{1}{2}, k + 1) - E_\phi^{n+\frac{1}{2}}(i, j + \frac{1}{2}, k)}{\Delta z 2(k + 1)} - \frac{E_z^{n+1}(i, j + 1, k + \frac{1}{2}) - E_z^{n+1}(i, j, k + \frac{1}{2})}{\Delta \phi \cdot r(i)} \right] \quad (\text{B-2e})$$

$$H_\phi^{n+1}(i + \frac{1}{2}, j, k + \frac{1}{2}) = H_\phi^{n+\frac{1}{2}}(i + \frac{1}{2}, j, k + \frac{1}{2}) + \frac{\Delta t}{2\mu} \left[ \frac{E_z^{n+\frac{1}{2}}(i + 1, j, k + \frac{1}{2}) - E_z^{n+\frac{1}{2}}(i, j, k + \frac{1}{2})}{\Delta r 2(i + 1)} - \frac{E_r^{n+1}(i + \frac{1}{2}, j, k + 1) - E_r^{n+1}(i + \frac{1}{2}, j, k)}{\Delta z(k + 1)} \right] \quad (\text{B-2f})$$

$$H_z^{n+1}(i + \frac{1}{2}, j + \frac{1}{2}, k) = H_z^{n+\frac{1}{2}}(i + \frac{1}{2}, j + \frac{1}{2}, k) + \frac{\Delta t}{2\mu \cdot r(i + \frac{1}{2})} \left[ \frac{E_r^{n+\frac{1}{2}}(i + \frac{1}{2}, j + 1, k) - E_r^{n+\frac{1}{2}}(i + \frac{1}{2}, j, k)}{\Delta \phi} - \frac{r(i + 1) \cdot E_\phi^{n+1}(i + 1, j + \frac{1}{2}, k) - r(i) \cdot E_\phi^{n+1}(i, j + \frac{1}{2}, k)}{\Delta r 2(i + 1)} \right] \quad (\text{B-2g})$$

Another easy way to obtain all the above equations is to permute the indices of the equation (B-1a). The resulting equations form a linear system of equations that can be solved with available numerical packages. In the following paragraphs, we will describe the approach to the solutions in a matrix form.



## Appendix C      Maple Outputs of the Expressions of the Coefficients of the Characteristic Equation

$$A_6 = (4*u^4*e^4*Wfi^4 + 4*u*e^3*b2*Wfi^4*Wz^4 + 2*u^2*e^2*dr^2*Wz^2*Wfi^2*b3*b2*b4*b1 + 8*u^4*e^4*i^4*dr^4*Wz^2*b4*b1 + 8*u^2*e^2*Wz^2*Wfi^4*b3*b2 + 8*u^2*e^2*Wz^2*Wfi^4*b4*b1 + 2*u^4*e^4*i^2*dr^4*Wz^2*b4*b1 + 8*u^4*e^4*i^2*dr^2*Wfi^2*b3*b2 + 8*u^4*e^4*i^3*dr^4*Wz^2*b4*b1 + 4*Wz^4*Wfi^4*b3*b2*b4*b1 + 2*u^4*e^4*dr^2*Wz^2*Wfi^2 + 8*u^3*e^3*Wz^2*Wfi^2*i*dr^2*b4*b1 + 8*u^3*e^3*Wz^2*b3*b2*dr^4*i^3*b4*b1 + 4*u^4*e^4*b3*b2*dr^4*i^4*b4*b1 + 4*u^4*e^4*b3*b2*dr^4*i^3*b4*b1 + u^4*e^4*b3*b2*dr^4*i^2*b4*b1 + 4*u^4*e^4*dr^4*i^4*Wz^4 + u^4*e^4*dr^4*i^2*Wz^4 + 4*u^4*e^4*dr^4*i^3*Wz^4 + u^4*e^4*Wfi^2*dr^2*b3*b2 + 4*u^4*e^4*Wfi^2*i*dr^2*b4*b1 + u^4*e^4*Wfi^2*dr^2*b4*b1 + 8*u^5*e^5*Wz^2*dr^4*i^4 + 4*u^4*e^4*Wfi^2*i*dr^2*b3*b2 + 2*u^5*e^5*Wz^2*dr^4*i^2 + u^5*e^5*b3*b2*dr^4*i^2 + 4*u^5*e^5*b3*b2*dr^4*i^3 + 4*u^5*e^5*b3*b2*dr^4*i^4 + 4*u^5*e^5*Wfi^2*i*dr^2 + 8*u^5*e^5*dr^2*i^2*Wfi^2 + 8*u^3*e^3*Wfi^4*Wz^2 + 4*u^5*e^5*dr^4*i^3*b4*b1 + u^5*e^5*dr^4*i^2*b4*b1 + 4*u^5*e^5*dr^4*i^4*b4*b1 + 4*u^6*e^6*dr^4*i^3 + u^5*e^5*Wfi^2*dr^2 + 4*u^6*e^6*dr^4*i^4 + u^6*e^6*dr^4*i^2 + 4*u^2*e^2*b3*b2*Wfi^2*i*dr^2*Wz^4 + 4*u^2*e^2*Wz^4*b3*b2*dr^4*i^3*b4*b1 + 4*u^2*e^2*dr^4*i^4*Wz^4*b3*b2*b4*b1 + u^2*e^2*Wz^4*b3*b2*dr^4*i^2*b4*b1 + u^2*e^2*Wfi^2*dr^2*Wz^4*b3*b2 + 4*u^2*e^2*Wfi^4*Wz^4 + 4*u^2*e^2*Wfi^2*i*Wz^4*b4*b1*dr^2 + u^2*e^2*Wfi^2*Wz^4*b4*b1*dr^2 + 2*u^3*e^3*Wz^2*dr^4*i^2*b3*b2*b4*b1 + 8*u^3*e^3*Wz^2*b3*b2*dr^4*i^4*b4*b1 + 4*u^2*e^2*Wfi^4*b3*b2*b4*b1 + u^3*e^3*Wfi^2*dr^2*Wz^4 + 4*u^3*e^3*Wfi^4*b3*b2 + 4*u^3*e^3*Wfi^4*b4*b1 + 2*u^3*e^3*Wfi^2*dr^2*Wz^2*b4*b1 + u^3*e^3*Wz^4*dr^4*i^2*b3*b2 + 4*u^3*e^3*Wz^4*dr^4*i^3*b3*b2 + 8*u^3*e^3*Wz^4*dr^2*i^2*Wfi^2 + 2*u^3*e^3*Wfi^2*dr^2*Wz^2*b3*b2 + 4*u^3*e^3*Wz^4*dr^4*i^3*b4*b1 + u^3*e^3*Wz^4*dr^4*i^2*b4*b1 + 16*i^2*u^2*e^2*dr^2*Wz^2*Wfi^2*b3*b2*b4*b1 + 4*u^3*e^3*Wz^4*dr^4*i^4*b4*b1 + 4*u^3*e^3*Wfi^2*i*dr^2*Wz^4 + 8*u^3*e^3*Wz^2*Wfi^2*i*dr^2*b3*b2 + 8*i*u^2*e^2*dr^2*Wz^2*Wfi^2*b3*b2*b4*b1 + 8*i^2*u^2*e^2*Wfi^2*dr^2*Wz^4*b3*b2 + 4*u*e*Wfi^4*Wz^4*b4*b1 + 8*u*e*Wz^2*Wfi^4*b3*b2*b4*b1 + 8*u*e*Wz^4*dr^2*i^2*b3*b2*b4*b1*Wfi^2 + 8*i^2*u^4*e^4*Wfi^2*dr^2*b4*b1 + 16*i^2*u^4*e^4*dr^2*Wz^2*Wfi^2 + 8*i*u^4*e^4*dr^2*Wz^2*Wfi^2 + 4*u*e*Wz^4*Wfi^2*b3*b2*i*dr^2*b4*b1 + u*e*Wfi^2*dr^2*Wz^4*b3*b2*b4*b1 + 8*u^5*e^5*Wz^2*dr^4*i^3 + 16*u^3*e^3*Wz^2*b3*b2*dr^2*i^2*Wfi^2 + 4*u^3*e^3*Wfi^2*b3*b2*i*dr^2*b4*b1 + 8*u^3*e^3*dr^2*i^2*b3*b2*b4*b1*Wfi^2 + 16*u^3*e^3*Wz^2*Wfi^2*i^2*dr^2*b4*b1 + 4*u^3*e^3*Wz^4*dr^4*i^4*b3*b2 + u^3*e^3*Wfi^2*dr^2*b3*b2*b4*b1 + 8*u^2*e^2*i^2*dr^2*b4*Wz^4*b1*Wfi^2 + 8*u^4*e^4*i^3*dr^4*Wz^2*b3*b2 + 2*u^4*e^4*i^2*dr^4*Wz^2*b3*b2 + 8*u^4*e^4*i^4*dr^4*Wz^2*b3*b2)/((u*dr^2*e*i^2 + Wfi^2)*(u*e + b4*b1)*(u*e + b3*b2)*(4*u*dr^2*e*i^2 + 4*u*dr^2*e*i + u*dr^2*e + 4*Wfi^2)*(u*e + Wz^2)^2)$$

$$A_5 = (8*u^4*e^4*Wfi^4 - 8*u*e^3*b2*Wfi^4*Wz^4 - 24*Wz^4*Wfi^4*b3*b2*b4*b1 + 16*u^3*e^3*Wz^2*Wfi^2*i*dr^2*b4*b1 + 16*u^3*e^3*Wz^2*b3*b2*dr^4*i^3*b4*b1 + 8*u^4*e^4*b3*b2*dr^4*i^4*b4*b1 + 8*u^4*e^4*b3*b2*dr^4*i^3*b4*b1 + 2*u^4*e^4*b3*b2*dr^4*i^2*b4*b1 + 8*u^4*e^4*dr^4*i^4*Wz^4 + 2*u^4*e^4*dr^4*i^2*Wz^4 + 8*u^4*e^4*dr^4*i^3*Wz^4 - 2*u^4*e^4*Wfi^2*dr^2*b3*b2 + 8*u^4*e^4*Wfi^2*i*dr^2*b4*b1 + 2*u^4*e^4*Wfi^2*dr^2*b4*b1 - 16*u^5*e^5*Wz^2*dr^4*i^4 - 8*u^4*e^4*Wfi^2*i*dr^2*b3*b2 - 4*u^5*e^5*Wz^2*dr^4*i^2 - 2*u^5*e^5*b3*b2*dr^4*i^2 - 8*u^5*e^5*b3*b2*dr^4*i^3 - 8*u^5*e^5*b3*b2*dr^4*i^4 - 8*u^5*e^5*Wfi^2*i*dr^2 -$$

$$\begin{aligned}
& 16*u^5*e^5*dr^2*i^2*Wfi^2+16*u^3*e^3*Wfi^4*Wz^2-8*u^5*e^5*dr^4*i^3*b4*b1- \\
& 2*u^5*e^5*dr^4*i^2*b4*b1-8*u^5*e^5*dr^4*i^4*b4*b1-24*u^6*e^6*dr^4*i^3- \\
& 2*u^5*e^5*Wfi^2*dr^2-24*u^6*e^6*dr^4*i^4-6*u^6*e^6*dr^4*i^2- \\
& 8*u^2*e^2*b3*b2*Wfi^2*i*dr^2*Wz^4+8*u^2*e^2*Wz^4*b3*b2*dr^4*i^3*b4*b1+8* \\
& u^2*e^2*dr^4*i^4*Wz^4*b3*b2*b4*b1+2*u^2*e^2*Wz^4*b3*b2*dr^4*i^2*b4*b1- \\
& 2*u^2*e^2*Wfi^2*dr^2*Wz^4*b3*b2+8*u^2*e^2*Wfi^4*Wz^4+8*u^2*e^2*Wfi^2*i* \\
& Wz^4*b4*b1*dr^2+2*u^2*e^2*Wfi^2*Wz^4*b4*b1*dr^2+4*u^3*e^3*Wz^2*dr^4*i^2 \\
& *b3*b2*b4*b1+16*u^3*e^3*Wz^2*b3*b2*dr^4*i^4*b4*b1+8*u^2*e^2*Wfi^4*b3*b2* \\
& b4*b1+2*u^3*e^3*Wfi^2*dr^2*Wz^4+8*u^3*e^3*Wfi^4*b3*b2+8*u^3*e^3*Wfi^4*b \\
& 4*b1+4*u^3*e^3*Wfi^2*dr^2*Wz^2*b4*b1+2*u^3*e^3*Wz^4*dr^4*i^2*b3*b2+8*u^ \\
& 3*e^3*Wz^4*dr^4*i^3*b3*b2+16*u^3*e^3*Wz^4*dr^2*i^2*Wfi^2- \\
& 4*u^3*e^3*Wfi^2*dr^2*Wz^2*b3*b2+8*u^3*e^3*Wz^4*dr^4*i^3*b4*b1+2*u^3*e^3* \\
& Wz^4*dr^4*i^2*b4*b1+8*u^3*e^3*Wz^4*dr^4*i^4*b4*b1+8*u^3*e^3*Wfi^2*i*dr^2* \\
& Wz^4-16*u^3*e^3*Wz^2*Wfi^2*i*dr^2*b3*b2-8*u^3*e^3*Wfi^4*Wz^4*b4*b1- \\
& 16*u^3*e^3*Wz^2*Wfi^4*b3*b2*b4*b1-16*u^3*e^3*Wz^4*dr^2*i^2*b3*b2*b4*b1*Wfi^2- \\
& 8*u^3*e^3*Wz^4*Wfi^2*b3*b2*i*dr^2*b4*b1-2*u^3*e^3*Wfi^2*dr^2*Wz^4*b3*b2*b4*b1- \\
& 16*u^5*e^5*Wz^2*dr^4*i^3+8*u^3*e^3*Wfi^2*b3*b2*i*dr^2*b4*b1+16*u^3*e^3*dr \\
& ^2*i^2*b3*b2*b4*b1*Wfi^2+8*u^3*e^3*Wz^4*dr^4*i^4*b3*b2+2*u^3*e^3*Wfi^2*dr \\
& ^2*b3*b2*b4*b1)/((u*dr^2*e^i^2+Wfi^2)*(u*e+b4*b1)*(u*e+b3*b2)*(4*u*dr^2*e^i^2 \\
& +4*u*dr^2*e^i+u*dr^2*e+4*Wfi^2)*(u*e+Wz^2)^2)
\end{aligned}$$

$$\begin{aligned}
A_4 = & (-4*u^4*e^4*Wfi^4-4*u^3*e^3*b3*b2*Wfi^4*Wz^4- \\
& 2*u^2*e^2*dr^2*Wz^2*Wfi^2*b3*b2*b4*b1-8*u^4*e^4*i^4*dr^4*Wz^2*b4*b1- \\
& 8*u^2*e^2*Wz^2*Wfi^4*b3*b2-8*u^2*e^2*Wz^2*Wfi^4*b4*b1- \\
& 2*u^4*e^4*i^2*dr^4*Wz^2*b4*b1-8*u^4*e^4*i^2*dr^2*Wfi^2*b3*b2- \\
& 8*u^4*e^4*i^3*dr^4*Wz^2*b4*b1+60*Wz^4*Wfi^4*b3*b2*b4*b1- \\
& 2*u^4*e^4*dr^2*Wz^2*Wfi^2+56*u^3*e^3*Wz^2*Wfi^2*i*dr^2*b4*b1- \\
& 8*u^3*e^3*Wz^2*b3*b2*dr^4*i^3*b4*b1-4*u^4*e^4*b3*b2*dr^4*i^4*b4*b1- \\
& 4*u^4*e^4*b3*b2*dr^4*i^3*b4*b1-u^4*e^4*b3*b2*dr^4*i^2*b4*b1- \\
& 4*u^4*e^4*dr^4*i^4*Wz^4-u^4*e^4*dr^4*i^2*Wz^4-4*u^4*e^4*dr^4*i^3*Wz^4- \\
& u^4*e^4*Wfi^2*dr^2*b3*b2-4*u^4*e^4*Wfi^2*i*dr^2*b4*b1- \\
& u^4*e^4*Wfi^2*dr^2*b4*b1-8*u^5*e^5*Wz^2*dr^4*i^4- \\
& 4*u^4*e^4*Wfi^2*i*dr^2*b3*b2-2*u^5*e^5*Wz^2*dr^4*i^2- \\
& u^5*e^5*b3*b2*dr^4*i^2-4*u^5*e^5*b3*b2*dr^4*i^3-4*u^5*e^5*b3*b2*dr^4*i^4- \\
& 4*u^5*e^5*Wfi^2*i*dr^2-8*u^5*e^5*dr^2*i^2*Wfi^2-8*u^3*e^3*Wfi^4*Wz^2- \\
& 4*u^5*e^5*dr^4*i^3*b4*b1-u^5*e^5*dr^4*i^2*b4*b1- \\
& 4*u^5*e^5*dr^4*i^4*b4*b1+60*u^6*e^6*dr^4*i^3- \\
& u^5*e^5*Wfi^2*dr^2+60*u^6*e^6*dr^4*i^4+15*u^6*e^6*dr^4*i^2- \\
& 4*u^2*e^2*b3*b2*Wfi^2*i*dr^2*Wz^4-4*u^2*e^2*Wz^4*b3*b2*dr^4*i^3*b4*b1- \\
& 4*u^2*e^2*dr^4*i^4*Wz^4*b3*b2*b4*b1-u^2*e^2*Wz^4*b3*b2*dr^4*i^2*b4*b1- \\
& u^2*e^2*Wfi^2*dr^2*Wz^4*b3*b2-4*u^2*e^2*Wfi^4*Wz^4- \\
& 4*u^2*e^2*Wfi^2*i*Wz^4*b4*b1*dr^2-u^2*e^2*Wfi^2*Wz^4*b4*b1*dr^2- \\
& 2*u^3*e^3*Wz^2*dr^4*i^2*b3*b2*b4*b1-8*u^3*e^3*Wz^2*b3*b2*dr^4*i^4*b4*b1- \\
& 4*u^2*e^2*Wfi^4*b3*b2*b4*b1-u^3*e^3*Wfi^2*dr^2*Wz^4- \\
& 4*u^3*e^3*Wfi^4*b3*b2- \\
& 4*u^3*e^3*Wfi^4*b4*b1+14*u^3*e^3*Wfi^2*dr^2*Wz^2*b4*b1- \\
& u^3*e^3*Wz^4*dr^4*i^2*b3*b2-4*u^3*e^3*Wz^4*dr^4*i^3*b3*b2- \\
& 8*u^3*e^3*Wz^4*dr^2*i^2*Wfi^2-2*u^3*e^3*Wfi^2*dr^2*Wz^2*b3*b2- \\
& 4*u^3*e^3*Wz^4*dr^4*i^3*b4*b1-u^3*e^3*Wz^4*dr^4*i^2*b4*b1- \\
& 16*i^2*u^2*e^2*dr^2*Wz^2*Wfi^2*b3*b2*b4*b1-4*u^3*e^3*Wz^4*dr^4*i^4*b4*b1- \\
& 4*u^3*e^3*Wfi^2*i*dr^2*Wz^4-8*u^3*e^3*Wz^2*Wfi^2*i*dr^2*b3*b2-
\end{aligned}$$

$$\begin{aligned}
& 8*i^2*u^2*e^2*dr^2*Wz^2*Wfi^2*b3*b2*b4*b1- \\
& 8*i^2*u^2*e^2*Wfi^2*dr^2*Wz^4*b3*b2-4*u^e*Wfi^4*Wz^4*b4*b1- \\
& 8*u^e*Wz^2*Wfi^4*b3*b2*b4*b1-8*u^e*Wz^4*dr^2*i^2*b3*b2*b4*b1*Wfi^2- \\
& 8*i^2*u^4*e^4*Wfi^2*dr^2*b4*b1-16*i^2*u^4*e^4*dr^2*Wz^2*Wfi^2- \\
& 8*i^u^4*e^4*dr^2*Wz^2*Wfi^2-4*u^e*Wz^4*Wfi^2*b3*b2*i^dr^2*b4*b1- \\
& u^e*Wfi^2*dr^2*Wz^4*b3*b2*b4*b1- \\
& 8*u^5*e^5*Wz^2*dr^4*i^3+48*u^3*e^3*Wz^2*b3*b2*dr^2*i^2*Wfi^2- \\
& 4*u^3*e^3*Wfi^2*b3*b2*i^dr^2*b4*b1- \\
& 8*u^3*e^3*dr^2*i^2*b3*b2*b4*b1*Wfi^2+48*u^3*e^3*Wz^2*Wfi^2*i^2*dr^2*b4*b1 \\
& -4*u^3*e^3*Wz^4*dr^4*i^4*b3*b2-u^3*e^3*Wfi^2*dr^2*b3*b2*b4*b1- \\
& 8*u^2*e^2*i^2*dr^2*b4*Wz^4*b1*Wfi^2-8*u^4*e^4*i^3*dr^4*Wz^2*b3*b2- \\
& 2*u^4*e^4*i^2*dr^4*Wz^2*b3*b2- \\
& 8*u^4*e^4*i^4*dr^4*Wz^2*b3*b2)/((u^dr^2*e^i^2+Wfi^2)*(u^e+b4*b1)*(u^e+b3*b2) \\
& *(4*u^dr^2*e^i^2+4*u^dr^2*e^i+u^dr^2*e+4*Wfi^2)*(u^e+Wz^2)^2)
\end{aligned}$$

$A_3=(-$

$$\begin{aligned}
& 16*u^4*e^4*Wfi^4+16*u^e*b3*b2*Wfi^4*Wz^4+256*u^3*e^3*b4*Wz^2*i^2*dr^2* \\
& Wfi^2*b2+128*u^3*e^3*b4*Wz^2*i^dr^2*b2*Wfi^2+128*u^3*e^3*Wfi^2*b3*i^dr^2* \\
& Wz^2*b1+256*u^3*e^3*Wfi^2*b3*b1*dr^2*Wz^2*i^2- \\
& 80*Wz^4*Wfi^4*b3*b2*b4*b1+96*u^3*e^3*Wz^2*Wfi^2*i^dr^2*b4*b1- \\
& 32*u^3*e^3*Wz^2*b3*b2*dr^4*i^3*b4*b1-16*u^4*e^4*b3*b2*dr^4*i^4*b4*b1- \\
& 16*u^4*e^4*b3*b2*dr^4*i^3*b4*b1-4*u^4*e^4*b3*b2*dr^4*i^2*b4*b1- \\
& 16*u^4*e^4*dr^4*i^4*Wz^4-4*u^4*e^4*dr^4*i^2*Wz^4- \\
& 16*u^4*e^4*dr^4*i^3*Wz^4+4*u^4*e^4*Wfi^2*dr^2*b3*b2- \\
& 16*u^4*e^4*Wfi^2*i^dr^2*b4*b1- \\
& 4*u^4*e^4*Wfi^2*dr^2*b4*b1+32*u^5*e^5*Wz^2*dr^4*i^4+16*u^4*e^4*Wfi^2*i^dr \\
& ^2*b3*b2+8*u^5*e^5*Wz^2*dr^4*i^2+4*u^5*e^5*b3*b2*dr^4*i^2+16*u^5*e^5*b3*b \\
& 2*dr^4*i^3+16*u^5*e^5*b3*b2*dr^4*i^4+16*u^5*e^5*Wfi^2*i^dr^2+32*u^5*e^5*dr^ \\
& 2*i^2*Wfi^2- \\
& 32*u^3*e^3*Wfi^4*Wz^2+16*u^5*e^5*dr^4*i^3*b4*b1+4*u^5*e^5*dr^4*i^2*b4*b1+ \\
& 16*u^5*e^5*dr^4*i^4*b4*b1-80*u^6*e^6*dr^4*i^3+4*u^5*e^5*Wfi^2*dr^2- \\
& 80*u^6*e^6*dr^4*i^4-20*u^6*e^6*dr^4*i^2+16*u^2*e^2*b3*b2*Wfi^2*i^dr^2*Wz^4- \\
& 16*u^2*e^2*Wz^4*b3*b2*dr^4*i^3*b4*b1- \\
& 16*u^2*e^2*dr^4*i^4*Wz^4*b3*b2*b4*b1- \\
& 4*u^2*e^2*Wz^4*b3*b2*dr^4*i^2*b4*b1+4*u^2*e^2*Wfi^2*dr^2*Wz^4*b3*b2- \\
& 16*u^2*e^2*Wfi^4*Wz^4-16*u^2*e^2*Wfi^2*i^Wz^4*b4*b1*dr^2- \\
& 4*u^2*e^2*Wfi^2*Wz^4*b4*b1*dr^2-8*u^3*e^3*Wz^2*dr^4*i^2*b3*b2*b4*b1- \\
& 32*u^3*e^3*Wz^2*b3*b2*dr^4*i^4*b4*b1-16*u^2*e^2*Wfi^4*b3*b2*b4*b1- \\
& 4*u^3*e^3*Wfi^2*dr^2*Wz^4-16*u^3*e^3*Wfi^4*b3*b2- \\
& 16*u^3*e^3*Wfi^4*b4*b1+24*u^3*e^3*Wfi^2*dr^2*Wz^2*b4*b1- \\
& 4*u^3*e^3*Wz^4*dr^4*i^2*b3*b2-16*u^3*e^3*Wz^4*dr^4*i^3*b3*b2- \\
& 32*u^3*e^3*Wz^4*dr^2*i^2*Wfi^2+8*u^3*e^3*Wfi^2*dr^2*Wz^2*b3*b2- \\
& 16*u^3*e^3*Wz^4*dr^4*i^3*b4*b1-4*u^3*e^3*Wz^4*dr^4*i^2*b4*b1- \\
& 16*u^3*e^3*Wz^4*dr^4*i^4*b4*b1- \\
& 16*u^3*e^3*Wfi^2*i^dr^2*Wz^4+32*u^3*e^3*Wz^2*Wfi^2*i^dr^2*b3*b2+16*u^e* \\
& Wfi^4*Wz^4*b4*b1+32*u^e*Wz^2*Wfi^4*b3*b2*b4*b1+32*u^e*Wz^4*dr^2*i^2*b3 \\
& *b2*b4*b1*Wfi^2+16*u^e*Wz^4*Wfi^2*b3*b2*i^dr^2*b4*b1+4*u^e*Wfi^2*dr^2*W \\
& z^4*b3*b2*b4*b1+32*u^5*e^5*Wz^2*dr^4*i^3+128*u^3*e^3*Wz^2*b3*b2*dr^2*i^2 \\
& *Wfi^2-16*u^3*e^3*Wfi^2*b3*b2*i^dr^2*b4*b1- \\
& 32*u^3*e^3*dr^2*i^2*b3*b2*b4*b1*Wfi^2+128*u^3*e^3*Wz^2*Wfi^2*i^2*dr^2*b4* \\
& b1-16*u^3*e^3*Wz^4*dr^4*i^4*b3*b2-
\end{aligned}$$

$$\frac{4*u^3*e^3*Wfi^2*dr^2*b3*b2*b4*b1}{((u*dr^2*e*i^2+Wfi^2)*(u*e+b4*b1)*(u*e+b3*b2)*(4*u*dr^2*e*i^2+4*u*dr^2*e*i+u*dr^2*e+4*Wfi^2)*(u*e+Wz^2)^2)}$$

## Appendix D      Modified ADI-FDTD Algorithm for Solving Conductive Materials

for the first half time step:

$$E_r^{n+\frac{1}{2}}(i+\frac{1}{2}, j, k) = \frac{1}{\left(1 + \frac{\Delta t \cdot \sigma}{2\varepsilon}\right)} E_r^n(i+\frac{1}{2}, j, k) + \frac{\Delta t}{2\varepsilon \left(1 + \frac{\Delta t \cdot \sigma}{2\varepsilon}\right)} \left[ \frac{H_z^{n+\frac{1}{2}}(i+\frac{1}{2}, j+\frac{1}{2}, k) - H_z^{n+\frac{1}{2}}(i+\frac{1}{2}, j-\frac{1}{2}, k)}{\Delta\phi \cdot r(i+\frac{1}{2})} - \frac{H_\phi^n(i+\frac{1}{2}, j, k+\frac{1}{2}) - H_\phi^n(i+\frac{1}{2}, j, k-\frac{1}{2})}{\Delta z l(k)} \right] \quad (D-1a)$$

$$E_\phi^{n+\frac{1}{2}}(i, j+\frac{1}{2}, k) = \frac{1}{\left(1 + \frac{\Delta t \cdot \sigma}{2\varepsilon}\right)} E_\phi^n(i, j+\frac{1}{2}, k) + \frac{\Delta t}{2\varepsilon \left(1 + \frac{\Delta t \cdot \sigma}{2\varepsilon}\right)} \left[ \frac{H_r^{n+\frac{1}{2}}(i, j+\frac{1}{2}, k+\frac{1}{2}) - H_r^{n+\frac{1}{2}}(i, j+\frac{1}{2}, k-\frac{1}{2})}{\Delta z l(k)} - \frac{H_z^n(i+\frac{1}{2}, j+\frac{1}{2}, k) - H_z^n(i-\frac{1}{2}, j+\frac{1}{2}, k)}{\Delta r l(i)} \right] \quad (D-1b)$$

$$E_z^{n+\frac{1}{2}}(i, j, k+\frac{1}{2}) = \frac{1}{\left(1 + \frac{\Delta t \cdot \sigma}{2\varepsilon}\right)} E_z^n(i, j, k+\frac{1}{2}) + \frac{\Delta t}{2\varepsilon \cdot r(i) \cdot \left(1 + \frac{\Delta t \cdot \sigma}{2\varepsilon}\right)} \left[ \frac{r(i+\frac{1}{2}) \cdot H_\phi^{n+\frac{1}{2}}(i+\frac{1}{2}, j, k+\frac{1}{2}) - r(i-\frac{1}{2}) \cdot H_\phi^{n+\frac{1}{2}}(i-\frac{1}{2}, j, k+\frac{1}{2})}{\Delta r l(i)} - \frac{H_r^n(i, j+\frac{1}{2}, k+\frac{1}{2}) - H_r^n(i, j-\frac{1}{2}, k+\frac{1}{2})}{\Delta\phi} \right] \quad (D-1c)$$

$$E_z^{n+\frac{1}{2}}(0, j, k+\frac{1}{2}) = \frac{1}{\left(1 + \frac{\Delta t \cdot \sigma}{2\varepsilon}\right)} E_z^n(0, j, k+\frac{1}{2}) + \frac{2\Delta t}{\varepsilon \cdot \Delta r 2(l) \left(1 + \frac{\Delta t \cdot \sigma}{2\varepsilon}\right)} H_\phi^{n+\frac{1}{2}}(\frac{1}{2}, j, k+\frac{1}{2}) \quad (D-1d)$$

for the second half time step:

$$E_r^{n+1}(i + \frac{1}{2}, j, k) = \frac{1}{\left(1 + \frac{\Delta t \cdot \sigma}{2\varepsilon}\right)} E_r^{n+\frac{1}{2}}(i + \frac{1}{2}, j, k) +$$

$$\frac{\Delta t}{2\varepsilon \left(1 + \frac{\Delta t \cdot \sigma}{2\varepsilon}\right)} \left[ \frac{H_z^{n+\frac{1}{2}}(i + \frac{1}{2}, j + \frac{1}{2}, k) - H_z^{n+\frac{1}{2}}(i + \frac{1}{2}, j - \frac{1}{2}, k)}{\Delta \phi \cdot r(i + \frac{1}{2})} - \frac{H_\phi^{n+1}(i + \frac{1}{2}, j, k + \frac{1}{2}) - H_\phi^{n+1}(i + \frac{1}{2}, j, k - \frac{1}{2})}{\Delta z l(k)} \right] \quad (D-2a)$$

$$E_\phi^{n+1}(i, j + \frac{1}{2}, k) = \frac{1}{\left(1 + \frac{\Delta t \cdot \sigma}{2\varepsilon}\right)} E_\phi^{n+\frac{1}{2}}(i, j + \frac{1}{2}, k) +$$

$$\frac{\Delta t}{2\varepsilon \left(1 + \frac{\Delta t \cdot \sigma}{2\varepsilon}\right)} \left[ \frac{H_r^{n+\frac{1}{2}}(i, j + \frac{1}{2}, k + \frac{1}{2}) - H_r^{n+\frac{1}{2}}(i, j + \frac{1}{2}, k - \frac{1}{2})}{\Delta z l(k)} - \frac{H_z^{n+1}(i + \frac{1}{2}, j + \frac{1}{2}, k) - H_z^{n+1}(i - \frac{1}{2}, j + \frac{1}{2}, k)}{\Delta r l(i)} \right] \quad (D-2b)$$

$$E_z^{n+1}(i, j, k + \frac{1}{2}) = \frac{1}{\left(1 + \frac{\Delta t \cdot \sigma}{2\varepsilon}\right)} E_z^{n+\frac{1}{2}}(i, j, k + \frac{1}{2}) +$$

$$\frac{\Delta t}{2\varepsilon \cdot r(i) \cdot \left(1 + \frac{\Delta t \cdot \sigma}{2\varepsilon}\right)} \left[ \frac{(i + \frac{1}{2}) \cdot \Delta r \cdot H_\phi^{n+\frac{1}{2}}(i + \frac{1}{2}, j, k + \frac{1}{2}) - (i - \frac{1}{2}) \cdot \Delta r \cdot H_\phi^{n+\frac{1}{2}}(i - \frac{1}{2}, j, k + \frac{1}{2})}{\Delta r l(i)} - \frac{H_r^{n+1}(i, j + \frac{1}{2}, k + \frac{1}{2}) - H_r^{n+1}(i, j - \frac{1}{2}, k + \frac{1}{2})}{\Delta \phi} \right] \quad (D-2c)$$

$$E_z^{n+1}(0, j, k + \frac{1}{2}) = \frac{1}{\left(1 + \frac{\Delta t \cdot \sigma}{2\varepsilon}\right)} E_z^{n+\frac{1}{2}}(0, j, k + \frac{1}{2}) + \frac{2\Delta t}{\varepsilon \cdot \Delta r 2(l) \left(1 + \frac{\Delta t \cdot \sigma}{2\varepsilon}\right)} H_\phi^{n+\frac{1}{2}}(\frac{1}{2}, j, k + \frac{1}{2}) \quad (D-2d)$$